ATLAS+CMS DARK MATTER FORUM RECOMMENDATIONS

Author/contributor list to be added as document is finalized.

May 19, 2015

Contents

1
Introduction

Dark matter has not yet been seen in particle physics experiments, and there is not yet any evidence for non-gravitational interactions between dark matter and Standard Model particles. If such interactions exist, pairs of dark matter particles could be produced at the LHC, leading to so-called 'mono-X' signatures.

Early Run 1 searches for 'mono-X' signatures at ATLAS and CMS employed a set of effective field theories (EFTs) [GIR+10] to model the possible signals. If a contact interaction is the correct description of dark matter pair production at colliders, the missing energy distribution of the signal depends only on the mass of the dark matter particles and the spin structure of the interaction; only the overall rate is a free parameter. Both experiments studied a variety EFTs with different spin structures. Provided the contact interaction approximation holds, these EFTs also provide a straightforward way to translate results amongst LHC results and the different types of non-collider searches for dark matter.

From the Run 1 results, however, it has become clear [BDSMR14] that a contact interaction is often not the correct description for the signals to which the LHC is truly sensitive. The LHC is exploring a regime where the mediating process may play a more interesting role, leading to mono-X signals that can be kinematically distinct from those predicted by the EFT, as well as qualitatively different signatures requiring new search strategies. While the EFT integrates out the degrees of freedom of the (heavy) intermediate particle, "simplified models" [A+12] with directly-accessible mediators describe this richer phenomenology. Such models can be used both to interpret mono-X searches and to guide the design of complementary searches for additional signatures.

Many proposals for such models began to emerge, for example Refs. [AJW12, AHW13, DNRT13, BDM14, BB13a, BB14, AWZ14a, A+14b, MMA+14, HKSW15, BFG15] and, at the end of 2014, ATLAS and CMS organized a forum, the ATLAS-CMS Dark Matter Forum, to form a consensus with the participation of experts on theories of dark matter. This is the final report of that forum.

One of the guiding principles of this report is to channel the efforts of the ATLAS and CMS Collaboration towards a minimal set of dark matter models that should influence the design of the early

Run-2 searches, rather than providing exhaustive and elaborate interpretations and re-interpretations of the results. At the same time, a thorough survey of realistic collider signals of dark matter is a crucial input to the overall design of the search program.

The goal of this report is such a survey, though confined within some broad assumptions and focused on benchmarks for kinematically-distinct signals which are most urgently needed. As far as time and resources have allowed, the assumptions have been carefully motivated by theoretical consensus and comparisons of simulation. But to achieve a true consensus with only a few months before Run 2 would begin, it was important to narrow the scope and timescale to the following:

1. A prioritized, small set of benchmark simplified models should be agreed upon by both collaborations for Run-2 searches.

2. The matrix element implementation of the simplified models should be standardized, and other common technical details (order of the calculation, showering) harmonized as much as practical. It would be desirable to have a common choice of LO/NLO, ME-parton shower matching and merging, factorization and renormalization scales for each of the simplified models. This will also lead to a single set of theory uncertainties, which will be easier to deal with when comparing results from the two collaborations.

3. The forum could also discuss the conditions under which the EFT interpretation may still be desirable.

4. The forum should prepare a report summarizing these items, suitable both as a reference for the internal ATLAS and CMS audiences and as an explanation for theory and non-collider readers. This report represents the views of the participants of the forum.

1.1 Grounding Assumptions

The first choice made for the Run-2 benchmarks is on the nature of the Dark Matter itself: it is assumed to be a particle, stable on collider timescales and non-interacting with the detector, and a Dirac fermion. The latter is a practical choice, given that the Forum relied upon a large body of theoretical work which made this assumption. Many of the conclusions in this report should also apply to MET signals of Majorana fermion DM or scalar DM with some minor modification to account for their different angular distributions, especially when considering cut-and-count analysis. Thus the choice of Dirac fermion dark matter is deemed sufficient for the benchmarks aiding the design of the upcoming Run-2 searches. Nevertheless, a more complete set of models will certainly be required upon a discovery; see e.g. [CHH15] for an example of an observable that may distinguish the spin of the DM particle.

We also assume that Minimal Flavor Violation (MFV) applies to the recommended models. This means that the flavor structure of the couplings between dark matter and ordinary particles follows the structure as the Standard Model. This choice is both natural, as there is no required additional theory of flavor beyond what is already present in the SM, and and it provides a mechanism to ensure that the models do not violate flavor constraints. As a consequence, spin-0 resonances exchanged in the $s-$channel must have Yukawa couplings to SM fermions. Flavor-safe models can still be constructed beyond the MFV assumption [ABG14], but their phenomenology is left for future studies.

In the parameter scan for the recommended models, we make the assumption of minimal width for the particles mediating the interaction between SM and DM. This means that only the decays that are strictly necessary for the self-consistency of the model (e.g. to DM and to quarks) are accounted for in the definition of the mediator width. In turn, this forbids any further decays to other invisible particles of the Dark Sector that may increase the width. However, studies within the Forum show that, for cut and count analyses, the kinematic distributions of many models and therefore the sensitivity of the search do not depend significantly on the mediator width up to extreme values where the particle nature of the mediator comes into question.

The particle content of the models chosen as benchmarks is limited to one single kind of DM whose self-interactions are not relevant for LHC phenomenology, and to one type of SM/DM interaction at a time. These assumptions only add a limited number of new particles to the SM. These simplified models, independently sought by different experimental analyses, can be used as starting points to build more complete theories. Even though this factorized picture does not always lead to full theories and leaves out details that are necessary for the self-consistency of single models (e.g. the mass generation for mediator particles), it is a starting point to prepare a set of distinct but yet complementary collider searches for Dark Matter, as it leads to benchmarks that are easily comparable across channels.

2

Recommended models for all $\not{E}_T$ +X analyses

This chapter of the report is dedicated to simplified models that produced, primarily, monojet signatures. Details of the implementation of these models in Monte Carlo generators is provided in Appendix A.

2.1 Vector and axial vector mediator, $s-$channel exchange

A simple extension of the Standard Model (SM) is an additional $U(1)$ gauge symmetry, where a dark matter (DM) candidate particle has charges only under this new group. Assuming that some SM particles are also charged under this group, then a new gauge boson can mediate interactions between the SM and DM.

We consider the case of a DM particle that is a Dirac fermion and where the production proceeds via the exchange of a spin-1 mediator in the $s-$channel, illustrated in Fig. 2.1.

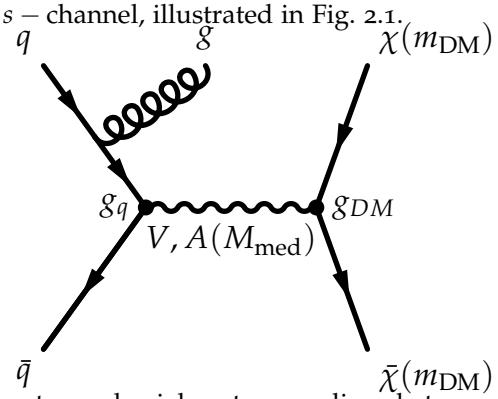

Figure 2.1: Representative Feynman diagram showing the pair production of dark matter particles in association with a parton from the initial state via a vector or axial-vector mediator. The cross section and kinematics depend upon the mediator and dark matter masses, and the mediator couplings to dark matter and quarks respectively: $(M_{\mathrm{med}}, m_{\mathrm{DM}}, g_{\mathrm{DM}}, g_{\mathrm{q}})$.

We consider vector and axial-vector couplings between the spin-1 mediator and SM and DM fields, with the corresponding interaction Lagrangians:

$$\mathcal{L}_{\mathrm{vector}} = g_{\mathrm{q}} \sum_{q=udscbt} Z'_\mu \bar{q}\gamma^\mu q + g_{\mathrm{DM}} Z'_\mu \bar{\chi}\gamma^\mu \chi \tag{2.1}$$

$$\mathcal{L}_{\mathrm{axial-vector}} = g_{\mathrm{q}} \sum_{q=udscbt} Z'_\mu \bar{q}\gamma^\mu\gamma^5 q + g_{\mathrm{DM}} Z'_\mu \bar{\chi}\gamma^\mu\gamma^5 \chi. \tag{2.2}$$

The coupling g_{q} is assumed to be universal to all quarks. It is also possible to consider another model in which mixed vector and axial-vector couplings are considered, for instance the couplings to the quarks are vector whereas those to DM are axial-vector. We recommend the models with pure vector couplings or pure axial vector couplings.

To do **Studies have been performed to see if the case of a mixed coupling can be simply extracted from the other models by some reweighting procedure to take account of the difference in cross section. This would assume that the difference between the pure and mixed couplings case does not affect the kinematics of the**

When no additional visible or invisible decays contribute to the width of the mediator, the width is fixed by the choices of couplings g_q and g_{DM}. We refer to the width in this situation as the minimal width[1]. For the vector and axial-vector models,

[1] See page 25 for a discussion of the effect of larger widths.

$$\Gamma^{V/A}_{\text{min}} = \Gamma^{V/A}_{\bar{\chi}\chi} + \sum_q \Gamma^{V/A}_{\bar{q}q}. \tag{2.3}$$

The leading order expressions for the partial widths are:

$$\Gamma^{V}_{\bar{\chi}\chi} = \frac{g^2_{DM} M_{med}}{12\pi}\left(1+\frac{2m^2_{DM}}{M^2_{med}}\right)\beta_{DM}\theta(M_{med}-2m_{DM}) \tag{2.4}$$

$$\Gamma^{V}_{\bar{q}q} = \frac{3g^2_{q} M_{med}}{12\pi}\left(1+\frac{2m^2_{q}}{M^2_{med}}\right)\beta_{q}\theta(M_{med}-2m_{q}) \tag{2.5}$$

$$\Gamma^{A}_{\bar{\chi}\chi} = \frac{g^2_{DM} M_{med}}{12\pi}\beta^{3/2}_{DM}\theta(M_{med}-2m_{DM}) \tag{2.6}$$

$$\Gamma^{A}_{\bar{q}q} = \frac{3g^2_{q} M_{med}}{12\pi}\beta^{3/2}_{q}\theta(M_{med}-2m_{q})\,, \tag{2.7}$$

$\theta(x)$ denotes the Heaviside step function, and $\beta_f = \sqrt{1-\frac{4m^2_f}{M^2_{med}}}$ is the velocity of the fermion f in the mediator rest frame. Note the color factor 3 in the quark terms. Figure 2.2 shows the minimal width as a function of mediator mass for both vector and axial-vector mediators assuming g_q =g_{DM} =1. With this choice of the couplings, the dominant contribution to the minimal width comes from the quarks due to the color factor enhancement and the large number of them.

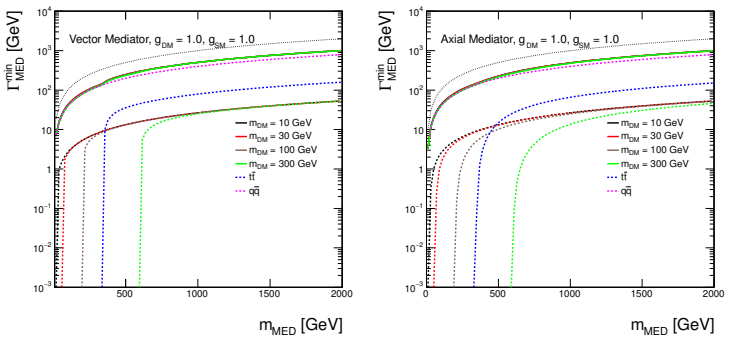

Figure 2.2: Minimal width as a function of mediator mass for vector and axial-vector mediator assuming couplings of 1. The total width is shown as solid lines for Dark Matter masses of 10 GeV, 30 GeV, 100 GeV and 300 GeV in black, red, brown and green, respectively. The individual contributions from Dark Matter are indicated by dotted lines with the same colors. The contribution from all quarks but top is shown as magenta dotted line and the contribution from top quarks only is illustrated by the dotted blue line. The dotted black line shows the extreme case $\Gamma_{\text{min}} = M_{\text{med}}$.

The simplified models described here have four free parameters: mediator mass M_{med}, Dark Matter mass m_{DM}, coupling of the mediator to quarks g_q and coupling of the mediator to Dark Matter g_{DM}. In order to determine an optimal choice of the parameter grid for presentation of the early Run-2 results, dependencies of the kinematic quantities and cross sections on the individual parameters need to be studied. The following paragraphs list the main observations from the scans over the parameters that support the final proposal for the parameter grid.

Scan over the couplings Figure 2.3 reveals there are no differences in the shape of the $\not{E}_T$ distribution among the samples where the pair of m_{DM} =10 GeV Dark Matter particles are produced on-shell from the mediator of M_{med} =1 TeV, generated with different choices of the coupling strength. This a generator-level prediction with no kinematic selections or detector simulation. Coupling values in the range 0.1–1.45, holding $g_{\mathrm{q}} = g_{\mathrm{DM}}$, correspond to a rough estimate of the lower sensitivity of mono-jet analyses and a maximum coupling value such that $\Gamma_{\mathrm{min}} < M_{\mathrm{med}}$. Based on similar plots for different choices of M_{med} and m_{DM}, we conclude that the shapes of kinematic distributions are not altered either for the on-shell Dark Matter production where $M_{\mathrm{med}} > 2m_{\mathrm{DM}}$, or for the off-shell Dark Matter production where $M_{\mathrm{med}} < 2m_{\mathrm{DM}}$. Only the cross sections change. Differences in kinematic distributions are expected only close to the transition region where both on-shell and off-shell decays occur.

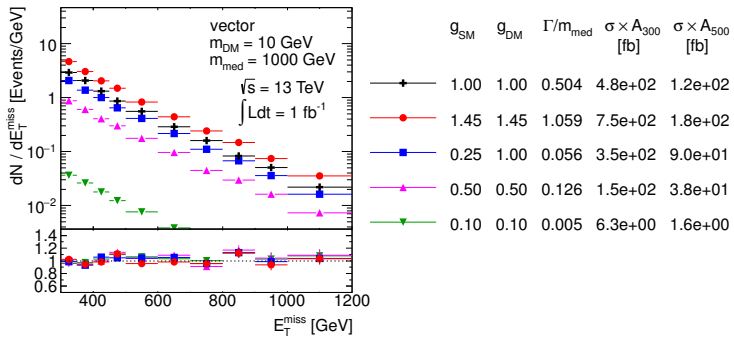

g_{SM}	g_{DM}	Γ/m_{med}	$\sigma \times A_{300}$ [fb]	$\sigma \times A_{500}$ [fb]
1.00	1.00	0.504	4.8e+02	1.2e+02
1.45	1.45	1.059	7.5e+02	1.8e+02
0.25	1.00	0.056	3.5e+02	9.0e+01
0.50	0.50	0.126	1.5e+02	3.8e+01
0.10	0.10	0.005	6.3e+00	1.6e+00

Figure 2.3: Scan over couplings. The $\not{E}_T$ distribution is compared for the vector mediator models using the parameters as indicated. Ratios of the normalized distributions with respect to the first one are shown. A_{300} and A_{500} in the table denote the acceptance of the $\not{E}_T > 300$ GeV and $\not{E}_T > 500$ GeV cut, respectively.

One situation requiring a careful consideration is the case of extremely heavy and narrow mediators, which can arise for small coupling strengths. Upon close examination, it was determined that this case is not peculiar. However, the complete story is a cautionary tale about understanding the details of the generator tools. Figure 2.4 suggests a change in the shape of the $\not{E}_T$ distribution for a M_{med} =5 TeV mediator once $\Gamma_{\mathrm{min}}/M_{\mathrm{med}}$ is of the order of a percent or lower. This, however, does not come from physics, but is an artifact of the generator implementation, where a cutoff for the regions far away from the mediator mass is sometimes used. This is illustrated in Fig. 2.5 showing the invariant mass of the Dark Matter pair in the samples generated for a M_{med} =7 TeV mediator with different coupling strengths. In all cases, it is expected to observe a peak around the mediator mass with a tail extending to $m_{\bar{\chi}\chi} \to 0$, significantly enhanced by parton distribution functions at low Bjorken x. For coupling strength 1 and 3, the massive enhancement at $m_{\bar{\chi}\chi} \to 0$ implies that resonant production at $m_{\bar{\chi}\chi} = 7$ TeV is statistically suppressed such that barely any events are generated there. However, for narrower mediators with couplings below 1, the peak around 7 TeV is clearly visible in the generated sample and the dominant tail at $m_{\bar{\chi}\chi} \to 0$ is artificially cut off, leading to unphysical cross section predictions and kinematic shapes. This

explains why the sample with the narrowest mediator in Fig. 2.4 is heavily suppressed in terms of production cross section and also gives different $\not{E}_T$ shape. In general, for such extreme parameter choices the EFT model should give the correct answer.

To do **Refer to results of ongoing study in Section 6. (??)**

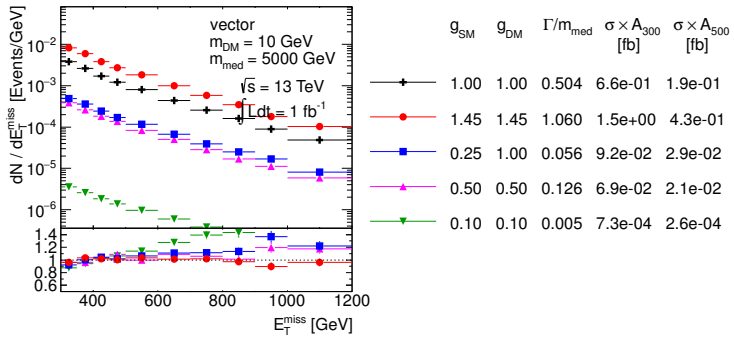

Figure 2.4: Scan over couplings. The $\not{E}_T$ distribution is compared for the vector mediator models using the parameters as indicated. Ratios of the normalized distributions with respect to the first one are shown. A_{300} and A_{500} in the table denote the acceptance of the $\not{E}_T > 300$ GeV and $\not{E}_T > 500$ GeV cut, respectively.

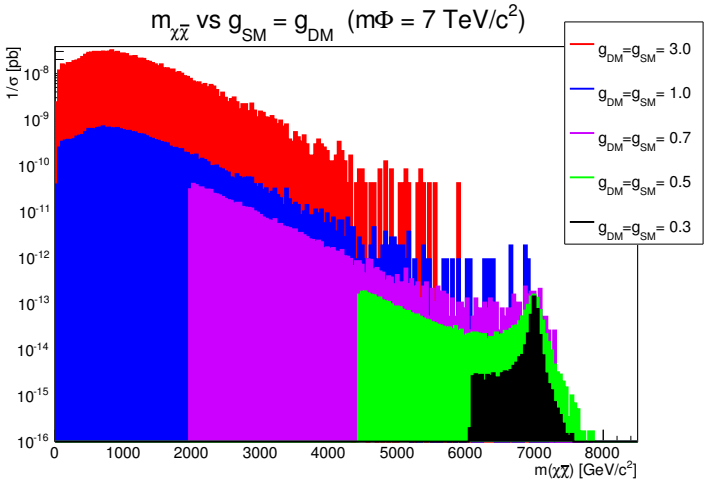

Figure 2.5: Invariant mass of the Dark Matter pair in the samples with $M_{\text{med}} = 7$ TeV and different coupling strengths.

The conclusion is that the choice $g_q = g_{DM}$ is a reasonable reduction in the parameter space since kinematic distributions are robust to changes in the specific values. There are no complications associated with small couplings, but, also, the early part of Run-1 will not be sensitive to them. We recommend a range of couplings that limit the calculated width of the mediator to be near or below M_{med}.

For direct mediator searches, asymmetric couplings ($g_q \neq g_{DM}$) might also be considered. For example, one might fix the mediator mass and produce a scan in g_{DM} vs g_q. Such searches, such as those for dijet and ttbar resonances, may restrict g_q to a greater degree than g_{DM}.

Scan over the Dark Matter mass For a fixed mediator mass M_{med} and couplings, both the cross section and the kinematic distributions remain similar for different Dark Matter masses as long as $M_{\text{med}} > 2m_{DM}$. This simply reflects the fact that most mediators are produced on-shell, and the details of the invisible decay are unimportant. This is illustrated in Fig. 2.6 for an example of M_{med} =1 TeV 10 GeV $< m_{DM} <$ 300 GeV. It is observed that the cross

section decreases as the m_{DM} approaches $M_{\mathrm{med}}/2$. Once the Dark Matter pair is produced off-shell, the cross section of the simplified model is suppressed and the $\not{E}_T$ spectrum hardens, as demonstrated with the choice of m_{DM} =1 TeV in the same plot. Figure 2.7 reveals the $\not{E}_T$ spectrum hardens further with increasing m_{DM}, accompanied by the gradual decrease of the cross section. From these observations one can conclude:

- A coarse binning along m_{DM} is sufficient at $M_{\mathrm{med}} \gg 2m_{\mathrm{DM}}$.
- Finer binning is needed in order to capture the changes in the cross section and kinematic quantities close to the production threshold on both sides around $M_{\mathrm{med}} = 2m_{\mathrm{DM}}$.
- Due to the significant cross section suppression of the off-shell Dark Matter pair production, it is not necessary to populate the parameter space $M_{\mathrm{med}} \ll 2m_{\mathrm{DM}}$ since the LHC is not going to be able to probe the models there.

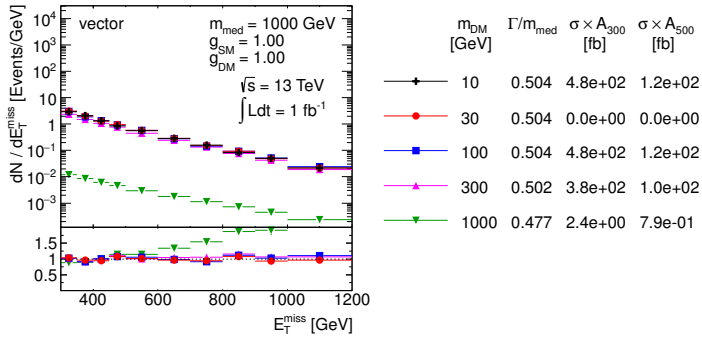

Figure 2.6: Scan over Dark Matter mass. The $\not{E}_T$ distribution is compared for the vector mediator models using the parameters as indicated. Ratios of the normalized distributions with respect to the first one are shown. A_{300} and A_{500} in the table denote the acceptance of the $\not{E}_T > 300$ GeV and $\not{E}_T > 500$ GeV cut, respectively.

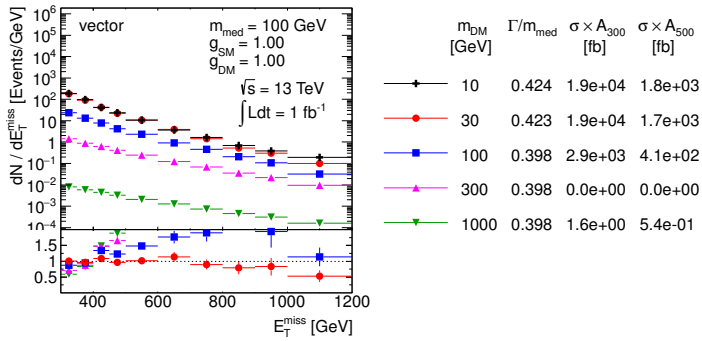

Figure 2.7: Scan over Dark Matter mass. The $\not{E}_T$ distribution is compared for the vector mediator models using the parameters as indicated. Ratios of the normalized distributions with respect to the first one are shown. A_{300} and A_{500} in the table denote the acceptance of the $\not{E}_T > 300$ GeV and $\not{E}_T > 500$ GeV cut, respectively.

Scan over the mediator mass Changing the mediator mass for fixed Dark Matter mass and couplings leads to significant differences in cross section and shapes of the kinematic variables for $M_{\mathrm{med}} > 2m_{\mathrm{DM}}$ as shown in Fig. 2.8. As expected, higher mediator masses lead to harder $\not{E}_T$ spectra. On the other hand, the $\not{E}_T$ shapes are similar in the off-shell Dark Matter production regime. This is illustrated in Fig. 2.9. Therefore, a coarse binning in m_{DM} is sufficient at $M_{\mathrm{med}} \ll 2m_{\mathrm{DM}}$.

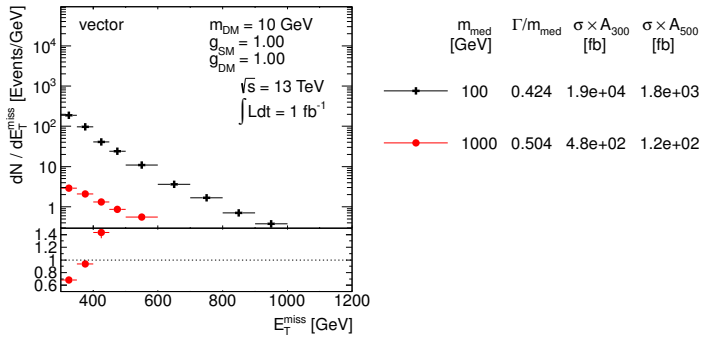

Figure 2.8: Scan over mediator mass. The $\not{E}_T$ distribution is compared for the vector mediator models using the parameters as indicated. Ratios of the normalized distributions with respect to the first one are shown. A_{300} and A_{500} in the table denote the acceptance of the $\not{E}_T > 300$ GeV and $\not{E}_T > 500$ GeV cut, respectively.

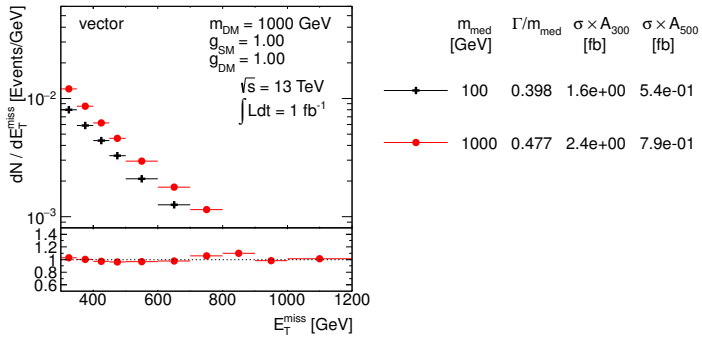

Figure 2.9: Scan over mediator mass. The $\not{E}_T$ distribution is compared for the vector mediator models using the parameters as indicated. Ratios of the normalized distributions with respect to the first one are shown. A_{300} and A_{500} in the table denote the acceptance of the $\not{E}_T > 300$ GeV and $\not{E}_T > 500$ GeV cut, respectively.

Proposed parameter grid The final step in proposing a parameter grid is to evaluate the sensitivity of Run-2 LHC data with respect to rate and/or kinematics. Projected sensitivities for a 14 TeV mono-jet analysis are available from ATLAS [ATL14]. The expected upper limit at 95% confidence level on the product of cross section, acceptance and efficiency, $\sigma \times A \times \epsilon$, in the final Run-1 ATLAS mono-jet analysis [A$^+$15b] is 51 fb and 7.2 fb for $\not{E}_T > 300$ GeV and $\not{E}_T > 500$ GeV, respectively. ATLAS estimates a factor of two increase in sensitivity with the 2015 data. Given that cross section for V+jets processes increases by roughly a factor 2 when going from $\sqrt{s} = 8$ TeV to 13 TeV, similar fiducial cross section limits can be expected with the first Run-2 data as from the final Run-1 analysis. The generator level cross section times the acceptance at $\not{E}_T > 500$ GeV for the model with couplings $g_q = g_{DM} = 1$, light Dark Matter of m_{DM} =10 GeV and a M_{med} =1 TeV vector mediator is at the order of 100 fb, i.e. the early Run-2 mono-jet analysis is going to be sensitive to heavier mediators than this. The value of $\sigma \times A$ at $\not{E}_T > 500$ GeV for 5 TeV vector mediator is at the order of 0.1 fb, therefore this model probably lies beyond the reach of the LHC.

To do **Can we get more precise number and a citation? Is this in Sarah's V+jets paper? (??)**

Based on these arguments, the following M_{med} grid points are chosen, roughly equidistant in the logarithmic scale: 10 GeV, 20 GeV, 50 GeV, 100 GeV, 200 GeV, 300 GeV, 500 GeV, 1000 GeV and 2000 GeV. Given the fact that significant changes in cross section happen around the $M_{med} = 2m_{DM}$ threshold, the m_{DM} grid points are taken at approximately $M_{med}/2$, namely: 10 GeV, 50 GeV, 150 GeV, 500 GeV and 1000 GeV. Points on the on-shell

diagonal are always chosen to be 5 GeV away from the threshold, to avoid numerical instabilities in the event generation. The detailed studies of the impact of the parameter changes on the cross section and kinematic distributions presented earlier in this section support removing some of the grid points and rely on interpolation. The optimized grids proposed for the vector and axial-vector mediators are given in Table. 2.1, containing 29 mass points each. One point at very high mediator mass (5 TeV) is added for each of the DM masses scanned, to aid the reinterpretation of results in terms of contact interaction operators (EFTs) as discussed in Section 5.4.

m_{DM} / GeV	M_{med} / GeV									
1	10	20	50	100	200	300	500	1000	2000	5000
10	10	15	50	100						
50	10		50	95	200	300				
150	10				200	295	500			
500	10						500	995	2000	
1000	10							1000	1995	5000

Table 2.1: Simplified model benchmarks for $s-$channel simplified models (spin-1 mediators decaying to Dirac DM fermions in the V and A case, taking the minimum width for $g_q = g_{DM} = 1$)

The presentation of the results in the g_q–g_{DM} plane for fixed masses benefits from cross section scaling and is discussed in Section 2.3.

2.2 *Scalar and pseudoscalar mediator, s − channel exchange*

One of the simplest UV complete extensions of the effective field theory approach is the addition of a scalar/pseudoscalar mediator between DM and SM. A gauge singlet mediator can have tree-level interactions with a singlet DM particle that is either a Dirac or Majorana fermion, or DM that is a scalar itself. The spin-0 mediator can either be a real or complex scalar; a complex scalar contains both scalar and pseudoscalar particles, whereas the real field only contains the scalar particle. See Refs. [BFG15] for a thorough discussion. In this document we consider only two of the possible choices for this simplified model: one where the interaction with the SM is mediated by a real scalar, and the second where we consider only a light pseudoscalar, assuming that the associated scalar is decoupled from the low-energy spectrum.

Couplings to the SM fermions can be arranged by mixing with the SM Higgs. Such models have interesting connections with Higgs physics, and can be viewed as generalizations of the Higgs portal to DM. The most general scalar mediator models will have renormalizable interactions between the SM Higgs and the new scalar ϕ or pseudoscalar a, as well as ϕ/a interactions with electroweak gauge bosons. Such interactions are model dependent, often subject to constraints from electroweak precision tests, and would suggest specialized searches which cannot be generalized to a broad class of models (unlike, for instance, the $\not{E}_T$ + jets searches). As a result, for this class of minimal simplified models with spin-0

mediators, we will focus primarily on couplings to fermions and loop-induced couplings to gluons.

Working under the assumption of Minimal Flavor Violation (MFV) implies scalar couplings to fermions are proportional to the fermion mass. However, the overall normalization constant of this coupling can differ for for up- and down-type quarks and charged leptons. Assuming that DM is a fermion χ that couples to the SM only through a scalar ϕ or pseudoscalar a, the most general tree-level Lagrangians compatible with the MFV assumption are [CRTW14, ADR+14]:

$$\mathcal{L}_\phi = g_\chi \phi \bar{\chi}\chi + \frac{\phi}{\sqrt{2}} \sum_i \left(g_u y_i^u \bar{u}_i u_i + g_d y_i^d \bar{d}_i d_i + g_\ell y_i^\ell \bar{\ell}_i \ell_i \right) , \quad (2.8)$$

$$\mathcal{L}_a = i g_\chi a \bar{\chi}\gamma_5\chi + \frac{ia}{\sqrt{2}} \sum_i \left(g_u y_i^u \bar{u}_i \gamma_5 u_i + g_d y_i^d \bar{d}_i \gamma_5 d_i + g_\ell y_i^\ell \bar{\ell}_i \gamma_5 \ell_i \right) . \quad (2.9)$$

Here, the sums run over the all SM generations; the Yukawa couplings y_i^f are normalized to $y_i^f = \sqrt{2} m_i^f / v$ where $v \simeq 246$ GeV represents the Higgs vacuum expectation value (VEV). While the couplings g_u, g_d, g_ℓ to SM fermions are factors multiplying the SM Yukawa structure, we parametrise the DM-mediator coupling as g_χ, without any additional Yukawa structure between the mediator and the dark sector.

As already stated we only choose a minimal set of interactions that do not include interactions with the SM Higgs field. For simplicity and ease of comparison, we assume universal SM-mediator couplings $g_v \equiv g_u = g_d = g_\ell$ in the remainder of this work. This allows the relative discovery and exclusion power of each search to be directly compared, though again we emphasize the importance of multiple search channels, not an exclusive focus on the single, most powerful channel under the assumption of universal couplings.

Given these simplifications, the minimal set of parameters under consideration is

$$\left\{ m_\chi,\ m_{\phi/a},\ g_\chi,\ g_v \right\} . \quad (2.10)$$

Despite our simplifying assumption, one should keep the more general possibility in mind, as even simple extensions of the mediating sector can result in $g_u \neq g_d \neq g_\ell$. A well-known realization of this would be the coupling of the pseudoscalar to up-type quarks (proportional to $m_u \cot\beta$) and down-type quarks and charged leptons (proportional to $m_{d/\ell} \tan\beta$) in two-Higgs doublet extensions of the SM. Here $\tan\beta$ denoting the ratio of VEVs of the two Higgs doublets. This possibility of non-equal couplings motivates searches in complementary channels which probe couplings to different flavors of quarks and leptons.

We choose the minimal mediator width given by

$$\Gamma_{\phi,a} = \sum_f N_c \frac{y_f^2 g_v^2 m_{\phi,a}}{16\pi}\left(1-\frac{4m_f^2}{m_{\phi,a}^2}\right)^{x/2} + \frac{g_\chi^2 m_{\phi,a}}{8\pi}\left(1-\frac{4m_\chi^2}{m_{\phi,a}^2}\right)^{x/2} + \frac{\alpha_s^2 y_t^2 g_v^2 m_{\phi,a}^3}{32\pi^3 v^2}\left|f_{\phi,a}\left(\frac{4m_t^2}{m_{\phi,a}^2}\right)\right|^2 \tag{2.11}$$

where $x = 3$ for scalars and $x = 1$ for pseudoscalars, and the loop integrals are

$$f_\phi(\tau) = \tau\left[1+(1-\tau)\arctan^2\left(\frac{1}{\sqrt{\tau-1}}\right)\right], \qquad f_a(\tau) = \tau\arctan^2\left(\frac{1}{\sqrt{\tau-1}}\right) \tag{2.12}$$

for $\tau < 1$ and

$$f_\phi(\tau) = \tau\left[1+(1-\tau)\left(-\frac{1}{4}\left(\log\frac{1+\sqrt{1-\tau}}{1-\sqrt{1-\tau}}+i\pi\right)^2\right)\right], f_a(\tau) = \tau\left(-\frac{1}{4}\left(\log\frac{1+\sqrt{1-\tau}}{1-\sqrt{1-\tau}}+i\pi\right)^2\right) \tag{2.13}$$

for $\tau > 1$, where $\tau = 4m_t^2/m_{\phi,a}^2$.

The first term in the width corresponds to the decay into SM fermions, and the sum runs over all kinematically available fermions, $N_c = 3$ for quarks. The second term is the decay into DM, assuming that is kinematically allowed. The factor of two between the decay into SM fermions and into DM is a result of our choice of normalization of the Yukawa couplings due to spin dependencies. The last two terms correspond to decay into gluons. Since we have assumed that $g_q = g_u = g_d = g_\ell$, we have included in the partial decay widths $\Gamma(\phi/a \to gg)$ only the contributions stemming from top loops, which provide the by far largest corrections given that $y_t \gg y_b$ etc. At the loop level the mediators can decay not only to gluons but also to pairs of photons and other final states if kinematical accessible. However the decay rates $\Gamma(\phi/a \to gg)$ are always larger than the other loop-induced partial widths, and in consequence the total decay widths $\Gamma_{\phi/a}$ are well approximated by the corresponding sum of the individual partial decay widths involving DM, fermion or gluon pairs. It should be noted that if $m_{\phi/a} > 2m_t$ the total widths of ϕ/a will typically be dominated by the partial widths to top quarks.

The minimal width for scalar and pseudo-scalar mediators with $g_q = g_{DM} = 1$ are shown in Fig. 2.10, illustrating the effect of choosing the SM Higgs-like Yukawa couplings for the SM fermions. For the mediator mass above twice the top quark mass m_t, the minimal width receives the dominant contribution from the top quark. For lighter mediator masses, Dark Matter dominates as the couplings to lighter quarks are Yukawa suppressed.

Similarly as in the case of the vector and axial-vector couplings of spin-1 mediators, scans in the parameter space are performed also for the scalar and pseudo-scalar couplings of the spin-0 mediators in order to decide on the optimized parameter grid for the

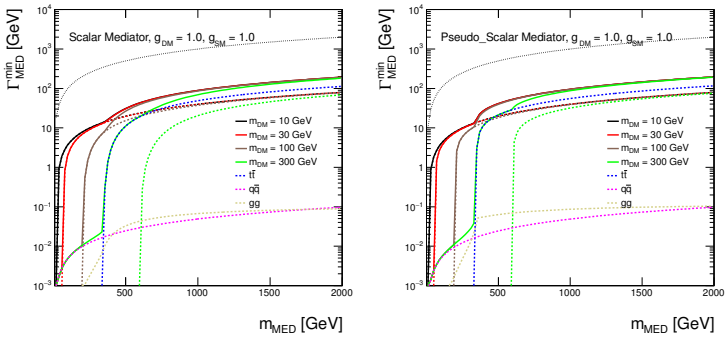

Figure 2.10: Minimal width as a function of mediator mass for scalar and pseudo-scalar mediator assuming couplings of 1. The total width is shown as solid lines for Dark Matter masses of m_{DM} =10 GeV, 30 GeV, 100 GeV and 300 GeV in black, red, brown and green, respectively. The individual contributions from Dark Matter are indicated by dotted lines with the same colors. The contribution from all quarks but top is shown as magenta dotted line and the contribution from top quarks only is illustrated by the dotted blue line. The dotted beige line shows the contribution fron the coupling to gluons. The dotted black line shows the extreme case $\Gamma_{\mathrm{min}} = M_{\mathrm{med}}$.

presentation of Run-2 results. Figures 2.11- 2.15 show the scans over the couplings, Dark Matter mass and mediator mass and the same conclusions apply as in Section 2.1.

Since the top quark gives the dominant contribution to the mediator width due to SM Higgs-like Yukawa couplings, the effect of the kinematic threshold at $M_{\mathrm{med}} = 2m_t$ was studied in detail. A scan over the mediator mass is shown in Fig. 2.15 where M_{med} = 300 GeV and 500 GeV are chosen to be below and above $2m_t$. The off-shell Dark Matter production regime is assumed by taking $m_{\mathrm{DM}} = 1$ TeV in order to study solely the effects of the couplings to quarks. No differences in the kinematic distributions are observed and also the cross sections remain similar in this case. Therefore, it is concluded that no significant changes appear for mediator masses around the $2m_t$ threshold.

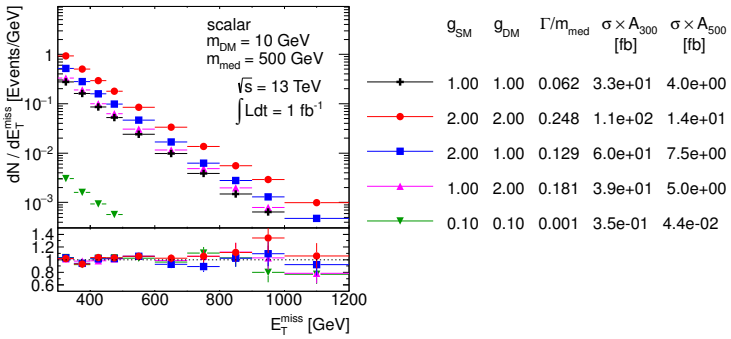

g_{SM}	g_{DM}	Γ/m_{med}	$\sigma \times A_{300}$ [fb]	$\sigma \times A_{500}$ [fb]
1.00	1.00	0.062	3.3e+01	4.0e+00
2.00	2.00	0.248	1.1e+02	1.4e+01
2.00	1.00	0.129	6.0e+01	7.5e+00
1.00	2.00	0.181	3.9e+01	5.0e+00
0.10	0.10	0.001	3.5e-01	4.4e-02

Figure 2.11: Scan over couplings. The $\not{E}_T$ distribution is compared for the scalar mediator models using the parameters as indicated. Ratios of the normalized distributions with respect to the first one are shown. A_{300} and A_{500} in the table denote the acceptance of the $\not{E}_T > 300$ GeV and $\not{E}_T > 500$ GeV cut, respectively.

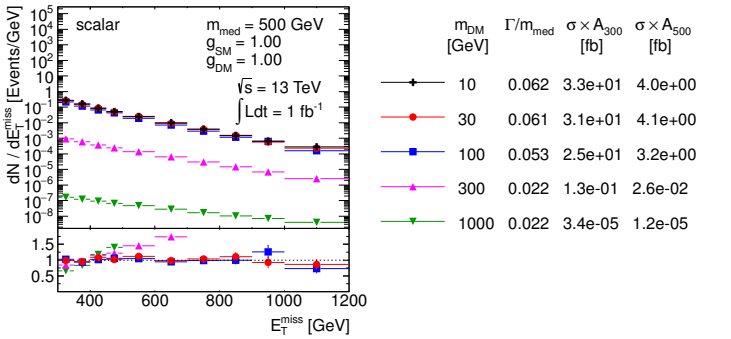

m_{DM} [GeV]	Γ/m_{med}	$\sigma \times A_{300}$ [fb]	$\sigma \times A_{500}$ [fb]
10	0.062	3.3e+01	4.0e+00
30	0.061	3.1e+01	4.1e+00
100	0.053	2.5e+01	3.2e+00
300	0.022	1.3e-01	2.6e-02
1000	0.022	3.4e-05	1.2e-05

Figure 2.12: Scan over Dark Matter mass. The $\not{E}_T$ distribution is compared for the scalar mediator models using the parameters as indicated. Ratios of the normalized distributions with respect to the first one are shown. A_{300} and A_{500} in the table denote the acceptance of the $\not{E}_T > 300$ GeV and $\not{E}_T > 500$ GeV cut, respectively.

The optimized parameter grid in the M_{med}–m_{DM} plane for scalar and pseudo-scalar mediators is motivated by similar arguments

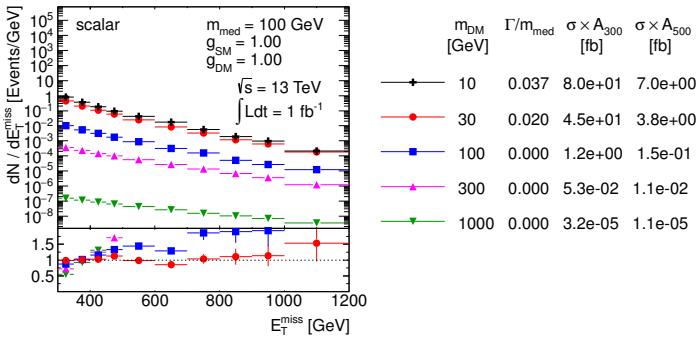

m_{DM} [GeV]	Γ/m_{med}	$\sigma \times A_{300}$ [fb]	$\sigma \times A_{500}$ [fb]
10	0.037	8.0e+01	7.0e+00
30	0.020	4.5e+01	3.8e+00
100	0.000	1.2e+00	1.5e-01
300	0.000	5.3e-02	1.1e-02
1000	0.000	3.2e-05	1.1e-05

Figure 2.13: Scan over Dark Matter mass. The $\not{E}_T$ distribution is compared for the scalar mediator models using the parameters as indicated. Ratios of the normalized distributions with respect to the first one are shown. A_{300} and A_{500} in the table denote the acceptance of the $\not{E}_T > 300$ GeV and $\not{E}_T > 500$ GeV cut, respectively.

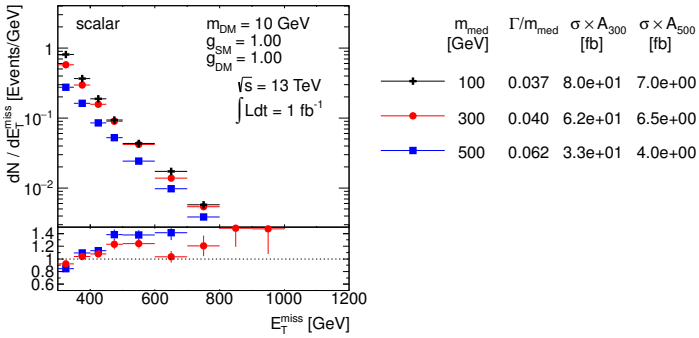

m_{med} [GeV]	Γ/m_{med}	$\sigma \times A_{300}$ [fb]	$\sigma \times A_{500}$ [fb]
100	0.037	8.0e+01	7.0e+00
300	0.040	6.2e+01	6.5e+00
500	0.062	3.3e+01	4.0e+00

Figure 2.14: Scan over mediator mass. The $\not{E}_T$ distribution is compared for the scalar mediator models using the parameters as indicated. Ratios of the normalized distributions with respect to the first one are shown. A_{300} and A_{500} in the table denote the acceptance of the $\not{E}_T > 300$ GeV and $\not{E}_T > 500$ GeV cut, respectively.

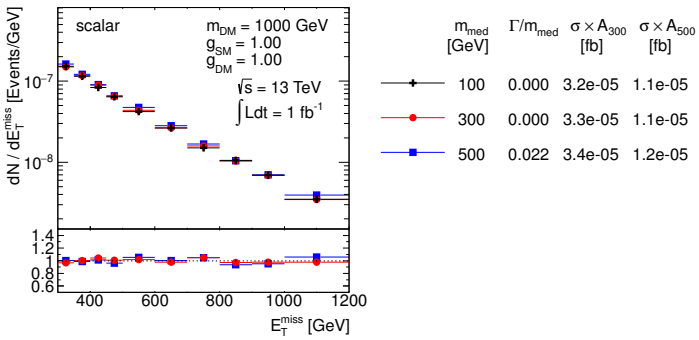

m_{med} [GeV]	Γ/m_{med}	$\sigma \times A_{300}$ [fb]	$\sigma \times A_{500}$ [fb]
100	0.000	3.2e-05	1.1e-05
300	0.000	3.3e-05	1.1e-05
500	0.022	3.4e-05	1.2e-05

Figure 2.15: Scan over mediator mass. The $\not{E}_T$ distribution is compared for the scalar mediator models using the parameters as indicated. Ratios of the normalized distributions with respect to the first one are shown. A_{300} and A_{500} in the table denote the acceptance of the $\not{E}_T > 300$ GeV and $\not{E}_T > 500$ GeV cut, respectively.

as in the previous section. Therefore, a similar pattern is followed here, taking again $g_q = g_{DM} = 1$. Only the sensitivity to the highest mediator masses has to be revisited. The generator level cross section times the acceptance at $\not{E}_T > 500$ GeV for the model with couplings $g_q = g_{DM} = 1$, light Dark Matter of m_{DM} =10 GeV and a M_{med} =500 GeV scalar mediator is at the order of 10 fb, i.e. just at the edge of the early Run-2 sensitivity. Increasing the mediator mass to 1 TeV pushes the product $\sigma \times A$ down to approximately 0.1 fb, below the LHC sensitivity. Therefore, we choose to remove the 2 TeV mediator mass from the grid and present the final grid with 26 mass points only in Fig. 2.2. One point at very high mediator mass (5 TeV) is added for each of the DM masses scanned, to aid the reinterpretation of results in terms of contact interaction operators (EFTs).

m_{DM} (GeV)	M_{med} (GeV)								
1	10	20	50	100	200	300	500	1000	5000
10	10	15	50	100					5000
50	10		50	95	200	300			5000
150	10				200	295	500		5000
500	10						500	995	5000
1000	10							1000	5000

Table 2.2: Simplified model benchmarks for $s-$channel simplified models (spin-0 mediators decaying to Dirac DM fermions in the scalar and pseudoscalar case, taking the minimum width for $g_q = g_{DM} = 1$)

The proposal for the scan in the g_q–g_{DM} plane is described in the following section.

2.3 *Cross section scaling*

The aim of the parameter grid optimization is to reduce the parameter space for simulation using neighboring grid points to populate the missing parts. Two ways of doing this are:

- Interpolation is used in-between the grid points that are close enough such that finer granularity is not needed for the presentation purposes, or between the points where smooth or no changes of the results are expected. The latter argument is exactly the one that motivates the reduction of the grid points in the M_{med}–m_{DM} plane.

- Recalculation of the results can be used when the dependencies with respect to the neighboring grid points are known.

The results of the scan over the couplings presented in the previous sections indicate there are no changes in kinematic distributions for different choices of the coupling strengths. This means that the acceptance remains the same in the whole g_q–g_{DM} plane and it is sufficient to perform the detector simulation only for one single choice of g_q, g_{DM}. The resulting truth-level selection acceptance and the detector reconstruction efficiency can then be applied to all remaining grid points in the g_q–g_{DM} plane where only the

generator-level cross section needs to be known. This significantly reduces the computing time as the detector response is by far the most expensive part of the Monte Carlo sample production. However, the number of generated samples can be reduced even further if a parameterization of the cross section dependence from one grid point to another exists.

Let us now elaborate on a cross section scaling procedure. The propagator on the $s-$channel exchange is written in a Breit-Wigner form as $\frac{1}{q^2-M_{\text{med}}^2+iM_{\text{med}}\Gamma}$, where q is the momentum transfer calculated from the two partons entering the hard process after the initial state radiation, which is equivalent to the invariant mass of the Dark Matter pair. The size of the momentum transfer with respect to the mediator mass allows to classify the production in the following way:

To do **This procedure needs a clarification: this can work only for fixed masses (??)**

- off-shell production when $q^2 \gg M_{\text{med}}$ leading to suppressed cross sections,
- on-shell production when $q^2 \sim M_{\text{med}}$ leading to enhanced cross sections,
- effective field theory (EFT) limit when $q^2 \ll M_{\text{med}}$.

All three categories can be distinguished in Fig. 2.16 showing the upper limit on the interaction scale $M^* \equiv M_{\text{med}}/\sqrt{g_q g_{\text{DM}}}$ for vector mediator. In the case of the off-shell production and the EFT limit, the first term in the propagator dominates which reduces the dependence on the mediator width. Therefore, in these cases one can approximate the cross section as

$$\sigma \propto g_q^2 g_{\text{DM}}^2. \tag{2.14}$$

The on-shell production regime is the most interesting one as it gives the best chances for a discovery at the LHC given the cross section enhancement. The propagator term with the width cannot be neglected in this case and, in the narrow width approximation which requires $\Gamma \ll M_{\text{med}}$, one can integrate

$$\int \frac{ds}{(s-M_{\text{med}}^2)^2 + M_{\text{med}}^2\Gamma^2} = \frac{\pi}{M_{\text{med}}\Gamma} \tag{2.15}$$

which further implies the cross section scaling

$$\sigma \propto \frac{g_q^2 g_{\text{DM}}^2}{\Gamma}. \tag{2.16}$$

The narrow with approximation is important here as it ensures an integration over parton distribution functions (PDFs) can be neglected. In other words, it is assumed the integrand in Eq. 2.15 is non-zero only for a small region of s, such that the PDFs can be taken to be constant in this range. Since $\Gamma \sim g_q^2 + g_{\text{DM}}^2$, one can

simplify this rule in the extreme cases as follows

$$\sigma \propto \frac{g_q^2 g_{DM}^2}{g_q^2 + g_{DM}^2} \xrightarrow{g_q \ll g_{DM}} g_q^2 \tag{2.17}$$

$$\sigma \propto \frac{g_q^2 g_{DM}^2}{g_q^2 + g_{DM}^2} \xrightarrow{g_q \gg g_{DM}} g_{DM}^2 \,. \tag{2.18}$$

However, it is important to keep in mind that there is no simple scaling rule for how the cross section changes with the Dark Matter mass and the mediator mass, or for mediators with a large width, because PDFs matter in such cases as well. Therefore, the scaling procedure outlined above is expected to work only for fixed masses and fixed mediator width, assuming the narrow width approximation applies.

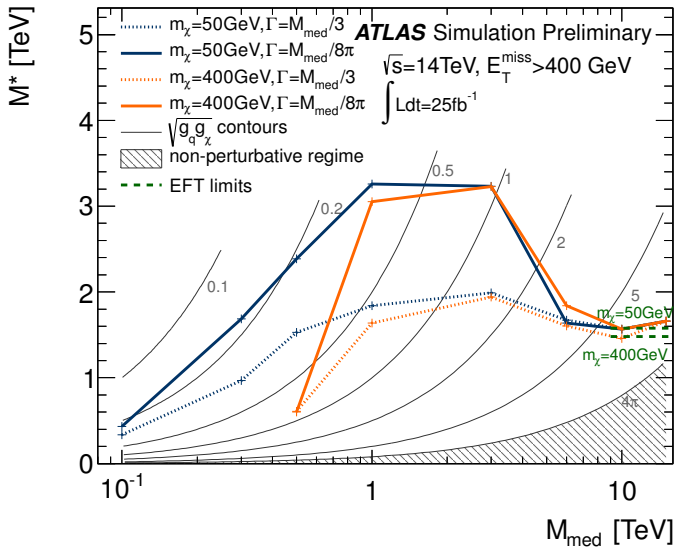

Figure 2.16: Comparison of the 95% CL lower limits on the scale of the interaction of a Z'-like simplified model at 14 TeV, in terms of the mediator mass. Corresponding limits from EFT models are shown on the same plot as green dashed lines to show equivalence between the two models for high mediator masses. Taken from Ref. [ATL14].

To do **Indicate mMed=GammaMin in the plots (gDM = 6, gSM = 1.5 for V and gSM = gDM = 5 for S) (??)**

Figures 2.17 and 2.18 show the minimal width in the g_q–g_{DM} plane for all vector, axial-vector, scalar and pseudo-scalar mediators for $M_{med} = 100$ GeV and 1000 GeV, respectively, taking $m_{DM} = 10$ GeV. The individual colors indicate the lines of constant width along which the cross section scaling works. For vector and axial-vector mediators, the minimal width is predominantly defined by g_q due to the number of quark flavors and the color factor. On the contrary, both the Standard Model and Dark Matter partial width have comparable contributions in case of scalar and pseudo-scalar mediators if the top quark channel is open ($M_{med} > 2m_t$). However, mostly g_{DM} defines the minimal width for $M_{med} < 2m_t$ due to the Yukawa-suppressed light quark couplings.

The performance of the cross section scaling is demonstrated in Fig. 2.19 where two mass points $M_{med} = 100$ GeV and 1 TeV with $m_{DM} = 10$ GeV are chosen and rescaled from the starting point $g_q = g_{DM} = 1$ according to Eq. 2.16 to populate the whole g_q–g_{DM} plane. This means the width is not kept constant in this test and this is done in purpose in order to point out deviations from the

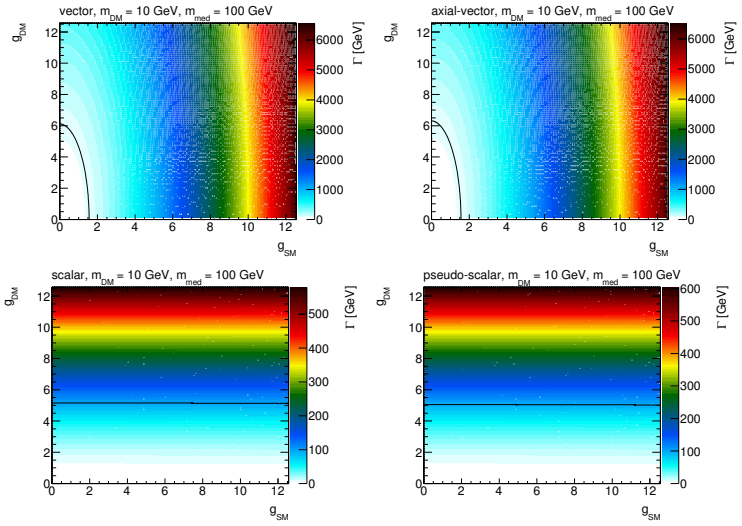

Figure 2.17: Minimal width for vector, axial-vector, scalar and pseudo-scalar mediators as a function of the individual couplings g_q and g_{DM}, assuming $M_{med} = 100$ GeV and $m_{DM} = 10$ GeV. The limiting case $\Gamma_{min} = M_{med}$ is indicated by the black line.

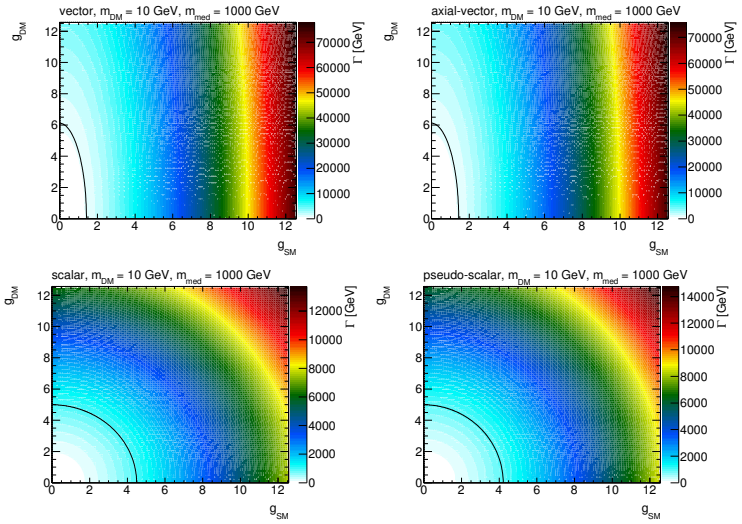

Figure 2.18: Minimal width for vector, axial-vector, scalar and pseudo-scalar mediators as a function of the individual couplings g_q and g_{DM}, assuming $M_{med} = 1$ TeV and $m_{DM} = 10$ GeV. The limiting case $\Gamma_{min} = M_{med}$ is indicated by the black line.

scaling when the width is altered. For each mass point, the rescaled cross section is compared to the generator cross section and the ratio of the two is plotted. For the given choice of the mass points, the scaling seems to work approximately with the precision of $\sim 20\%$ in the region where $\Gamma_{\text{min}} < M_{\text{med}}$. Constant colors indicate the lines along which the cross section scaling works precisely and there is a remarkable resemblance of the patterns shown in the plots of the mediator width. To prove the scaling along the lines of constant width works, one such line is chosen in Fig. 2.20 for a scalar mediator, defined by $M_{\text{med}} = 300$ GeV, $m_{\text{DM}} = 100$ GeV, $g_{\text{q}} = g_{\text{DM}} = 1$, and the rescaled and generated cross sections are found to agree within 3%.

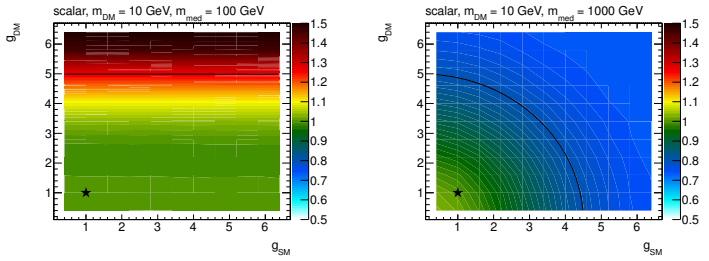

Figure 2.19: Ratio of the rescaled and generated cross sections in the g_{q}–g_{DM} plane. The point at $g_{\text{q}} = g_{\text{DM}} = 1$, taken as a reference for the rescaling, is denoted by a star symbol. Scalar model with $M_{\text{med}} = 100$ GeV (left) and 1 TeV (right) is plotted for $m_{\text{DM}} = 10$ GeV. The limiting case $\Gamma_{\text{min}} = M_{\text{med}}$ is shown as a black line.

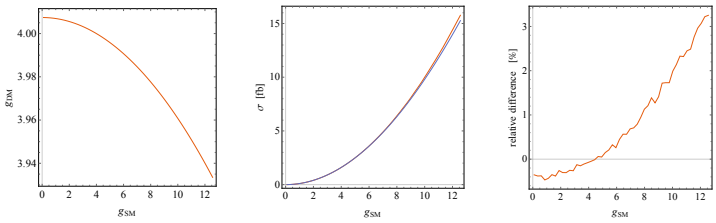

Figure 2.20: Scaling along the lines of constant width. The line of constant width for $M_{\text{med}} = 300$ GeV and $m_{\text{DM}} = 100$ GeV, intercepting $g_{\text{q}} = g_{\text{DM}} = 4$ is shown on left. The generated and rescaled cross sections are compared in the middle, the corresponding ratio is shown on right.

Proposed parameter grid We propose to present the results in the g_{q}–g_{DM} plane using the following prescription:

- Since the shapes of kinematic quantities do not change for different couplings, use the acceptance and efficiency for the available $m_{\text{DM}} = 50$ GeV, $M_{\text{med}} = 300$ GeV, $g_{\text{q}} = g_{\text{DM}} = 1$ grid point from the M_{med}–m_{DM} plane for the scalar and pseudo-scalar mediator. In case of the vector and axial-vector mediator, use the grid point $m_{\text{DM}} = 50$ GeV, $M_{\text{med}} = 1$ TeV, $g_{\text{q}} = g_{\text{DM}} = 1$.

- Generate additional samples in order to get generator cross sections only. For scalar and pseudo-scalar mediator, choose $m_{\text{DM}} = 50$ GeV, $M_{\text{med}} = 300$ GeV with the following values for $g_{\text{q}} = g_{\text{DM}}$: 0.1, 2, 3, 4, 5, 6. For vector and axial vector mediator, choose $m_{\text{DM}} = 50$ GeV, $M_{\text{med}} = 1$ TeV with the following values for $g_{\text{q}} = g_{\text{DM}}$: 0.1, 0.25, 0.5, 0.75, 1.25, 1.5. The upper values are defined by the minimal width reaching the mediator mass.

- Rescale the generator cross sections along the lines of constant width in order to populate the whole g_{q}–g_{DM} plane.

To do **We may agree on a smaller set of coupling values to get the cross-sections (those samples are not fully simulated anyway, and maybe the Forum can provide this information centrally.). (??)**

Rescaling to different mediator width In general there may be an interest to consider larger mediator masses than Γ_{min} in order to accommodate further couplings of the mediator. The cross section scaling method described above can be used to reinterpret the results presented for the minimal width, since multiplying the width by factor n is equivalent to changing the coupling strength by factor $\sqrt{n}$, i.e.

$$\sigma(g_q, g_{DM}, n\Gamma_{\text{min}}(g_q, g_{DM})) \propto \frac{g_q^2 g_{DM}^2}{\Gamma_{\text{min}}(\sqrt{n}g_q, \sqrt{n}g_{DM})} . \tag{2.19}$$

The cross section for the sample with couplings g_q and g_{DM} and modified mediator width $\Gamma = n\Gamma_{\text{min}}$ can therefore be rescaled from a sample generated with the minimal width corresponding to the couplings scaled by $\sqrt{n}$ as described in the following formula.

$$\sigma(g_q, g_{DM}, n\Gamma_{\text{min}}(g_q, g_{DM})) = \frac{1}{n^2}\sigma(\sqrt{n}g_q, \sqrt{n}g_{DM}, \Gamma_{\text{min}}(\sqrt{n}g_q, \sqrt{n}g_{DM})) \tag{2.20}$$

Here, it is again assumed the narrow width approximation applies. The advantage of doing this is in the fact that no event selection and detector response needs to be simulated since the changes in couplings do not have an effect on the shapes of kinematic distributions.

2.4 *Colored scalar mediator, $t-$channel exchange*

The preceding sections address models with a Dirac fermion coupled to the SM through exchange of a neutral spin-0 or spin-1 in an $s-$channel process. A $t-$channel process may couple the SM and DM directly, leading to a different phenomenology. Here, we examine a model where χ is a Standard Model (SM) singlet, a Dirac fermion[2]; the mediating particle, labeled ϕ, is charged and coloured; and the SM particle is a quark. Such models have been studied in Refs. [AWZ14b, PVZ14].

Following the example of Ref. [PVZ14], the interaction Lagrangian is written as

$$\mathcal{L}_{\text{int}} = g \sum_{i=1,2,3} (\phi_L^i \bar{Q}_L^i + \phi_{uR}^i \bar{u}_R^i + \phi_{dR}^i \bar{d}_R^i)\chi \tag{2.21}$$

where Q_L^i, u_R^i and d_R^i are the SM quarks and ϕ_L^i, ϕ_{uR}^i and ϕ_{dR}^i are the corresponding mediators, which (unlike the $s-$channel mediators) must be heavier than χ. These mediators have SM gauge representations under $(SU(3), SU(2))_Y$ of $(3,2)_{-1/6}$, $(3,1)_{2/3}$ and $(3,1)_{-1/3}$ respectively. Variations of the model previously studied include coupling to the left-handed quarks only [CEHL14, BDSJ+14], to the ϕ_{uR}^i [DNRT13] or ϕ_{dR}^i [PVZ14, A+14b], or some combination [BB13b, AWZ14a].

As for the $s-$channel models, we assume Minimal Flavour Violation (MFV), setting the mediator masses for each flavour; the

[2] Though outside the scope of this report, a colored vector $t-$channel mediator with vector dark matter may also be worthy of study. The UV completion of such models would look like an RS KK gluon,for example. In these case, it is expcted that the most interesting mediator masses will be of order several TeV.

To do **Note: [PVZ14] uses only i = 1,2, but I think it's fine to extend this to 3 here. (??)**

same logic also applies to the couplings g. The available parameters are then

$$\{m_{\mathrm{DM}},\, M_{\phi},\, g\}. \tag{2.22}$$

In practice, the third mediator mass and coupling could be separated from the other two, if higher order corrections to the MFV prediction arise due to the large top Yukawa coupling — a common variation is then to define this split between the first two generations and the third, so the parameters are extended to

$$\{m_{\mathrm{DM}},\, M_{\phi_{1,2}},\, M_{\phi_3},\, g_{1,2},\, g_3\}. \tag{2.23}$$

For the purposes of the rest of this section, we will assume the universal variant $M_{\phi_{1,2}} = M_{\phi_3}$, $g_{1,2} = g_3$.

The minimal width of each mediator is expressed, using the example of decay to an up quark, as

$$\begin{aligned}\Gamma(\phi_i \to \bar{u}_i \chi) = \frac{g_i^2}{16\pi M_{\phi_i}^3}(M_{\phi_i}^2 - m_{u_i}^2 - m_{\mathrm{DM}}^2) \\ \times \sqrt{(M_{\phi_i}^2 - (m_{u_i} + m_{\mathrm{DM}})^2)(M_{\phi_i}^2 - (m_{u_i} - m_{\mathrm{DM}})^2)}\,,\end{aligned} \tag{2.24}$$

which reduces to

$$\frac{g_i^2 M_{\phi_i}}{16\pi}\left(1 - \frac{m_{\mathrm{DM}}^2}{M_{\phi_i}^2}\right)^2 \tag{2.25}$$

in the limit $M_{\phi_i}, m_{\mathrm{DM}} \gg m_{u_i}$.

The leading-order processes involved in MET+jet production are shown in Fig. 2.21. Note that the generation index for ϕ is linked to the incoming fermion(s). Thus, mono-jet production via ϕ_u^3 is not possible at this order, while production through ϕ_d^3 is suppressed by the b parton PDF. This model can also give a signal in the di-jet + MET channel when, for example, the χ is exchanged in the $t-$channel and the resulting ϕ pair each decay to a jet + χ. Fig. 2.22 shows the leading order diagrams. Except for the gg induced process, di-jet production through ϕ_u^3 is not possible, and production through ϕ_d^3 is again suppressed. The diagram involving the $t-$channel exchange of χ is strongly dependent upon the Dirac fermion assumption. For a Majorana fermion, $q\bar{q}, \bar{q}\bar{q}$, and qq production would be possible with the latter having a pronounced enhancement at the LHC.

This model is similar to the MSSM with only light squarks and a neutralino, except for two distinct points: the χ is a Dirac fermion and the coupling g is not limited to be weak scale. In the MSSM, most of these processes are sub-dominant, even if resonantly enhanced, because the production is proportional to weak couplings.

In the more general theories considered here, g is free to take on large values of order 1 or more, and thus diagrams neglected in MSSM simulation can occur at a much higher rate here. While constraints from SUSY jets+MET analyses on these models should be translated to this model, LHC experiments should also test their sensitivity to them.

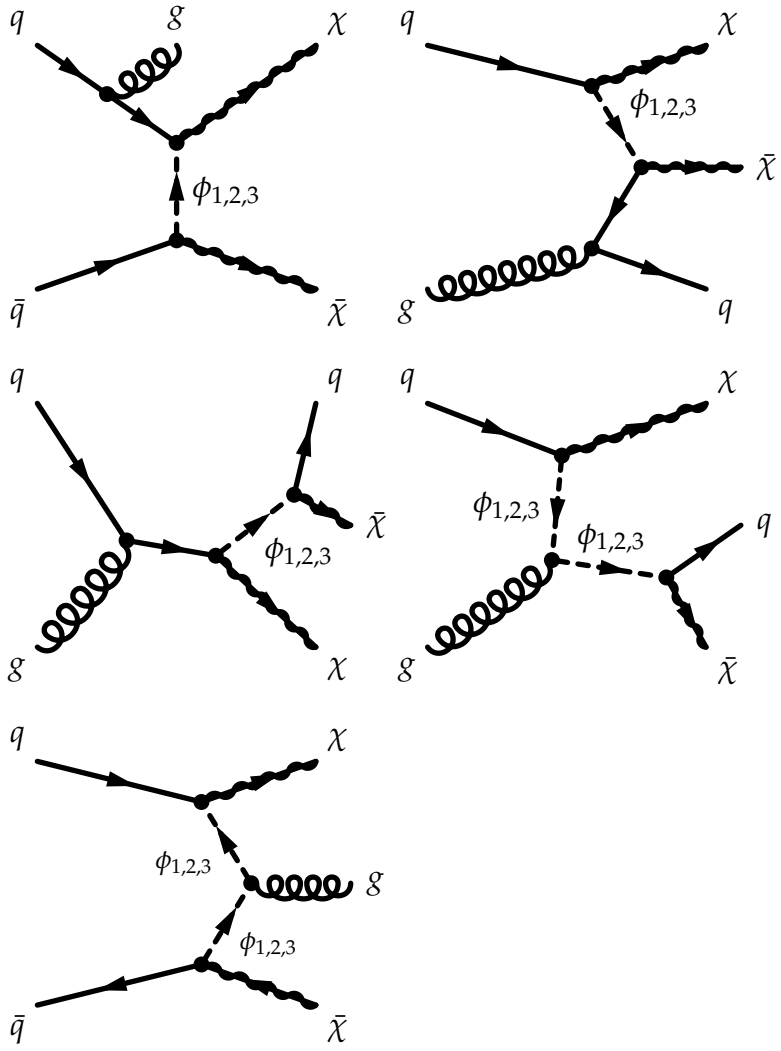

Figure 2.21: Leading order mono-jet $t-$channel processes, adapted from [PVZ14].

Parameter scans

Ref. [PVZ14] studies the parameter space and obtains bounds on this model from LHC Run 1 mono-jet and dijets+MET data.

As in the $s-$channel models, scans should be performed over m_{DM} and M_ϕ. The viable ranges of both parameters nearly coincide with the scan proposed for the $s-$channel; for simplicity we recommend adopting the $s-$channel mono-jet grid.

The rates of the first three diagrams of Fig. 2.21 scale as one with the coupling g. In the heavy mediator limit, then, the kinematic distributions depend only indirectly on the coupling through the effect on the minimal mediator width. In contrast with the $s-$channel case, however, the bounds one obtains from X+MET searches depends strongly on the width of the mediator, as is visible in Figs. 5 and 6 of Ref. [PVZ14], except in the heavy mediator

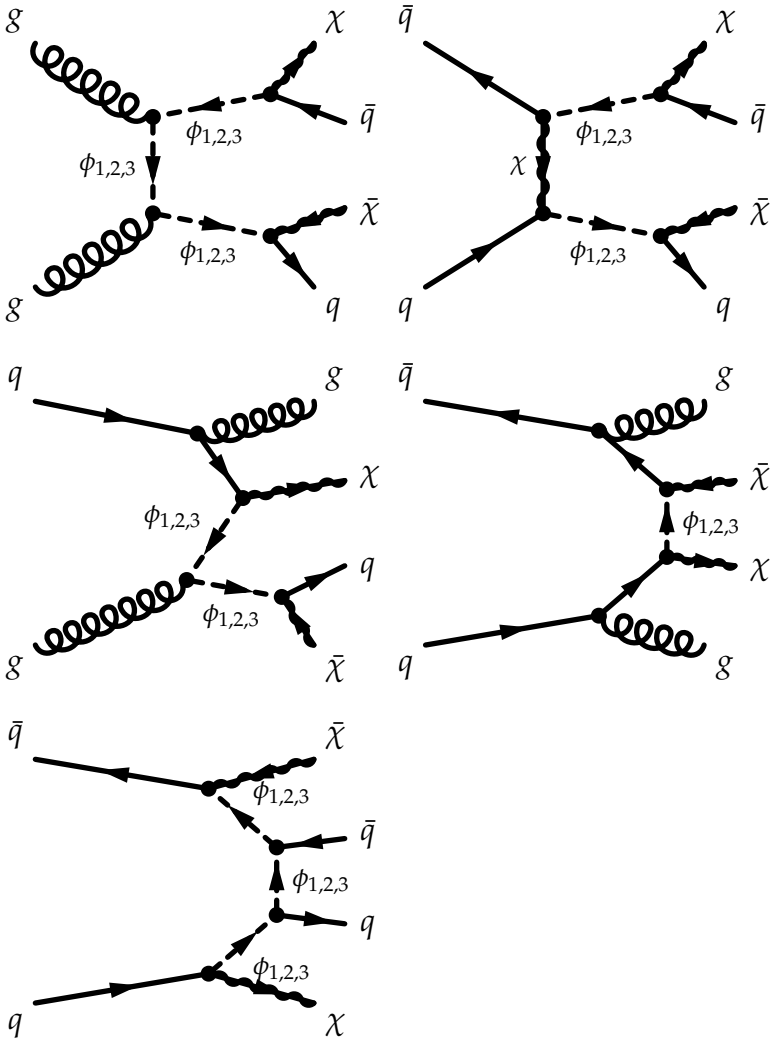

Figure 2.22: Leading order two-jet t – channel processes, adapted from [PVZ14].

limit ($M_\phi \approx 2\,\text{TeV}$). A scan over the width was not available for this report; thus we recommend scanning a range of possible widths as discussed in a more-limited way for the $s-$channel mono-jet, spanning from the minimal width to a value approaching the particle limit (for example, $\Gamma \approx M_\phi/3$ in Ref. [PVZ14]).

IMPLEMENTATION

The MadGraph implementation of the Ref. [PVZ14] is available from the Forum repository [For15g], following the matching and merging prescription described in its Section II and Appendix A.

2.5 *Spin-2 mediator*

In models with extra dimensions, the Kaluza-Klein excitations of the graviton could also serve as a mediator between the Standard Model and dark sector physics. Below a few TeV in mediator mass, production of a graviton with universal couplings is dominantly gluon-initiated, leading to forward-peaked angular distributions [AOP+02] distinct from the other models considered above. This kind of model was not studied in the forum and is not included in the recommendations, but it and models such as Ref. [LPS14] may warrant further study on a longer timescale.

3
Specific models for signatures with heavy flavor quarks

3.1 $t\bar{t}$+MET models

As described in Section 2.2, a model with a scalar/pseudoscalar particle mediating the DM-SM interactions is one of the simplest UV completions of our EFT models. With the MFV assumption, the top quark plays a primary role in the phenomenology. The model predicts not only the monojet process described earlier, but also production of dark matter in association with top pairs, as illustrated in Fig. 3.1.

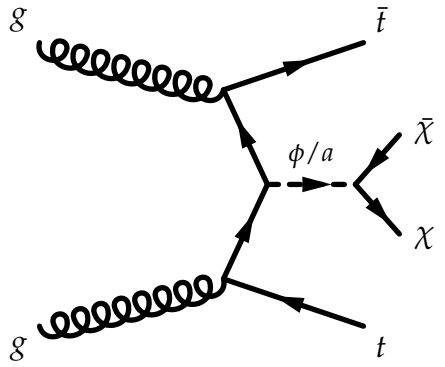

Figure 3.1: Representative Feynman diagram showing the pair production of dark matter particles in association with $t\bar{t}$.

3.1.1 Parameter scan

As discussed in Sec. 2, the MFV and universal coupling assumptions for spin-0 mediators leads to quark mass dependent Yukawa couplings and therefore dominant couplings to top quarks.Therefore DM+$t\bar{t}$ searches are strongly physically motivated and it is important to establish benchmarks for collider searches following the assumptions described in Sec. 2, in particular a Dirac fermion DM particle, universal couplings and minimum width, $\Gamma_{\phi,a}$.

The benchmark points scanning the model parameters have been selected to ensure that the kinematic features of the parameter space are sufficiently represented. Detailed studies were performed to identify points in the m_{DM}, $m_{\phi,a}$, g_{DM}, g_{q} (and $\Gamma_{\phi,a}$) parameter space that differ significantly from each other in terms of expected detector acceptance. Because missing transverse momentum is the key observable for searches, the mediator p_T spectra is taken to represent the main kinematics of a model. Another consideration in determining the set of benchmarks is to focus on the phase space

where we expect the searches to be sensitive during the 2015 LHC run. Based on a projected integrated luminosity of 30 fb^{-1} expected for 2015, we disregard model points with a cross section times branching ratio smaller than 0.1 fb.

The kinematics is most dependent on the masses m_{DM} and $m_{\phi,a}$. Figure 3.2 and 3.3 show typical dependencies for scalar and pseudoscalar couplings respectively. Typically, the mediator p_T spectra broadens with larger $m_{\phi,a}$. The kinematics are also quite different between on-shell and off-shell production. Furthermore, the kinematic differences between scalar and pseudoscalar are large with light mediator masses and are reduced for larger masses. It is therefore important to benchmark points covering on-shell and off-shell production with sufficient granularity.

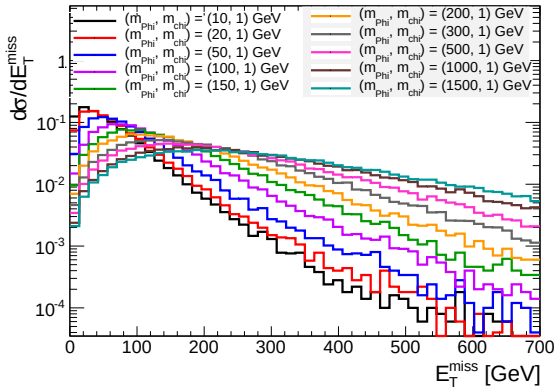

Figure 3.2: Example of the dependence of the kinematics on the scalar mediator mass. The Dark Matter mass is fixed to be m_{DM} =1GeV.

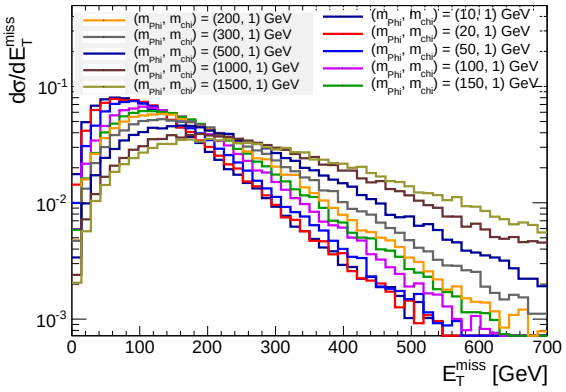

Figure 3.3: Example of the dependence of the kinematics on the pseudoscalar mediator mass. The Dark Matter mass is fixed to be m_{DM} =1GeV.

Typically only weak dependencies on width or equivalently couplings are observed (see Fig 3.5), except for large mediator masses of $\sim$ 1.5 TeV or for very small couplings of $\sim 10^{-2}$. These regimes where width effects are significant have production cross sections that are too small to be relevant for 30 fb^{-1} and are not considered here. However, with the full Run-2 dataset, such models may be within reach. The weak dependence on the typical width values can be understood as the parton distribution function are the dominant effect on mediator production. In other words, for couplings $\sim O(1)$ the width is large enough that the p_T of the mediator is

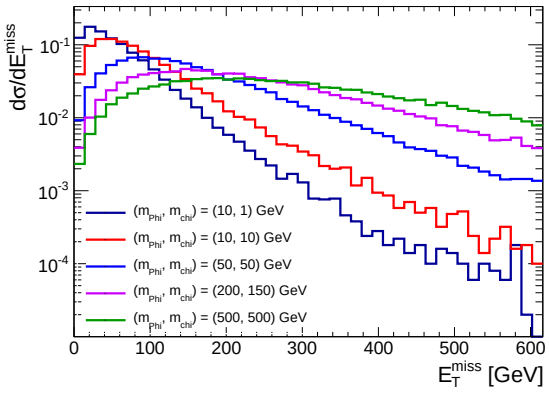

Figure 3.4: Example of the dependence of the kinematic for points of the grid proposed in Tab. 2.2 close to the $m_{\phi,a} \sim 2m_\chi$ limit.

determined mainly by the PDF.

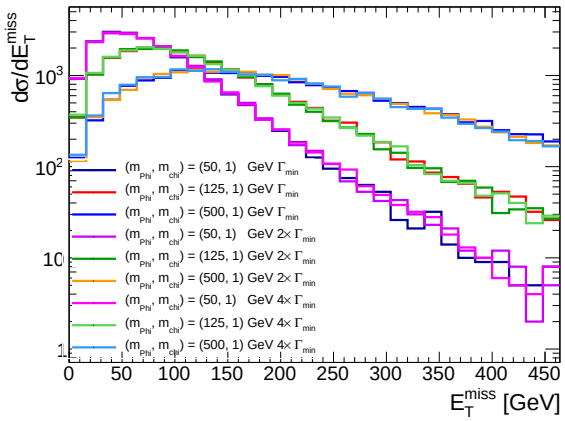

Figure 3.5: Study of the dependence of kinematics on the width of a scalar mediator. The width is increased up to four times the minimal width for each mediator and dark matter mass combination.

Another case where the width can impact the kinematics is when $m_{\phi,a}$ is slightly larger than $2m_\chi$. Here, the width determines the relative contribution between on-shell and off-shell production. An example is given in Fig. 3.6.

Given that the kinematics are similar for all couplings $\sim O(1)$, we recommend to generate only samples with $g_{\mathrm{DM}} = g_{\mathrm{q}} = 1$. It follows from this that these benchmark points should be a good approximation for non-unity couplings and for $g_{\mathrm{DM}} \neq g_{\mathrm{q}}$, provided that the sample is rescaled to the appropriate cross section times branching ratio.

While the simple scaling function

$$\sigma' \times BR' = [\sigma \times BR] \times \frac{{g'_{\mathrm{q}}}^2}{g_{\mathrm{q}}} \times \frac{{g'_{\mathrm{DM}}}^2}{g_{\mathrm{DM}}} \times \frac{\Gamma}{\Gamma'} \tag{3.1}$$

is sufficient for a limited range of coupling values (see Fig. 3.7 for example), we also choose to provide instead a table of cross section times branching ratio values over a large range of couplings to support interpretation of search results (see the Appendix C). The table lists couplings from $g = 0.1$ to $g = 3.5$, where the upper limit is chosen to close to the perturbative limit.

The points for the parameter scan chosen for this model are listed in Table 2.2, chosen to be harmonized with those for other

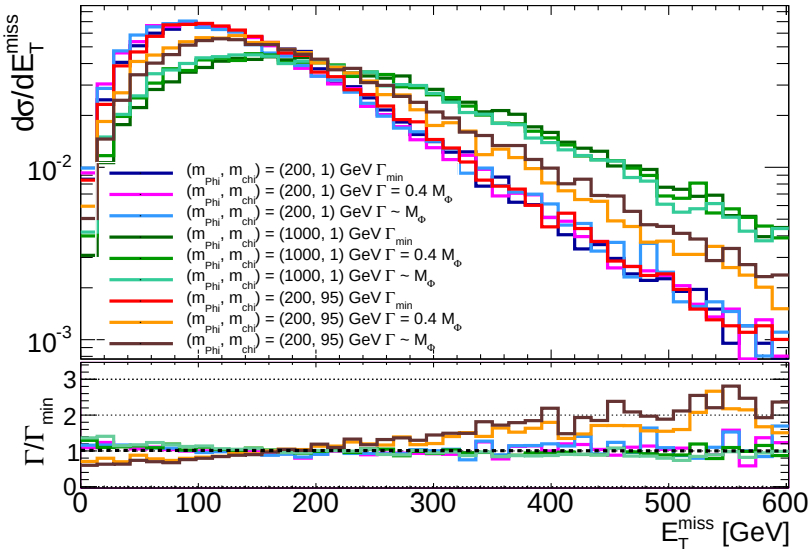

Figure 3.6: Dependence of the kinematics on the width of a scalar mediator. The width is increased up to the mediator mass. Choices of mediator and dark matter masses such that $m_{\phi,a}$ is slightly larger than $2m_\chi$ is the only case that shows a sizeable variation of the kinematics as a function of the width.

analyses employing the same scalar model as benchmark. Based on the sensitivity considerations above, DM masses are only simulated up to 500 GeV, leading to a total of 24 benchmark points.

3.2 $b\bar{b}$+MET models

In some theoretically motivated scenario (e.g. for high $tan\beta$ in 2HDM in the pMSSM), spin-0 mediators might couple more strongly to down generation quarks. This assumption motivates the study of final states involving b-quarks as a complementary search to the $t\bar{t}$+DM models presented in the previous section, to directly probe the $b-$ quark coupling. An example of such a model can be found in Ref. [BFG15]

As in the $t\bar{t}$ case, detailed studies were performed, analyzing these models and their key features. It was found that they show the same weak dependence of the kinematics of the event on width variation, except in few corner cases. In addition, it was found that the same benchmark parameters of the $t\bar{t}$ case could be chosen.

IMPLEMENTATION There are some subtleties to the Monte Carlo simulation relevant for this case that are discussed in Appendix A.

.

To do [**TODO: The following figures are placeholders for now and will be added later]. If these are supporting material for the MC generation, put in the appendix (??)**

3.3 *Models with a single top−quark + MET*

Many different theories predict final states with a single top and associated missing transverse momentum (monotop), some of them including dark matter candidates. A simplified model encompassing the processes leading to this phenomenology is described in

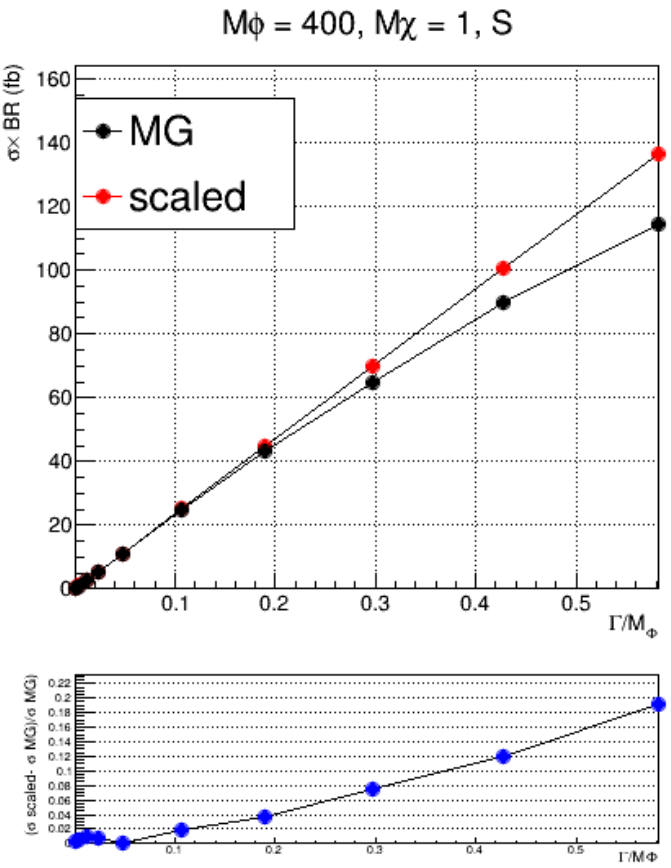

Figure 3.7: An example comparing a simple cross section scaling versus the computation from the generator, for a scalar model with $m_\phi = 400\,\text{GeV}$, $m_{\text{DM}} = 1\,\text{GeV}$ and all couplings set to unity. In this example, the scaling relationship holds for Γ_ϕ / m_ϕ below 0.2, beyond which finite width effects become important and the simple scaling breaks down.

Figure 3.8: Example of the dependence of the kinematics on the scalar mediator mass. The Dark Matter mass is fixed to be 1GeV.

Figure 3.9: Example of the dependence of the kinematics on the pseudoscalar mediator mass. The Dark Matter mass is fixed to be 1GeV.

Refs. [AFM11, AAB+14, BCDF15], and is adopted as one of the benchmarks for Run 2 LHC searches.

A dark matter candidate $\chi$and a new particle (vector or scalar) are added to the SM, in a theory that respects the $\text{SU}(2)_L \times \text{U}(1)_Y$ symmetry and produces a single top quark in association with either the DM particle or a new particle decaying invisibly.

Within this model, two distinct processes can lead to monotop production:

- resonant production, as shown in the diagram of Fig. 3.10 (a), where a color triplet scalar φ or vector field are exchanged in the $s-$channel, and decay into a spin $1/2$ invisible new fermion χ and a top quark;
- non-resonant production, as shown in the diagrams of Fig. 3.10 (b) and (c), where a flavor-changing interaction produces a top

quark in association with a new colored scalar or vector V. The new particles decay invisibly, e.g. to a pair of DM particles. V can also decay into a top quark and an up quark, leading to a same-sign top quark final state; a detailed study of the complementarity of this signature is beyond the scope of this Forum report.

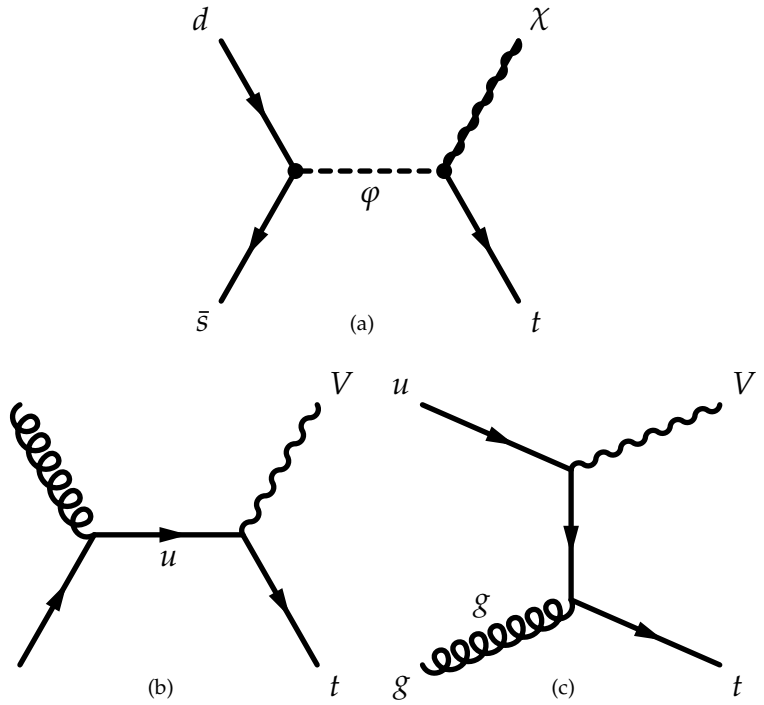

Figure 3.10: Feynman diagram of leading order processes leading to monotop events: production of a coloured scalar resonance φ decaying into a top quark and a spin-1/2 fermion χ (a), $s-$ (b) and $t-$ channel (c) non resonant production of a top quark in association with a spin-1 boson V.

In the following, resonant and non-resonant production are treated independently as separate benchmarks. Only the simpler case of a scalar resonance and the non-resonant vector are considered as early benchmarks for the resonant model; the other two cases with a more complicated phenomenology can be studied in the future.

Resonant production

In this case, a colored 2/3-charged scalar (φ) is produced and decays into a top quark and a spin-1/2 invisible particle, χ. The dynamics of the new sector is described by the following Lagrangian:

$$\mathcal{L} = \left[\varphi \bar{d}^c \left[a^q_{SR} + b^q_{SR}\gamma_5\right] d + \varphi \bar{u}\left[a^{1/2}_{SR} + b^{1/2}_{SR}\gamma_5\right]\chi + \text{h.c.}\right] \qquad (3.2)$$

where u (d) stands for any up ($down$)-quark, the index S stands for scalar field, and the index q runs over the three quark generations, and the color indices are not shown.

In the notation of [AAB+14], the couplings of the new colored fields to down-type quarks are embedded into the 3×3 antisymmetric matrices $a^q_{\{S\}R}$ (scalar couplings) and $b^q_{\{S\}R}$ (pseudoscalar couplings) while those to the new fermion χ and one single up-type quarks are given by the three-component vectors $a^{1/2}_{\{S\}R}$ and $b^{1/2}_{\{S\}R}$ in flavor space.

In the following, we only consider the model with a new colored scalar, as the requirement of invariance under $SU(2)_L \times U(1)_Y$ would require the introduction of further particles in the case of a new colored vector [BCDF15]. Note that the resulting model can be likened to the MSSM with an RPV coupling between a top squark and fermions and an RPC coupling between a top squark–top–neutralino.

NON-RESONANT PRODUCTION

For the non-resonant production, the top quark is produced in association with the new particle: either a new scalar or a new vector (V). For simplicity, we only consider the case of a vector new particle, as the scalar case would involve a mixing with the SM Higgs boson and therefore a larger number of free parameters. The Lagrangian describing the dynamics of the non-resonant case is:

$$\mathcal{L} = \left[V_\mu \bar{u} \gamma^\mu \left[a^1_{FC} + b^1_{FC} \gamma_5 \right] u + \text{h.c.} \right] \tag{3.3}$$

The strength of the interactions among these two states and a pair of up-type quarks is modeled via two 3×3 symmetric matrices in flavor space $a^{\{1\}}_{FC}$ for the vector couplings and $b^{\{1\}}_{FC}$ for the axial vector couplings.

MODEL PARAMETERS AND ASSUMPTIONS

The models considered as benchmarks for the first LHC searches contain further assumptions in terms of the flavour and chiral structure of the model with respect to the full Lagrangians of equations (3.2) and (3.3).

We only consider right-handed quark components, in order to simplify the model phenomenology. The representation of the left-handed components under the $\mathrm{SU}(2)_L$ symmetry would lead to a coupling to *down*-type quarks, since the effective theory is invariant under $\mathrm{SU}(2)_L \times \mathrm{U}(1)_Y$ gauge symmetry. This implies the vector to be an SU(2)L singlet, hence in turn setting the vector and axial vector matrices to have elements of equal values.

Furthermore, in order to be visible at the LHC in the monotop final state, these models must include a strong coupling between the new particle ϕ and $t\chi$. The same kind of assumption exists for the non-resonant production. This means that only the couplings between the new scalar resonance and light quarks (a_{VR}, a_{SR}), and the couplings between the new vector, the top quark and light quarks (a_{FC}), are set to non-zero values

$$\begin{aligned} (a^1_{FC})_{13} = (a^1_{FC})_{31} = a \,, \\ (a^q_{SR})_{11} = (a^{1/2}_{SR})_3 = a \end{aligned} \tag{3.4}$$

IMPLEMENTATION The Monte Carlo simulation relevant for this case is discussed in Appendix A.

3.3.1 *Parameter scan*

The relevant parameters for the resonant model are:

- The mass of the new scalar ϕ;
- The mass of the new fermion χ;
- The coupling of the new scalar to the new fermion and top quark a, related to the width of the scalar in the minimal width assumption;

The relevant parameters for the non-resonant model are:

- The mass of the new vector V;
- The coupling of the new vector to the up and top quark a, related to the width of the scalar in the minimal width assumption;
- The coupling of the new vector to the new fermion χ, related to the branching fraction of the vector into invisible and visible particle, and as a consequence to the width of the vector.

In the case of the non-resonant model, the current implementation of the model does not allow changing the new fermion mass directly as it is not explicitly implemented.

It has been checked for the non-resonant model that the relevant kinematics does not change when changing the width of the resonance, for widths up to 10% of the resonance mass. Figures 3.11 and 3.12 show the V mass distribution, the transverse momentum for V in the case of the $V \to t\bar{u}$ decay, for different V masses and widths. Since they only show kinematic quantities related to the mediator, these figures are relevant independently of the V decay mode (be it visible or invisible).

To do **Pictures will be improved in the next drafts. (??)**

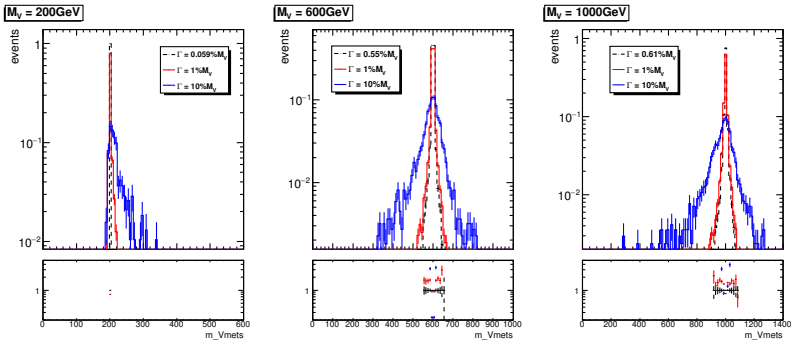

Figure 3.11: Distribution of V invariant mass for the $gu \to tV(\to t\bar{u})$ (on-shell V) for m_V = 200, 600, 1000 GeV (from left to right) and for three different visible decay width (computed from Madgraph directly according to the allowed decays and their couplings, 1% and 10%).

The limited timescale allowed to reach a consensus for the recommendations contained in this document has not allowed further studies on the parameter scan of these models. The two Collaborations have however agreed to continue studying these models and agree on a common parameter scan, following the same path as for other models described in this document.

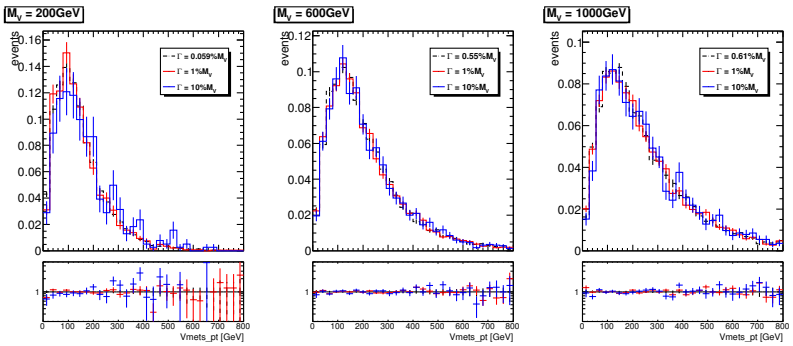

Figure 3.12: Distribution of the V p_T for the $gu \to tV(\to t\bar{u})$ (on-shell V) for m_V = 200, 600, 1000 GeV (from left to right) and for three different visible decay width (computed from Madgraph directly, 1% and 10%).

3.4 *Models with a single b−quark + MET*

Models of bottom-flavored Dark Matter have been proposed in Refs. [LKW13, ABHL14]. We focus on the b-FDM model of Ref. [ABHL14], created to explain the Galactic Center (GC) gamma-ray excess observed in data collected by the Fermi-LAT collaboration [DFH$^+$14].

To do **Add Feynman diagrams. (??)**

The model contains a Dirac fermion transforming as a flavor triplet. The third component of the triplet χ_b comprises the cosmological DM. A flavor singlet, color triplet scalar field Φ mediates the interactions between the DM and the Standard Model quarks.The model is similar to the MSSM with a light bottom squark and neutralino, and is thus a flavor-specific example of a $t-$ channel model.

The Lagrangian considered is given by

$$-\mathcal{L} \supset g\Phi^* \chi_b b_R + \text{h.c.} \tag{3.5}$$

Within the framework of minimal flavor violation, the other fermions in the flavor triplet can be made sufficiently heavy and weakly-coupled that they can be neglected in the analysis.

An annihilation cross section consistent with the gamma-ray excess can be achieved for perturbative values of the couplings while being consistent with LHC constraints on the colored mediator. For parameters capable of explaining the anomalous gamma-ray signal in terms of Dark Matter coupling preferentially to $b-$ quarks, the model predicts a direct detection cross section that is consistent with current constraints, but within the near future reach of Direct Detection experiments. The model will be decisively tested with data from the upcoming high-energy run at the LHC.

3.4.1 *Parameter scan*

The nature of the model doesn't allow to derive a simple scaling behaviour which would allow us reduce the number of points to be simulated. This is because of the interference of diagrams with QCD production of the mediator (which scale as g_s^2) with diagrams that are proportional to the coupling g.

The coupling can be chosen as a discrete set of values $g = 0.5, 1, 2, 3...$ for each mass point, which would allow a bound on

To do **1. Does the kinematic always change with m_{DM} and coupling, in all cases? This model is close to a $t-$ channel colored scalar mediator so the conclusions should be similar. 2. Is minimal width assumed for this model? (??)**

g to be determined. The coupling could also be chosen to fullfill constraints from the relic density (see Appendix C.1, with corresponding cross sections in Tables C.2 onwards). A sizable, $O(1)$ coupling benchmark such as $g = 1$ should be considered for each mass point since this would be a distinctive feature of this benchmark from SUSY models with sbottom squarks.

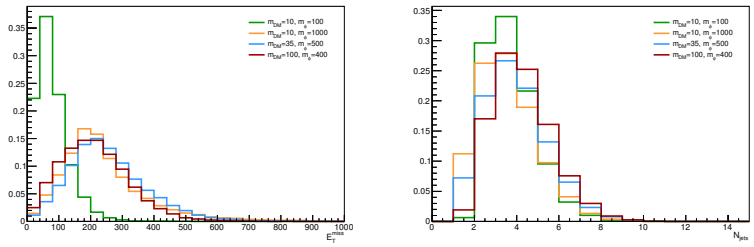

Figure 3.13: MET (left) and jet multiplicity (right) for various DM and mediator masses and couplings normalised to the relic density observed in the early universe.

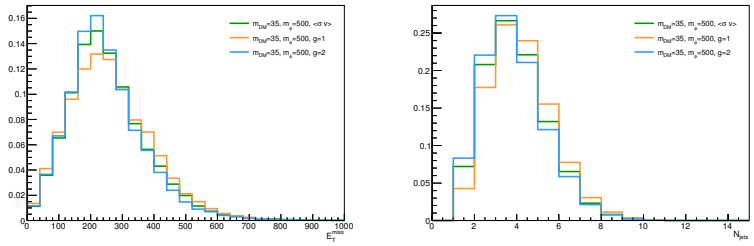

Figure 3.14: MET (left) and jet multiplicity (right) for $m_{\mathrm{DM}} = 35$ GeV and $MPhi = 500$ GeV for couplings corresponding to relic density weights and also $g = 1, 2$

In light of these considerations, we recommend to produce the following benchmark points in the parameter space for this model:

To do **Describe the coupling scan? (??)**

- $m_{\mathrm{DM}} = 10 - 500$ GeV with a binning of 50 GeV for $m_{\mathrm{DM}} < 100$ and 100 GeV otherwise;
- $MPhi = 10 - 1300$ with a binning of 100 GeV;
- $MPhi > m_{\mathrm{DM}} + m_b$, since the cross-sections in the off-shell region are too small to be sensitive with early LHC data;

Cross-sections for unit couplings can be found in Appendix C.2. The increase in the center of mass energy from 8 to 13 TeV leads to a cross-section increase that is a function of $MPhi$, with a smaller dependency for m_{DM}. Therefore, the sensitivity to this model will increase in early 13 TeV data compared to 8 TeV searches [A+15a].

3.4.2 *Model implementation*

We simulate the model using the `MG5_aMC` v2.2.3. The corresponding card files can be found on the Forum SVN repository [For15e].

To do **Do we have to match with Pythia PS? Do we have any recommendations for the initial state PDFs, given the heavy flavors? (??)**

4
Specific models for signatures with EW bosons

In this Section, we consider models with a photon, a W boson, a Z boson or a Higgs boson in the final state, accompanied by Dark Matter particles that either couple directly to the boson or are mediated by a new particle. The experimental signature is identified as *V+MET*.

These models are interesting both as some are demanded by gauge coupling relations in models where the gluon provides the experimentally detectable signature, and also as stand-alone models with final states that cannot be generated by the models in Section 2.

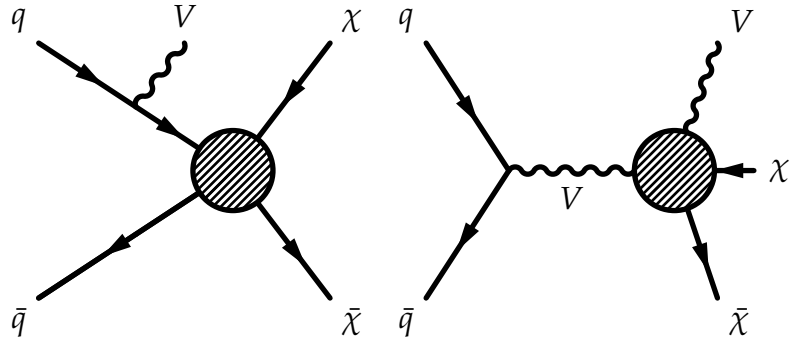

Figure 4.1: Sketch of benchmark models including a contact interaction for V+MET searches, adapted from [NCC+14].

The models considered can be divided into four categories:

Models including a contact operator, where the boson is radiated from the initial state
As depicted in the left diagram of Figure 4.1, these models follow the nomenclature and theory for the EFT benchmarks commonly used by MET+X searches [GIR+10]. These models have been used in past experimental searches [Kha14, Aad14b, K+14, Aad14b, A+14a, Aad14a], and they will not be described here [CHLR13, CNS+13, CHH15, BLW14].

Simplified models with a boson radiated either from the initial state or from the mediator
These models follow those already described in Section 2, replacing the gluon with a boson.

Models including a contact operator, where the boson is directly coupled to DM
Shown on the right-hand side of Figure 4.1, these models allow for a contact interaction vertex that directly couples the boson to Dark Matter.

V-specific simplified models These models postulate direct couplings of new mediators to bosons, e.g. they couple the Higgs boson to a new vector or to a new scalar [CDM+14, BLW14].

The following Sections describe the models within these categories, the parameters for each of the benchmark models chosen, the studies towards the choices of the parameters to be scanned, and finally point to the location of their Matrix Element implementation.

4.1 Simplified models with boson radiation

Monojet searches are generally more sensitive with respect to final states including bosons, due to the much larger rates of signal events featuring quark or gluon radiation with respect to radiation of bosons [ZBW13], in combination with the low branching ratios if leptons from boson decays are required in the final state. The rates for the Higgs boson radiation is too low for these models to be considered a viable benchmark [CDM+14]. However, the presence of photons, leptons from W and Z decays, and W or Z bosons decaying hadronically allow backgrounds to be rejected more effectively, making Z/gamma/W+$\not{E}_T$ searches still worth comparing with searches in the jet+$\not{E}_T$ final state.

To do **Additional motivations exist for this final state from SUSY searches. (??)**

4.1.1 Vector mediator exchanged in the $s-$channel

An example Feynman diagram for these processes can be constructed by taking Fig. 2.1 and replacing the gluon with γ, W or Z. The interest for searches with W bosons in the final state has been elevated by the increased cross section for certain choices of couplings for a spin-1 mediator [BT13]. Run-1 searches have considered three sample cases for the product of up and down quark couplings to the mediator, denoted as ξ:

- No couplings between mediator and either up or down quarks ($\xi = 0$);
- Same coupling between mediator and each of the quark types ($\xi = 1$);
- Coupling of opposite sign between mediator and each of the quark types ($\xi = -1$).

The $\xi = -1$ case leads to a large increase in the cross-section of the process, and modifies the spectrum of missing transverse energy or transverse mass used for the searches. The sensitivity of the W+$\not{E}_T$ search for this benchmark in this case surpasses that of the jet+$\not{E}_T$ search. However, as shown in Ref. [BCD+15], the cross-section increase is due to the production of longitudinally polarized W bosons, as a consequence of a violation of electroweak gauge symmetries. Unless further particles are introduced (in a fashion similar to the Higgs boson in the Standard Model), choosing a value of

$\xi = -1$ for this simplified model will lead to a manifest violation of unitarity at LHC energies. The simplified model with a vector mediator exchanged in the $s-$channel model can still be considered as a benchmark for searches with a W boson if $\xi = 1$. We leave the study of further models with cross-section enhancements due to different couplings to up and down quarks for studies beyond the early LHC searches covered in this document. An example of such model is the case of both DM and SM Higgs charged under a new $U(1)'$, with a a small mass mixing between SM Z-boson and the new Z'. This leads to different effective DM couplings to u_L and d_L, proportional to their coupling to the Z boson, detailed in Appendix B.

The scan in the parameters that characterize this simplified model for EW boson + $\not{E}_T$ searches follow what is already detailed in Section 2.

As in the case of the jet+$\not{E}_T$ models, the width does not have a significant impact on the kinematic distributions relevant for those searches. An example of the particle-level analysis acceptance using the generator-level cuts from Ref. [Aad15] for the photon+$\not{E}_T$ analysis, but raising the photon p_T cut to 150 GeV is shown in Figure 4.1, comparing a width that is set to $\Gamma = M_{med}/3$ to the minimal width (the ratio between the two widths ranges from 1.05 to 1.5 with increasing mediator masses).

Acceptance ratio for $\Gamma = \Gamma_{\text{min}}$ vs $\Gamma = M_{\text{med}}/3$				
	m_{DM}/GeV			
M_{med}/GeV	10	50	200	400
50	0.96	0.99		0.95
100	0.97			
300	1.00	1.02		
600			0.96	
1000	1.01	1.02	1.03	
3000	1.02	1.03		1.01

Table 4.1: Analysis acceptance for the photon+$\not{E}_T$ analysis when varying the mediator width, in the case of a vector mediator exchanged in the $s-$channel

Examples of relevant kinematic distributions for selected benchmark points are shown in Fig. 4.2. leading-order cross-sections for the chosen benchmark points are shown in Appendix B.

4.1.2 *Scalar mediator exchanged in the s − channel*

To do **Feynman diagram? (??)**

We recommend to generate this model for W, Z and photon searches in order to reproduce the kinematics of the dimension-5 contact operator described in Section 4.2.1 in a simplified model framework. Results can then be recast at the reinterpretation stage, by rescaling the cross-sections. The scan in m_{DM} and M_{med} should follow the one in Table 4.1, although individual analyses may choose to reduce the granularity of the scan according to their expected sensitivity.

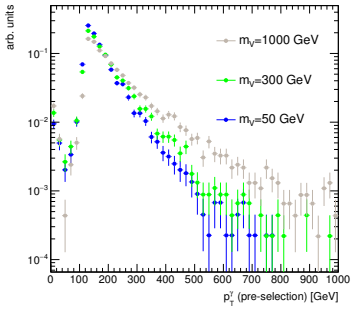

(a) Missing transverse momentum distribution for the photon+$\not{E}_T$ final state, for different mediator mass choices, for m_{DM} =10 GeV.

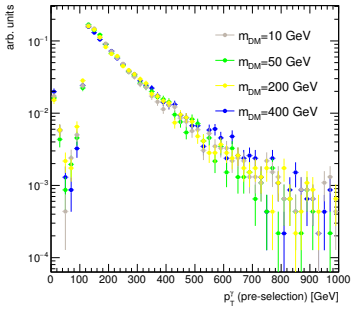

(b) Leading photon transverse momentum distribution for the photon+$\not{E}_T$ final state, for different DM mass choices, with M_{med} =1 TeV.

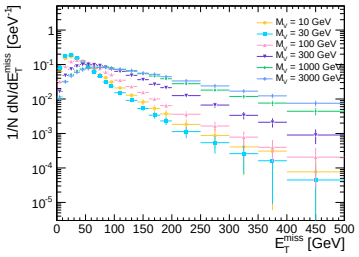

(c) Missing transverse momentum distribution for the leptonic Z+$\not{E}_T$ final state, for different mediator mass choices, for m_{DM} =15 GeV

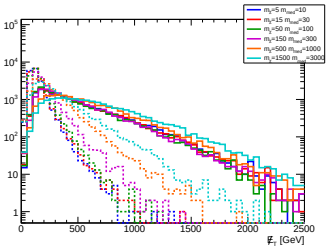

(d) Missing transverse momentum distribution for the hadronic W+$\not{E}_T$ final state.

Figure 4.2: Kinematic distributions relevant for searches with W, Z and photons in the final state, for the simplified model with a vector mediator exchanged in the $s-$channel.

4.1.3 *Colored scalar mediator exchanged in the t − channel*

The model parameters with emission of an EW boson generally follow those in Section 2, even though fewer diagrams are involved. A representative Feynman diagram can be constructed by replacing a gluon in Fig. 2.21 with a γ, W, Z boson. See Ref. [BDG+12] for a theoretical overview of this model with specific examples for the Z+$\not{E}_T$ final state.

Figure 4.3 shows the $\not{E}_T$ distribution for the hadronic Z+$\not{E}_T$ final state, with varying dark matter and mediator mass, before any selection. The acceptance for a series of simplified analysis cuts ($\not{E}_T$ >350 GeV, leading jet p_T > 40 GeV, minimum azimuthal angle between jet and $\not{E}_T$ > 0.4) applied at the generator level is shown in Figure 4.4.

The parameter scan for the $t-$ channel model is still under discussion

To do **The parameter scan, and the conclusions that can be drawn from the plots below, need to be cross-checked with those in the monojet channel. (??)**

4.1.4 *Model implementation*

These models are generated at leading order with MadGraph 2.2.2, using Pythia8 for the parton shower. Parameter cards can be found on the Forum SVN repository [For15a]. .

To do **Add models and instructions for other final states (??)**

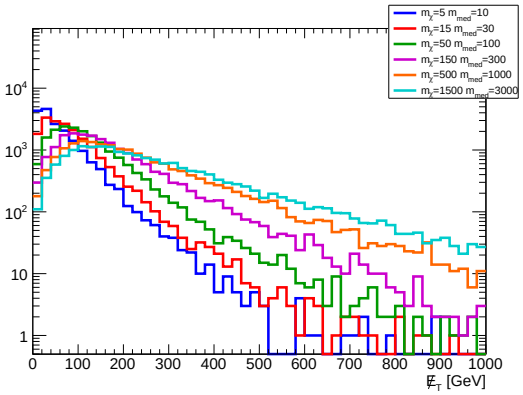

Figure 4.3: Missing transverse momentum distribution for the hadronic Z+$\not{E}_T$ final state, for the simplified model with a colored scalar mediator exchanged in the $t-$channel.

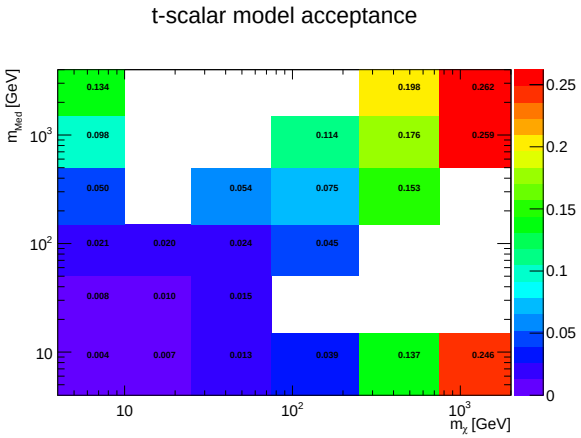

Figure 4.4: Acceptance table for the hadronic Z+$\not{E}_T$ final state, for the simplified model with a colored scalar mediator exchanged in the $t-$channel.

4.2 *EFT models with direct DM-boson couplings*

A complete list of effective operators with direct DM/boson couplings for Dirac DM, up to dimension 7, can be found in [CHLR13, CNS+13, CHH15]. Higher dimensional operators, up to dimension 8, leading to Higgs+$\not{E}_T$ signatures, are mentioned in [CNS+13, BLW14]. Despite the appearance of simplified models, we argue that the model independent approach of the EFTs is still relevant. Furthermore, not all EFT operators have a simplified model replacement.

Implementation discussed in the Appendix

4.2.1 *Dimension 5 operators*

The lowest dimension benchmark operators we consider are effective dimension 5, such as the one depicted in Figure 4.5.

Following the notation of [CNS+13], models from this category have a Lagrangian that includes terms such as:

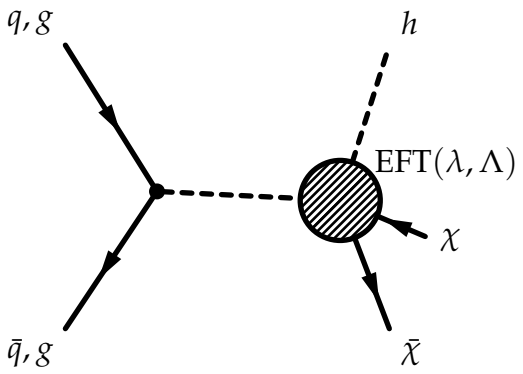

Figure 4.5: Diagram for EFT operators giving rise to a Higgs+$\not{E}_T$ signature.

$$\frac{m_W^2}{\Lambda_5^3}\,\bar{\chi}\chi\,W^{+\mu}W^-_{\mu} + \frac{m_Z^2}{2\Lambda_5^3}\,\bar{\chi}\chi\,Z^{\mu}Z_{\mu}\,, \tag{4.1}$$

where m_Z and m_W are the masses of the Z and W boson, W^{μ} and Z^{μ} are the fields of the gauge bosons, χ denote the Dark Matter fields and Λ_5 is the effective field theory scale . Note that these operators are of true dimension 7, but reduce to effective dimension 5 once the Higgs vacuum expectation values, contained in the W and Z mass terms, are inserted. As such, one expects these that operators would naturally arise in UV complete models where Dark Matter interacts via a Higgs portal where heavy mediators would couple to the Higgs or other fields in an extended Higgs sector. In such models the full theory may be expected to contain additional operators with Higgs-Dark Matter couplings.

To do **The nomenclature in different models differs from literature: Λ_5 vs λ (??)**

Concentrating for the moment on mono-gauge boson signals, the above operator induces signatures with $\not{E}_T$ in conjunction with Z and W bosons at tree level, while at loop level it induces couplings to photon pairs and $Z\gamma$ through W loops. In these models, a clear relation exists between final states with photons, EW bosons and Higgs boson.

As shown in Fig. 4.6 kinematics of this model can be approximated by that of a simplified model including a high-mass scalar mediator exchanged in the $s-$channel described in Section 4.1.2. For this reason, the list of benchmark models with direct boson-DM couplings for photon, Z and W only includes dimension 7 operators: the scalar model with initial state radiation of an EW boson is already recommended and its results can be rescaled. The Higgs+$\not{E}_T$ analysis, however, will not consider the scalar simplified model as benchmark, due to the very low sensitivity in early LHC analyses, and will instead use this dimension 5 operator.

4.2.1.1 *Parameter scan*

The two parameters of this model are the scale of new physics λ and the DM particle mass. SM-DM coupling and new physics scale are related by $g_{\mathrm{DM}} = (246\ \mathrm{GeV})/\lambda$.

To do **Clarify the reason why this happens in Madgraph through explicit Lagrangian terms? (??)**

The initial value of the new physics scale λ chosen for the sample generation is 3 TeV; this does not affect the signal kinematics, and the cross-section of the samples can be rescaled according to the λ^3 dependence when deriving the constraints on this scale.

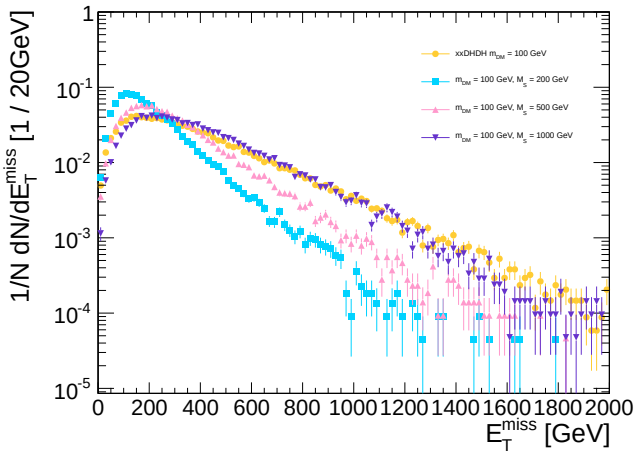

Figure 4.6: Comparison of the missing transverse momentum for the simplified model where a scalar mediator is exchanged in the $s-$channel and the model including a dimension-5 scalar contact operator, in the leptonic Z+$\not{E}_T$ final state

However, more care should be given when rescaling Higgs+$\not{E}_T$ operators of higher dimensions, as different diagrams have a different λ dependence.

To do **Include study of rescaling for dimension-8 operators by N. Whallon in dimension-8 section. (??)**

The DM mass values for the benchmark points to be simulated are chosen to span a sufficient Dark Matter range leading to different kinematics, that is within the LHC sensitivity for early searches and that is consistent across the various signatures and EFT operators. We therefore start the mass scan at m_{DM} =1 GeV, where collider experiments are complementary to direct and indirect detection and choose the last point corresponding to a DM mass of 1 TeV. We recommend a scan in seven mass points, namely:

$$m_{\mathrm{DM}} = 1, 10, 50, 100, 200, 400, 800, 1300\,\mathrm{GeV}.$$

A set of kinematic distributions from the Higgs+$\not{E}_T$ signature where the Higgs decays into two $b-$quarks is shown in Fig. 4.2, for points similar to those of the grid scan proposed.

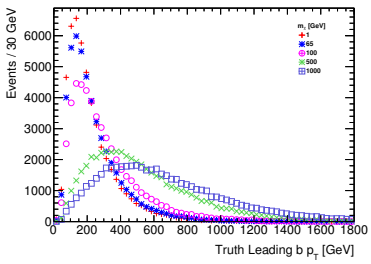

(a) Leading $b-$jet transverse momentum

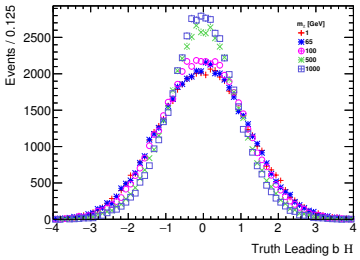

(b) Leading $b-$jet pseudorapidity

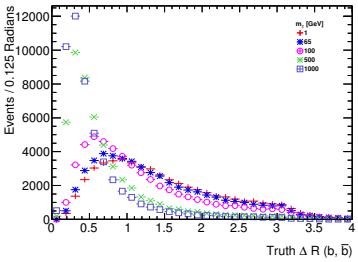

(c) Angular distance between the two leading $b-$jets

Figure 4.7: Comparison of the kinematic distributions for the two leading $b-$ jets (from the Higgs decay) in the model with direct interactions between the Higgs boson and the DM particle, when varying the DM mass.

4.2.2 *Dimension 7 operators*

The dimension-7 benchmark models contain the $SU(2)_L \times U(1)_Y$ gauge-invariant couplings between DM fields and the kinetic terms of the EW bosons. The CP-conserving scalar couplings of this type can be written as

$$\frac{c_1}{\Lambda_S^3}\,\bar{\chi}\chi\,B_{\mu\nu}B^{\mu\nu} + \frac{c_2}{\Lambda_S^3}\,\bar{\chi}\chi\,W^i_{\mu\nu}W^{i,\mu\nu}\,. \tag{4.2}$$

Here $B_{\mu\nu} = \partial_\mu B_\nu - \partial_\nu B_\mu$ and $W^i_{\mu\nu} = \partial_\mu W^i_\nu - \partial_\nu W^i_\mu + g_2\epsilon^{ijk}W^j_\mu W^k_\mu$ are the $U(1)_Y$ and $SU(2)_L$ field strength tensor, respectively, and g_2 denotes the weak coupling constant. In the case of the pseudoscalar couplings, one has instead

$$\frac{c_1}{\Lambda_P^3}\,\bar{\chi}\gamma_5\chi\,B_{\mu\nu}\tilde{B}^{\mu\nu} + \frac{c_2}{\Lambda_P^3}\,\bar{\chi}\gamma_5\chi\,W^i_{\mu\nu}\tilde{W}^{i,\mu\nu}\,, \tag{4.3}$$

where $\tilde{B}_{\mu\nu} = 1/2\,\epsilon_{\mu\nu\lambda\rho}B^{\lambda\rho}$ and $\tilde{W}^i_{\mu\nu} = 1/2\,\epsilon_{\mu\nu\lambda\rho}W^{i,\lambda\rho}$ are the dual field strength tensors. In addition to the CP-conserving interactions (4.2) and (4.3), there are also four CP-violating couplings that are obtained from the above operators by the replacement $\bar{\chi}\chi \leftrightarrow \bar{\chi}\gamma_5\chi$.

The effective interactions introduced in (4.2) and (4.3) appear in models of Rayleigh DM [WY12]. Ultraviolet completions where the operators are generated through loops of states charged under $U(1)_Y$ and/or $SU(2)_L$ have been proposed in [WY13] and their LHC signatures have been studied in [LSWY13]. If these new charged particles are light, the high-p_T gauge bosons that participate in the $\not{E}_T$ processes considered here are able to resolve the substructure of the loops. This generically suppresses the cross sections compared to the EFT predictions [HKU13], and thus will weaken the bounds on the interaction strengths of DM and the EW gauge bosons to some extent. Furthermore, the light charged mediators may be produced on-shell in pp collisions, rendering direct LHC searches potentially more restrictive than $\not{E}_T$ searches. Making the above statements precise would require further studies beyond the timescale of this forum.

Since for $\Lambda_S = \Lambda_P$ the effective interactions (4.2) and (4.3) predict essentially the same value of the mono-photon, mono-Z and mono-W cross section [CNS$^+$13, CHH15], we consider below only the former couplings. We emphasize however that measurements of the jet-jet azimuthal angle difference in $\not{E}_T + 2j$ events may be used to disentangle whether DM couples more strongly to the combination $B_{\mu\nu}B^{\mu\nu}$ ($W^i_{\mu\nu}W^{i,\mu\nu}$) or the product $B_{\mu\nu}\tilde{B}^{\mu\nu}$ ($W^i_{\mu\nu}\tilde{W}^{i,\mu\nu}$) of field strength tensors [CHLR13, CHH15].

After EW symmetry breaking the interactions (4.2) induce direct couplings between pairs of DM particles and gauge bosons. The corresponding Feynman rule reads

$$\frac{4i}{\Lambda_S^3}\,g_{V_1V_2}\left(p_1^{\mu_2}p_2^{\mu_1} - g^{\mu_1\mu_2}\,p_1\cdot p_2\right), \tag{4.4}$$

where p_i (μ_i) denotes the momentum (Lorentz index) of the vector field V_i and for simplicity the spinors associated with the DM fields

have been dropped. The couplings $g_{V_iV_j}$ take the form

$$\begin{aligned} g_{\gamma\gamma} &= c_w^2 c_1 + s_w^2 c_2 \,, \\ g_{\gamma Z} &= -s_w c_w \left(c_1 - c_2\right) \,, \\ g_{ZZ} &= s_w^2 c_1 + c_w^2 c_2 \,, \\ g_{WW} &= c_2 \,, \end{aligned} \tag{4.5}$$

with s_w (c_w) the sine (cosine) of the weak mixing angle. Note that our coefficients c_1 and c_2 are identical to the coefficients C_B and C_W used in [CHH15], while they are related via $k_1 = \frac{1}{{c_w}^2} c_1$ and $k_2 = \frac{1}{{s_w}^2} c_2$ to the coefficients k_1 and k_2 introduced in [CNS+13].

The coefficients c_1 and c_2 appearing in (4.5) determine the relative importance of each of the $\not{E}_T$ channels and their correlations. For example, one observes that:

- Only c_2 enters the coupling between DM and W bosons, meaning that only models with $c_2 \neq 0$ predict a mono-W signal;
- If $c_1 = c_2$ the mono-photon (mono-Z) signal does not receive contributions from diagrams involving Z (photon) exchange;
- Since numerically $c_w^2/s_w^2 \simeq 3.3$ the mono-photon channel is particularly sensitive to c_1.

4.2.2.1 *Parameter scan*

As stated above and shown in Ref. [NCC+14], the kinematic distributions for dimension-7 scalar and pseudoscalar operators only shows small differences. This has been verified from a generator-level study: the signal acceptance after a simplified analysis selection ($\not{E}_T$ >350 GeV, leading jet $p_T > 40$ GeV, minimum azimuthal difference between either of the two jets and the $\not{E}_T$ direction > 0.4) is roughly 70% for both. We therefore only suggest to generate one of the two models. TodoWhen we have the cross-sections for both, we can recommend the one with the highest cross-section.

The differences in kinematics for the various signatures are negligible when changing the coefficients k_1 and k_2, as shown in Figure 4.8. Only the case $k_1 = k_2 = 1$ is generated as benchmark; other cases are left for reinterpretation as they will only need a rescaling of the cross-sections shown in Appendix B for the various DM mass points considered.

4.2.3 *Higher dimensional operators*

Many higher dimensional operators can induce signals of photons or $W/Z/H$ bosons in the final state. A complete list can be found in Refs. [CDM+14, BLW14, PS14] and references therein.

Although with lower priority with respect to the operators above, a representative dimension-8 operators can be chosen as benchmark, with the form:

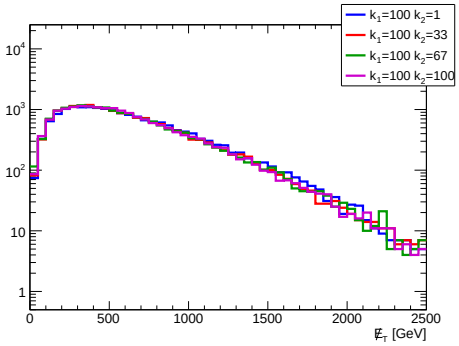

(a) Missing transverse momentum distribution.

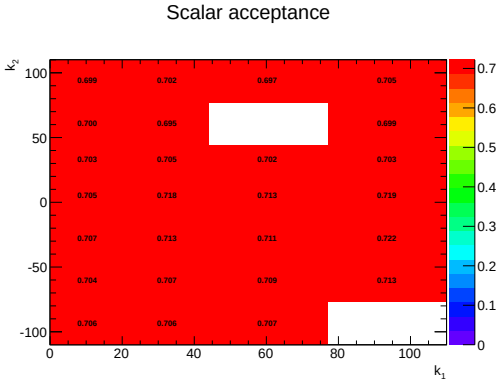

(b) Acceptance.

Figure 4.8: $\not{E}_T$ distribution and acceptance for the dimension-7 model with a hadronically decaying Z in the final state, for the scalar and pseudoscalar operators representing direct interactions between DM and bosons.

$$\frac{1}{\Lambda^4}\bar{\chi}\gamma^\mu\chi B_{\mu\nu}H^\dagger D^\nu H$$

In this case, the new physics scale is Λ is connected with the coupling of the DM as $y_\chi = \frac{1}{\Lambda^4}$.TodoIs more detail needed here? An advantage of this operator is that it includes all signatures with EW bosons, allowing to assess the relative sensitivity of the various channels with the same model. The kinematics for this operator is different with respect to other operators, leading to a harder $\not{E}_T$ spectrum, as illustrated by comparing the leading $b-$jet distribution for the dimension 5 operator to the dimension 8 operator.

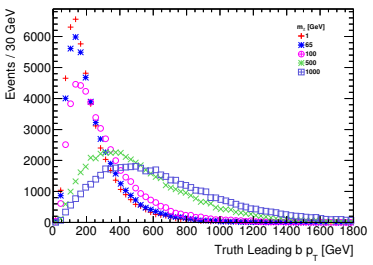

(a) Dimension 5 operator

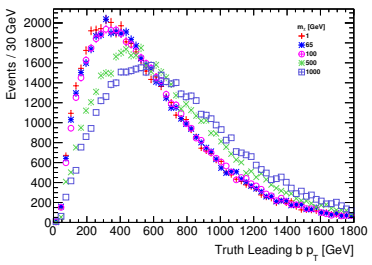

(b) Dimension 7 operator

Figure 4.9: Comparison of the transverse momentum for the leading $b-$ jet from the Higgs decay for a dimension 5 and dimension 7 operator with direct boson-DM couplings.

4.2.4 *Validity of EW contact operators and possible completions*

It is important to remember that the operators described in this section may present problems in terms of the validity of the contact interaction approach for the energy scales reached at the LHC.

As outlined in [BLW14], designing very high $\not{E}_T$ search signal regions that are exclusively motivated by the hard $\not{E}_T$ spectra of the dimension 7 and 8 operators will mean that the momentum transfer in the selected events is larger. This in turn means that processes at that energy scale (mediators, particles exchanged in loops) are accessible, and a simple contact interaction will not be able to correctly describe the kinematics of these signals.

Contact interaction operators like the ones in this section remain useful tools for comparison of the sensitivity of different search channels, and for reinterpretation of other models under the correct assumptions. To date, there are no UV-complete models available for most of those operators: the dimension-7 operators are particularly challenging since their completion involves loops. However, this may be the focus of future theoretical exploration, as discussed in Ref. [CHH15]. An example of a complete model for scalar DM corresponding to the dimension-5 operator is provided in the Appendix B. Providing results for the pure EFT limit of these models will prove useful to cross-check the implementation of future.

Given these considerations, the recommendations on the presentation of the results for these models are:

- Assess the percentage of events that pass the EFT validity condition, and present results using a truncation of the invalid events using the procedure in Section 5 alongside pure EFT results;
- Deliver fiducial limits on the cross section of any new physics events, without any model assumption, according to the guidelines in Appendix D.

MODEL IMPLEMENTATION DISCUSSED IN THE APPENDIX

4.3 *Specific simplified models including EW bosons, tailored to Higgs+MET searches*

Three benchmark simplified models [CDM+14, BLW14] are recommended for Higgs+$\not{E}_T$ searches:

- A model where a leptophobic vector mediator (Z'_B) is exchanged in the $s-$channel, radiates a Higgs boson and decays into two DM particles (Fig. 4.10 (a));
- A model where a scalar mediator S couples to the SM only through the SM Higgs and decays to two DM particles (Fig. 4.11);
- A model where a vector Z' is produced resonantly and decays into a Higgs boson plus an intermediate heavy pseudoscalar

particle A^0, in turn decaying into two DM particles (Fig. 4.10 (b)).

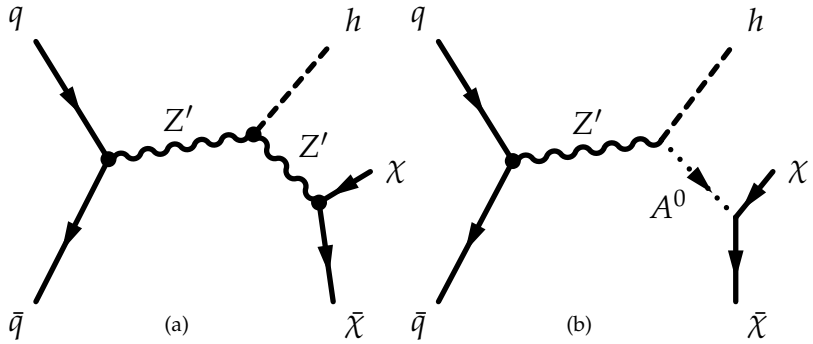

Figure 4.10: Feynman diagrams of leading order processes leading to Higgs+$\not{E}_T$ events: (a) a model with a vector mediator (Z') coupling with DM and with the Higgs boson h, and (b) a 2HDM model with a new invisibly decaying pseudoscalar A^0 from the decay of an on-shell resonance Z' giving rise to a Higgs+$\not{E}_T$ signature .

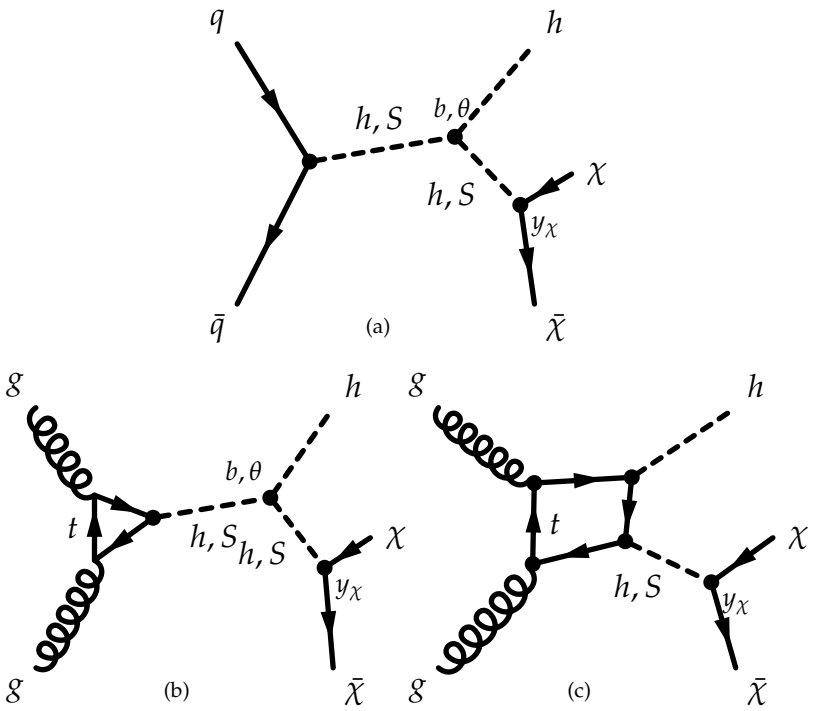

Figure 4.11: Feynman diagrams of leading order processes leading to Higgs+$\not{E}_T$ events for a model with a scalar mediator (S) coupling with DM and with the Higgs boson h.

These models are kinematically distinct from one another, as shown in the comparison of the $\not{E}_T$ spectra in Fig. 4.12 for high and low masses of the pseudoscalar mediator. Figure 4.12 (a) shows the $\not{E}_T$ distribution for models with high mediator masses ($m_S = 1$ TeV, $m_{Z'} = 1$ TeV, $m_{A^0} = 1$ TeV) and DM mass of either 50 (Z'_B and A^0 models) or 65 GeV (scalar mediator model). Figure 4.12 (b) shows the $\not{E}_T$ distribution for models with low pseudoscalar mediator masses ($m_{Z'_B} = 100$ GeV, $m_{Z'} = 1$ TeV, $m_{A^0} = 100$ GeV) and DM mass of 1 TeV for all models.

4.3.1 $\not{E}_T$ +Higgs from a baryonic Z'

The model shown in Fig. 4.10 (a) postulates a new gauge boson Z' corresponding to a new $U(1)_B$ baryon number symmetry. The stable baryonic states included in this model are the DM candidate particles. The mass of the Z' boson is acquired through a baryonic

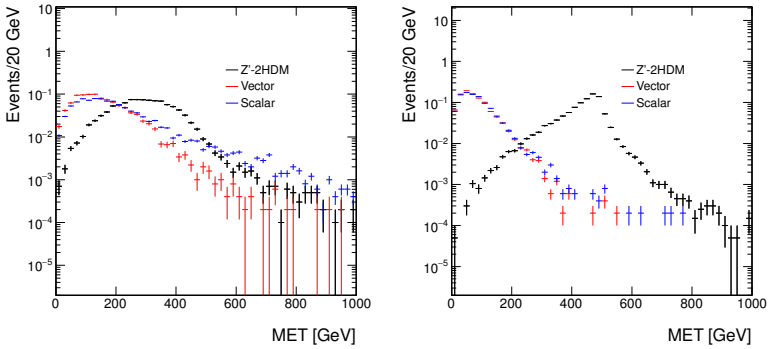

(a) High mediator mass (b) Low mediator mass

Figure 4.12: Comparison of the missing transverse momentum distributions at generator level in different simplified models leading to a Higgs+$\not{E}_T$ signature. The model parameter settings are detailed in the text.

Higgs h_B, which mixes with the SM Higgs boson. The interactions between the Z', the quarks and the DM are described by the following Lagrangian:

$$L = g_q \bar{q} \gamma^\mu q Z'_\mu + g_{DM} \bar{\chi} \gamma^\mu \chi Z'_\mu. \tag{4.6}$$

The quark couplings g_q are fixed to be equal to one third of the gauge coupling g_B, while the DM coupling to the Z' are proportional to the baryon number and to the gauge coupling ($g_\chi = B g_B$). No leptonic couplings of the Z' are allowed, thus evading dilepton constraints. After incorporating the mixing of the baryonic and SM Higgs bosons, this model is is described by the following Lagrangian term at energies below $m_{Z'}$:

$$L_{\text{eff}} = -\frac{g_q g_{DM}}{m^2_{Z'}} \bar{q} \gamma^\mu q \bar{\chi} \gamma_\mu \chi \left(1 + \frac{g_{hZ'Z'}}{m^2_{Z'}} h\right), \tag{4.7}$$

The first term of this equation gives rise to a term that is equivalent to the radiation of a jet (or another EW gauge boson) in the initial state. The second term describes the interaction between the Z' and the SM Higgs boson, via the coupling $g_{hZ'Z'} = \frac{m_{Z'} 2 sin\theta}{v_B}$, where $sin\theta$ is the mixing angle between the SM Higgs and the baryonic Higgs h_B, and v_B is the Baryonic Higgs vev.

4.3.1.1 *Parameter scan*

The model is described by six parameters:

1. the mediator mass M_{med}, (also referred to as $m_{Z'}$)
2. mass of dark matter, m_{DM}
3. coupling of Z' mediator to dark matter, g_{DM}
4. coupling of the mediator to quarks, g_q
5. mixing angle between baryonic Higgs h_B and the SM-like Higgs boson, $\sin\theta$
6. coupling of the mediator to SM-like Higgs boson, $g_{hZ'Z'}$

The width of the Z' mediator is calculated using all possible decays to SM particles (quarks) and to pairs of DM particles if kinematically allowed.

The dependence of the missing transverse momentum ($\not{E}_T$) on the model parameters is studied by varying the parameters one at a time. The variation of parameters other than M_{med} and m_{DM} does not result in significant variations of the $\not{E}_T$ spectrum, as shown in Figures 4.13. Figure 4.14 shows that for an on-shell mediator, varying m_{DM} with the other parameters fixed does not affect the $\not{E}_T$ distribution, while the distribution broadens significantly in the case of an off-shell mediator. For this reason, the same grid in M_{med}, m_{DM} as for the vector mediator of the jet+$\not{E}_T$ search (Table 2.1) is chosen as a starting point. The coupling $g_{hZ'Z'}$, along with g_{q} and g_{DM}, are subject to perturbativity bounds:

$$g_{\text{q}}, g_{\text{DM}} < 4\pi$$

and

$$g_{hZ'Z'} < \sqrt{4\pi} m_{Z'} \sin\theta$$

The value $g_{hZ'Z'}/m_{Z'} = 1.0$ is chosen as a benchmark value for the generation of Monte Carlo samples since it maximizes the cross section (as shown in the following paragraph) without violating the bounds. The mediator-DM coupling g_{DM} is fixed to 1, and the mediator-quark g_q coupling is fixed to $1/3$. The kinematic distributions do not change as a function of these parameters, so results for other values of $g_{hZ'Z'}/m_{Z'}$, g_{DM} and g_{q} can be obtained through rescaling by the appropriate cross sections.

Figs 4.15 and 4.16 show the kinematic distributions for the two leading jets in the $H \to \bar{b}b$ decay channel, for two values of the mediator mass and varying the DM mass.

Analyses should perform further studies, beyond those studies performed for the forum, to estimate the reach of the analysis with respect to all points in the grid and therefore decide on a smaller set of grid points to be generated.

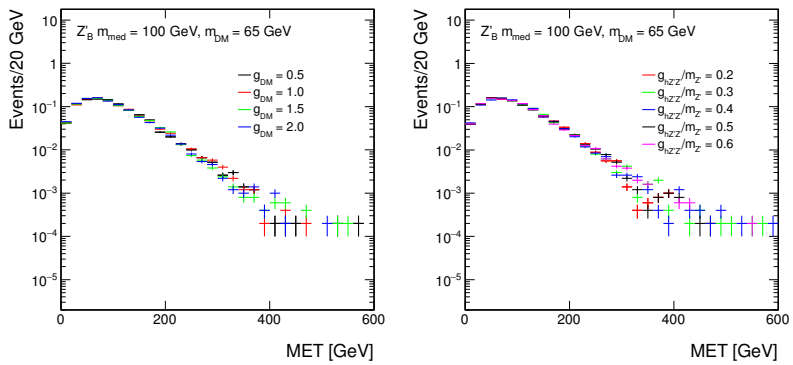

Figure 4.13: Missing transverse momentum distributions at generator level in the vector mediator scenario for different values of: the mediator-dark matter coupling g_{DM} (left), and the coupling between the mediator and the SM-like Higgs boson, scaled by the mediator mass, $g_{hZ'Z'}/m_{Z'}$ (right).

4.3.1.2 *Cross-section scaling*

The dependence of the cross section of the $pp \to H\chi\bar{\chi} + X$ process on $g_{hZ'Z'}$ is shown in Figure 4.17. The curves have been fit to

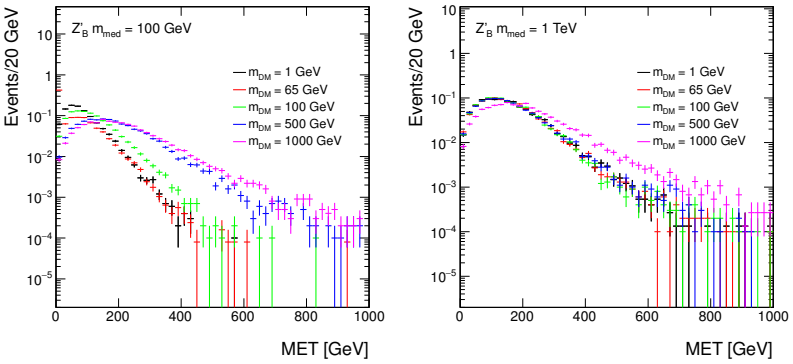

Figure 4.14: Missing transverse momentum distributions at generator level in the vector mediator scenario: for different values of the dark matter mass m_{DM} and a mediator mass of M_{med} = 100 GeV (left) and M_{med} = 1 TeV (right).

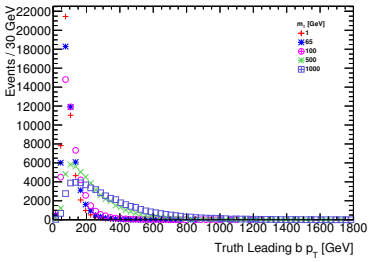

(a) Leading $b-$jet transverse momentum

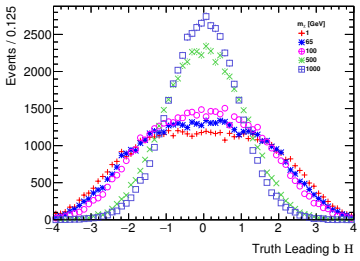

(b) Leading $b-$jet pseudorapidity

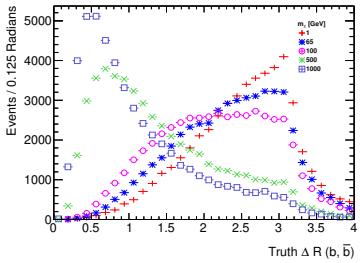

(c) Angular distance between the two leading $b-$jets

Figure 4.15: Comparison of the kinematic distributions for the two leading $b-$jets (from the Higgs decay) in the vector Z' simplified model, when fixing the Z' mass to 100 GeV and varying the DM mass.

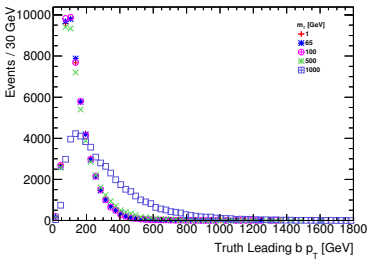

(a) Leading $b-$jet transverse momentum

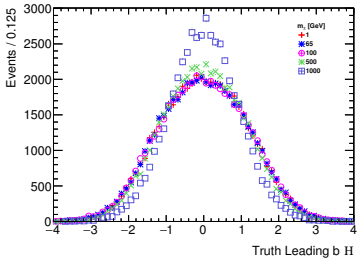

(b) Leading $b-$jet pseudorapidity

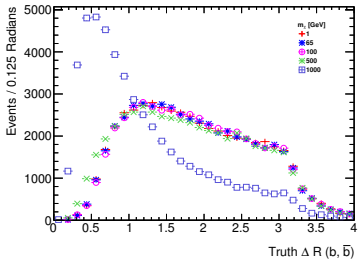

(c) Angular separation of the two leading b-jets

Figure 4.16: Comparison of the kinematic distributions for the two leading jets from the Higgs decay in the vector Z' simplified model, when fixing the Z' mass to 1000 GeV and varying the DM mass.

second-order polynomials. For $m_{med} = 100$ GeV, the fit function is

$$y = -0.12 - 3.4 \times 10^{-3} x + 2.7 \times 10^{-4} x^2$$

. For $m_{med} = 1$ TeV, the fit function is is

$$y = 0.0012 - 2.4 \times 10^{-7} x + 1.5 \times 10^{-7} x^2$$

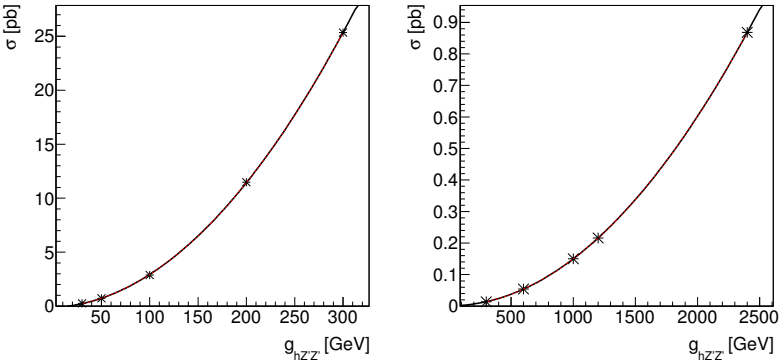

Figure 4.17: Cross section of the $pp \to H\chi\bar{\chi}$ process as a function of $g_{hZ'Z'}$ for $m_{Z'} = 100$ GeV (left) and $m_{Z'} = 1$ TeV (right). The fit functions are shown in the text.

4.3.2 $\not{E}_T$ +Higgs from a scalar mediator

A real scalar singlet S coupling to DM can be introduced as a portal between SM and the dark sector through the Higgs field. The new scalar mixes with the SM Higgs boson, and couples to DM through a Yukawa term y_χ. The relevant terms in the scalar potential are

$$\begin{aligned} V &\supset a|H|^2 S + b|H|^2 S^2 + \lambda_h |H|^4 \\ &\longrightarrow \tfrac{1}{2} a (h+v)^2 S + \tfrac{1}{2} b (h+v)^2 S^2 + \frac{\lambda_h}{4}(h+v)^4, \end{aligned} \tag{4.8}$$

where a, b are new physics couplings and λ_h is the Higgs quartic.

The additional Lagrangian terms for this model are:

$$L \supset -y_\chi \bar{\chi}\chi (cos\theta\, S - sin\theta\, h) - \frac{m_q}{v}\bar{q}q(cos\theta\, h + sin\theta\, S) \tag{4.9}$$

where θ is the mixing angle between the Higgs boson and the new scalar.

Mono-Higgs signals in this second model arise through processes shown in Fig. 4.11 (a,b), or through the radiation of a Higgs boson from the t quark in the production loop, in Fig. 4.11 (c). The first two processes depend on the $h^2 S$ and $h S^2$ cubic terms in Eq. (4.8). At leading order in $\sin\theta$, these terms are

$$V_{\text{cubic}} \approx \frac{\sin\theta}{v}(2m_h^2 + m_S^2) h^2 S + b\, v\, h\, S^2 + ... \tag{4.10}$$

with a and λ_h expressed in terms of $\sin\theta$ and m_h^2, respectively. At leading order of $\sin\theta$, the $h^2 S$ term is fixed once the mass eigenvalues m_h, m_S and mixing angle are specified. The $h\, S^2$ term is not fixed and remains a free parameter of the model, depending on the new physics coupling b.

4.3.2.1 Parameter scan

The model is described by five parameters:

1. the Yukawa coupling of heavy scalar to dark matter, g_{DM} (also referred to as y_χ)
2. the mixing angle between heavy scalar and SM-like Higgs boson, $\sin\theta$;
3. the new physics coupling, b;
4. mass of heavy scalar, m_S, also termed M_{med};
5. mass of dark matter, m_{DM};

The mixing angle is constrained from current Higgs data to satisfy $\cos\theta = 1$ within 10% and therefore $\sin\theta \lesssim 0.4$. This provides a starting point for the parameter scan in this model: we recommend to set $\sin\theta = 0.3$. Figure 4.19 shows that there is no dependence of the kinematics from the value of this angle, and different values

can be obtained via rescaling the results for this mixing angle according to the relevant cross-section. It can also be observed from Figures 4.20 and 4.18 that the kinematics of this model follows that of the equivalent jet+$\not{E}_T$ model: only small changes are observed in the on-shell region, while the relevant distributions diverge when the mediator is off-shell. For this reason, the same grid in M_{med}, m_{DM} as for the scalar mediator of the jet+$\not{E}_T$ search (Table 2.2) is chosen as a starting point. The Yukawa coupling to DM y_{DM} is set to 1, the new physics coupling between scalar and SM Higgs b = 3. Results for other values can be obtained via a rescaling of the results for these parameters.

To do **Estimate the sensitivity and possibly prune parameter scan. (??)**

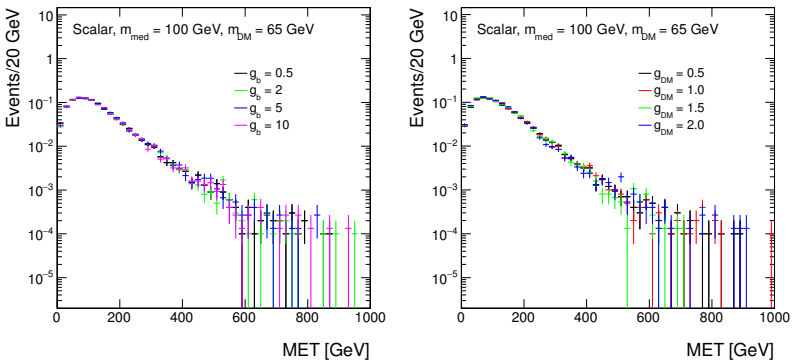

Figure 4.18: Missing transverse momentum distributions at generator level in the scalar mediator scenario, for different values of: the new physics coupling g_b (left), and the mediator-dark matter coupling g_{DM} (right).

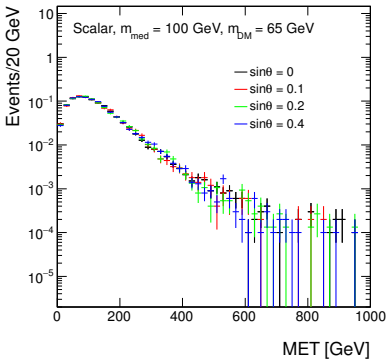

Figure 4.19: Missing transverse momentum distributions at generator level in the scalar mediator scenario: for different values of the mixing angle $\sin\theta$.

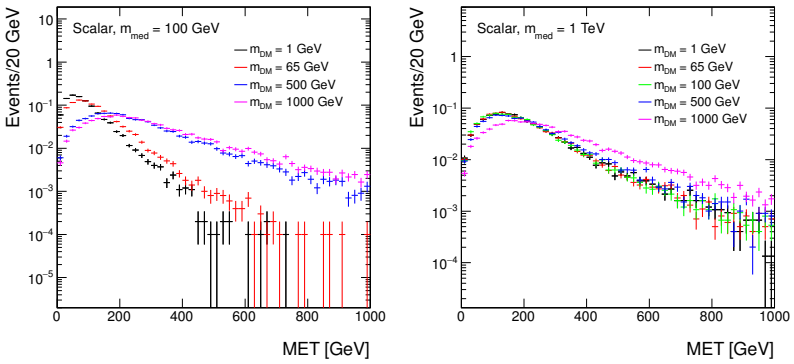

Figure 4.20: Missing transverse momentum distributions at generator level in the scalar mediator scenario: for different values of the dark matter mass m_{DM} and a mediator mass of $M_{\text{med}} = 100$ GeV (left) and $M_{\text{med}} = 1$ TeV (right).

Figs. 4.21 and 4.22 show the kinematic distributions for the two leading jets in the $H \to \bar{b}b$ decay channel, for two values of the mediator mass and varying the DM mass.

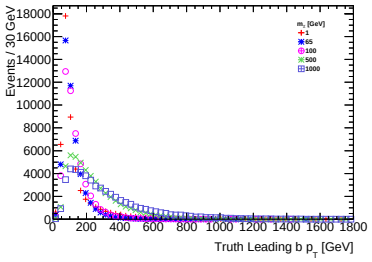

(a) Leading $b-$jet transverse momentum

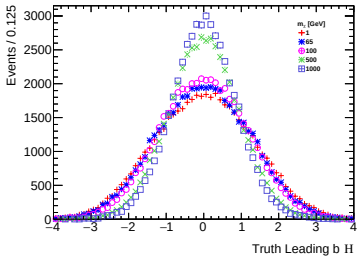

(b) Leading $b-$jet pseudorapidity

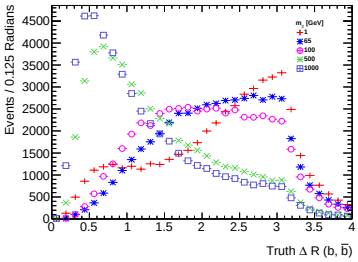

(c) Angular distance between the two leading $b-$jets

Figure 4.21: Comparison of the kinematic distributions for the two leading jets from the Higgs decay in the scalar simplified model, when fixing the new scalar mass to 100 GeV and varying the DM mass.

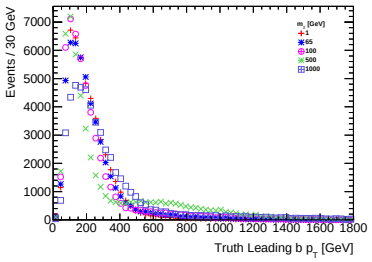

(a) Leading $b-$jet transverse momentum

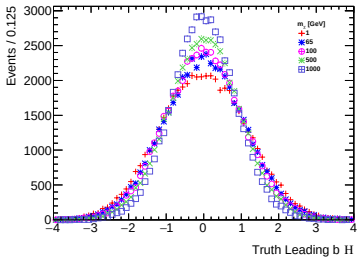

(b) Leading $b-$jet pseudorapidity

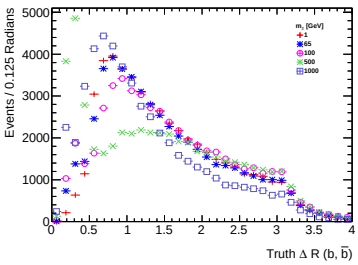

(c) Angular distance between the two leading $b-$jets

Figure 4.22: Comparison of the kinematic distributions for the two leading jets from the Higgs decay in the scalar simplified model, when fixing the new scalar mass to 1000 GeV and varying the DM mass.

4.3.3 *Higgs+$\not{E}_T$ signal from 2HDM model with a Z' and a new pseudoscalar*

In this simplified model [BLW14], a new Z' resonance decays to a Higgs boson h plus a heavy pseudoscalar state A^0 in the 2HDM

framework, which in turn decays to a DM pair. This model is represented in the diagram in Fig. 4.10 (b).

The motivation for coupling the dark matter to the pseudoscalar is that dark matter coupling to a Higgs or Z' boson is generically constrained by other signal channels and direct detection. An advantage of including this model is that it has different kinematics due to the on-shell Z' production, where for heavy Z' masses the $\not{E}_T$ and pT spectra are much harder. This model can satisfy electroweak precision tests and constraints from dijet resonance searches, and still give a potentially observable Higgs+$\not{E}_T$ signal.

This model comprises two doublets, where Φ_u couples to up-type quarks and Φ_d couples to down-type quarks and leptons:

$$-\mathcal{L} \supset y_u Q \tilde{\Phi}_u \bar{u} + y_d Q \Phi_d \bar{d} + y_e L \Phi_d \bar{e} + \text{h.c.} \tag{4.11}$$

After electroweak symmetry breaking, the Higgs doublets attain vevs v_u and v_d, and in unitary gauge the doublets are parametrized as

$$\begin{aligned} \Phi_d &= \frac{1}{\sqrt{2}} \begin{pmatrix} -\sin\beta\ H^+ \\ v_d - \sin\alpha\ h + \cos\alpha\ H - i\sin\beta\ A^0 \end{pmatrix} \quad , \\ \Phi_u &= \frac{1}{\sqrt{2}} \begin{pmatrix} \cos\beta\ H^+ \\ v_u + \cos\alpha\ h + \sin\alpha\ H + i\cos\beta\ A^0 \end{pmatrix} \end{aligned} \tag{4.12}$$

where h, H are neutral CP-even scalars and A^0 is a neutral CP-odd scalar. In this framework, $\tan\beta \equiv v_u/v_d$, and α is the mixing angle that diagonalizes the $h - H$ mass squared matrix. We take $\alpha = \beta - \pi/2$, in the limit where h has SM-like couplings to fermions and gauge bosons as per Ref. [CGT13], and $\tan\beta \geq 0.3$ as implied from the perturbativity of the top Yukawa coupling. The Higgs vevs lead to $Z - Z'$ mass mixing, with a mixing parameter given by

$$\begin{aligned} \epsilon &\equiv \frac{1}{M_{Z'}^2 - M_Z^2} \frac{g g_z}{2\cos\theta_w} (z_d v_d^2 + z_u v_u^2) \\ &= \frac{(M_Z^0)^2}{M_{Z'}^2 - M_Z^2} \frac{2 g_z \cos\theta_w}{g} z_u \sin^2\beta. \end{aligned} \tag{4.13}$$

The production cross section for this model scales as $(g_z)^2$, as the decay width for this process to leading order in ϵ (Eq. 4.13) is

$$\Gamma_{Z' \to h A^0} = (g_z \cos\alpha \cos\beta)^2 \frac{|p|}{24\pi} \frac{|p|^2}{M_{Z'}^2}. \tag{4.14}$$

where the center of mass momentum for the decay products $|p| = \frac{1}{2M_{Z'}} \lambda^{1/2}(M_{Z'}^2, m_h^2, m_{A^0}^2)$, and λ is the Källen triangle function[1].

[1] $\lambda(c_1, c_2, c_3) \equiv c_1^2 + c_2^2 + c_3^2 - 2(c_1c_2 + c_2c_3 + c_3c_1)$

4.3.3.1 *Parameter scan*

The model is described by five parameters:

- the pseudoscalar mass M_{A^0},
- the DM mass m_{DM},

- the Z' mass, $M_{Z'}$,
- $\tan\beta (\equiv v_u/v_d)$,
- the Z' coupling strength g_z.

To study the signal production and kinematic dependencies on these parameters, we produced signal samples varying each of the five parameters through MadGraph for the matrix element, PYTHIA for the parton shower, and DELPHES[dF+14] for a parameterized detector-level simulation.

As seen in Fig. 4.23, variations of $\tan\beta$ does not lead to any kinematic difference and the production cross section simply scales as a function of $\tan\beta$. Hence we recommend to fix $\tan\beta$ to unity in the signal generation.

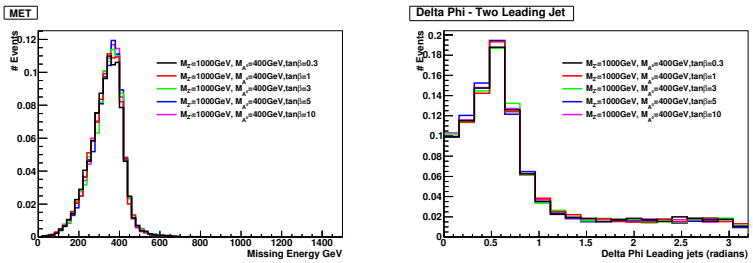

(a) $\not{E}_T$ distribution (b) $\Delta\phi$ distance between the two $b-$ jets

Figure 4.23: Kinematic distributions of the signal process varying $\tan\beta$, in the case of a Higgs boson decaying into two b quarks, after parameterized detector simulation: no kinematic dependency is observed

Similarly, variations of g_z do not lead to any kinematic changes. The value of g_z for a given $M_{Z'}$ and $\tan\beta$ can be set according to the maximum value allowed by electroweak global fits and dijet constraints, as described in [BLW14]. Since this parameter does not influence the kinematics, we leave it up to individual analyses on whether they generate benchmark points only according to these external constraints.

Since the DM pair are produced as a result of the decay of A^0, there are minimal kinematic changes when varying m_{DM} as long as $m_{\text{DM}} < M_{A^0}/2$ so that A^0 production is on-shell, as shown in Fig. 4.24 and 4.25 (before detector simulation).

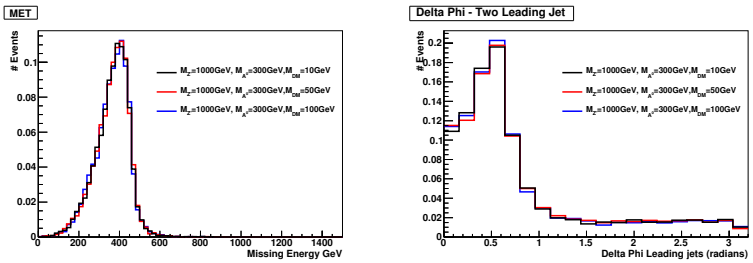

(a) $\not{E}_T$ distribution (b) $\Delta\phi$ distance between the two $b-$ jets

Figure 4.24: Kinematic distributions of the signal process varying m_{DM}: minimal kinematic dependency on m_{DM} as expected when A^0 is produced on-shell. Plots shown for $M_{Z'} = 1000$ GeV, $M_{A^0} = 300$ GeV.

We recommend to produce signal events for a fixed $g_z = 0.8$, $\tan\beta = 1$ and $m_{\text{DM}} = 100$ GeV. For these values, we scan the 2-D parameter space of $M_{Z'}, M_{A^0}$ with $M_{Z'} = 600, 800, 1000, 1200, 1400$ GeV, and $M_{A^0} = 300, 400, 500, 600, 700, 800$ GeV with $M_{A^0} < M_{Z'} - m_h$, for a total of 24 points. The choice of scan is justified by the sensitivity study in [BLW14]: the expected LHC sensitivity for Run-2

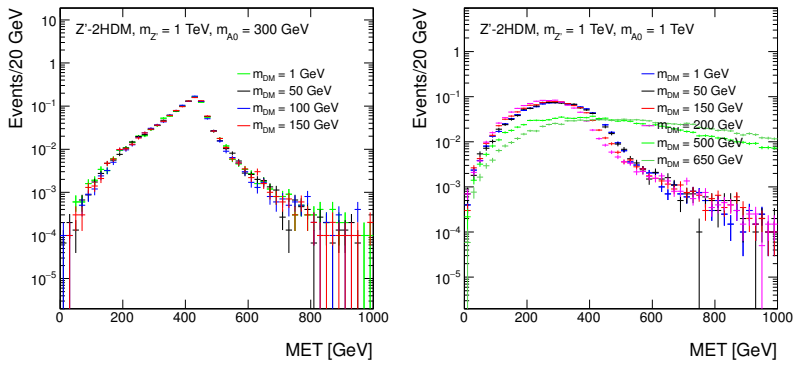

Figure 4.25: Missing transverse momentum distributions at generator level in the Z' +2HDM scenario for different values of the dark matter mass m_{DM}, with $m_{Z'} = 1$ TeV and $m_{A^0} = 300$ GeV (left) and $m_{A^0} = 1$ TeV (right).

is up to $M_{Z'} \sim 1.5$ TeV. For the parameter scan, the DM mass is fixed to 100 GeV. For two $M_{Z'}$, M_{A^0} value sets, we vary the DM mass to obtain sample cross section for rescaling results. All LO cross sections for the various parameter scan points are reported in Appendix B. The parameter scan excludes the off-shell region, as the cross-sections are suppressed and the LHC would not have any sensitivity to these benchmark points in early data.

The kinematic distributions with varying $M_{Z'}$ for fixed M_{A^0} are shown in Fig. 4.26, while the dependency on M_{A^0} is shown in Fig. 4.27.

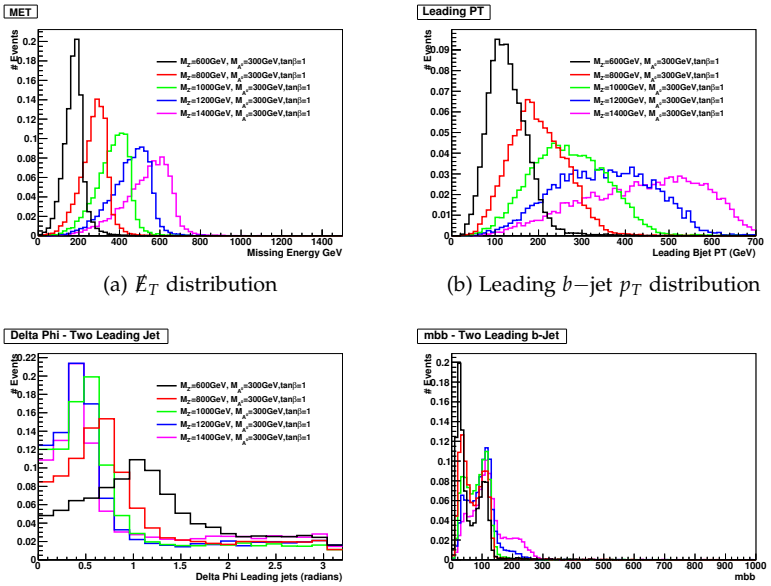

(a) $\not{E}_T$ distribution

(b) Leading $b-$jet p_T distribution

(c) $\Delta\phi$ distance between the two $b-$ jets

(d) Dijet invariant mass

Figure 4.26: Kinematic distributions of the signal process varying $M_{Z'}$, for $m_{\mathrm{DM}} = 100$ GeV, $M_{A^0} = 300$ GeV.

This model also allows for an additional source of Higgs plus $\not{E}_T$ signal with a similar kinematics (Fig. 4.28, shown with detector simulation samples) to the signal process from the decay of $Z' \to hZ$, where the Z decays invisibly. The partial decay width for the Z' is:

$$\Gamma_{Z' \to hZ} = (g_z \cos\alpha \sin\beta)^2 \frac{|p|}{24\pi} \left(\frac{|p|^2}{M_{Z'}^2} + 3\frac{M_Z^2}{M_{Z'}^2} \right), \qquad (4.15)$$

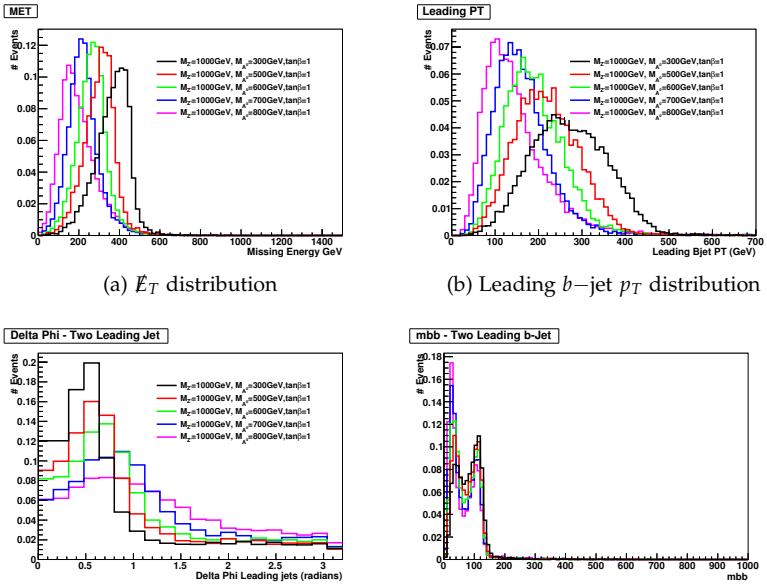

(a) $\not{E}_T$ distribution (b) Leading $b-$jet p_T distribution

(c) $\Delta\phi$ distance between the two $b-$ jets (d) Dijet invariant mass

Figure 4.27: Kinematic distributions of the signal process varying M_{A^0}, for $m_{\text{DM}} = 100$ GeV, $M_{Z'} = 1000$ GeV.

The values for the Z' masses scanned for those samples should follow those of the previous samples, namely values of $M_{Z'} = 600, 800, 1000, 1200, 1400$ GeV. This signal process has no M_A dependence.

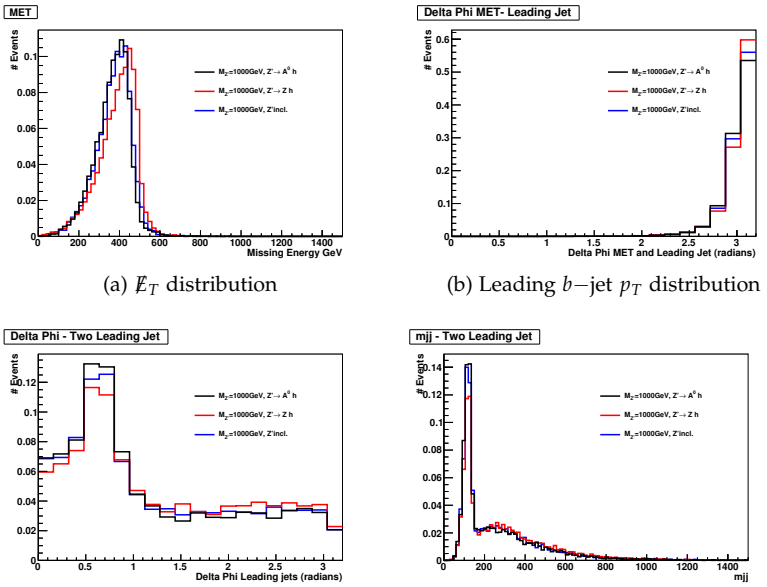

(a) $\not{E}_T$ distribution (b) Leading $b-$jet p_T distribution

(c) $\Delta\phi$ distance between the two $b-$ jets (d) Dijet invariant mass

Figure 4.28: Kinematic distributions of $Z' \to A^0 h$ exclusive production, $Z' \to Zh$ exclusive production and Z' inclusive production for $M_{Z'} = 1000$ GeV and $M_{A^0} = 300$ GeV

IMPLEMENTATION DISCUSSED IN THE APPENDIX

5 Validity of EFT approach

Effective Field Theories (EFTs) are an extremely useful framework for interpreting DM searches at the LHC. Given our current lack of knowledge about the nature of a DM particle and its interactions, a model independent interpretation of the collider bounds appears mandatory. This approach should be complemented with an interpretation within a choice of simplified models. However, these models cannot exhaust the set of possible completions of an effective Lagrangian. EFTs must be used with caution at colliders, where the energy scale of the interaction can be above the point where the EFT approximation is valid.

To illustrate the problem, consider an effective interaction

$$(\bar{\psi}\psi)(\bar{\chi}\chi)\frac{g}{\Lambda^2}$$

that couples SM and DM fields. The strength of this interaction can be parametrized by $f = \frac{g}{\Lambda^2}$. A monojet signature can be generated by applying perturbation theory in the QCD coupling (assuming ϕ is a quark, for example). A mono-X analysis will place a limit on f. For a fixed f, a small value of g will require a small value of Λ. The EFT approximation breaks down if $Q > \Lambda$, where Q is a typical hard scale of the process. One reasonable choice is $Q^2_{\rm tr} = p(\bar{\chi}\chi)^2$, i.e. the momentum flow through the $s-$ channel. On the other hand, large Λ implies large g, raising the question if perturbation theory is even applicable.

To do **right symbol? (??)**

Here we summarize some methods that can be used to ensure the validity of the EFT approximation. These methods are described in detail in Refs. [BDSMR14, BDSG$^+$14, BDSJ$^+$14, A$^+$15b, RWZ15]. We then propose a recommendation for the presentation of EFT results for Run-2 LHC benchmarks.

5.1 Outline of the procedure described in Refs. [BDSG$^+$14, A$^+$15b]

A standard approach has been to consider a simplified model and work backwards to determine the validity of the EFT approximation. For a tree-level interaction between DM and the Standard Model (SM) via some mediator with mass $M_{\rm med}$, the EFT approximation corresponds to expanding the propagator for the mediator in powers of $Q^2_{\rm tr}/M^2_{\rm med}$, truncating at lowest order, and combining

the remaining parameters into a single parameter m_*(also called Λ in the literature). For an example scenario with a Z'-type mediator (leading to some combination of operators D5 to D8 in the EFT limit) this corresponds to setting

$$\frac{g_{\rm DM}g_{\rm q}}{Q_{\rm tr}^2 - M^2} = -\frac{g_{\rm DM}g_{\rm q}}{M^2}\left(1 + \frac{Q_{\rm tr}^2}{M^2} + \mathcal{O}\left(\frac{Q_{\rm tr}^4}{M^4}\right)\right) \simeq -\frac{1}{{m_*}^2}, \qquad (5.1)$$

where $Q_{\rm tr}$ is the momentum carried by the mediator, and $g_{\rm DM}$, $g_{\rm q}$ are the DM-mediator and quark-mediator couplings respectively. Similar expressions exist for other operators. Clearly the condition that must be satisfied for this approximation to be valid is that $Q_{\rm tr}^2 < M^2 = g_{\rm DM}g_{\rm q}{m_*}^2$. In this framework, there are clearly three regions to consider:

- $Q_{\rm tr}^2 \sim M^2$, in which case the EFT misses a resonant enhancement, and it is conservative to ignore this enhancement;
- $Q_{\rm tr}^2 \ll M^2$, in which case the EFT is valid; and
- $Q_{\rm tr}^2 \gg M^2$, in which case the signal cross section should fall according to a power of $Q_{\rm tr}^{-1}$ instead of M^{-1}. This is the problematic kinematic region.

We can use the condition $Q_{\rm tr}^2 < M^2 = g_{\rm DM}g_{\rm q}{m_*}^2$ to restrict the kinematics of the signal and enforce the validity of the EFT approximation (after the imposition of the event selection of the analysis). This truncated signal can then be used to derive the new, truncated limit on m_* as a function of $(m_{\rm DM}, g_{\rm DM}g_{\rm q})$.

For the example D5-like operator, $\sigma \propto {m_*}^{-4}$, and so there is a simple rule for converting a rescaled cross section into a rescaled constraint on m_* if the original limit is based on a simple cut-and-count procedure. Defining $\sigma_{\rm EFT}^{\rm cut}$ as the cross section truncated such that all events pass the condition $\sqrt{g_{\rm DM}g_{\rm q}}m_*^{\rm rescaled} > Q_{\rm tr}$, we have

$$m_*^{\rm rescaled} = \left(\frac{\sigma_{\rm EFT}}{\sigma_{\rm EFT}^{\rm cut}}\right)^{1/4} m_*^{\rm original}, \qquad (5.2)$$

which can be solved for $m_*^{\rm rescaled}$ via either iteration or a scan (note that $m_*^{\rm rescaled}$ appears on both the LHS and RHS of the equation). Similar relations exist for a given UV completion of each operator. The details and application of this procedure to ATLAS results can be found in Ref. [A$^+$15b] for a range of operators. Since this method uses the physical couplings and energy scale $Q_{\rm tr}$, it gives the strongest possible constraints in the EFT limit while remaining robust by ensuring the validity of the EFT approximation.

If a search is not simply a counting experiment and exploits the shapes of kinematic distributions, the condition on the momentum transfer should be applied on the benchmarks using generator level information, by discarding events that are invalid. This provides the necessary rescaling of the cross section while keeping the information on the change in the kinematic distributions due to the removal of the invalid events.

5.2 Outline of the procedure described in Ref. [RWZ15]

In [RWZ15] a procedure to extract model independent and consistent bounds within the EFT is described. This procedure can be applied to any effective Lagrangian describing the interactions between the DM and the SM, and provides limits that can be directly reinterpreted in any completion of the EFT.

The range of applicability of the EFT is defined by a mass scale m_{cut}, a parameter which marks the upper limit of the range of energy scales at which the EFT can be used reliably, independently of the particular completion of the model. Regardless of the details of the full theory, the energy scale probing the validity of the EFT is less than or equal to the center-of-mass energy E_{cm}, the total invariant mass of the hard final states of the reaction. To be specific, consider the basic monojet process with kinematics $p_1 + p_2 \to k + p_{\bar{\chi}\chi}$. k is the momentum of the outgoing jet, whereas $p_{\bar{\chi}\chi}$ is the momentum of the $\bar{\chi}\chi$ pair and $p_{\bar{\chi}\chi} = Q_{\text{tr}}$. $E_{\text{cm}}^2 = (p_1 + p_2)^2 > Q_{\text{tr}}^2$. The condition ensuring the validity of the EFT is, by definition of m_{cut},

$$E_{\text{cm}} < M_{\text{cut}} \,. \tag{5.3}$$

For example, in the specific case of a tree level mediation with a single mediator, m_{cut} can be interpreted as the mass of that mediator.

There are then at least three free parameters describing an EFT: the DM mass m_{DM}, the scale m_* of the interaction, and the cutoff scale m_{cut}.

We can use the same technique as above to restrict the signal to the events for which $E_{\text{cm}} < M_{\text{cut}}$, using only these events to derive the exclusion limits on m_* as a function of $(m_{\text{DM}}, M_{\text{cut}})$. We can also define an *effective coupling strength* $m_{\text{cut}} = g_* \, m_*$, where $g_*$is a free parameter that substitutes the parameter m_{cut}, and therefore derive exclusions on m_*as a function of (m_{DM}, g_*). This allows us to see how much of the theoretically allowed parameter space has been actually tested and how much is still unexplored; For example, in the Z'-type model considered above, $g_*$is equal to $\sqrt{g_{\text{DM}} g_{\text{q}}}$. The resulting plots are shown in [RWZ15] for a particular effective operator.

The advantage of this procedure is that the obtained bounds can be directly and easily recast in any completion of the EFT, by computing the parameters m_*, m_{cut} in the full model as functions of the parameters of the complete theory. On the other hand, the resulting limits will be weaker than those obtained using Q_{tr} and a specific UV completion.

5.3 Comments on Unitarity Considerations

Like the title says.

5.4 Recommendation for presentation of EFT results

A full discussion of the presentation of collider results is left to work beyond this Forum, where ATLAS, CMS, the theory community and the Direct and Indirect Detection communities are involved. In this report we recommend two strategies for the presentation of results in terms of Effective Field Theories. We divide the EFT operators in two categories: those which can be mapped to one or more UV-complete simplified models, such as those commonly used in LHC searches so far and detailed in [GIR+10], and those for which no UV completion is available, such as those outlined in Section 4.2. Results for the first class of operators can be recast using simplified models with high mediator masses, therefore removing the need to explicitly simulate EFT events and provide experimental limits for those operators. For the second class of models, a truncation procedure should be applied and the truncated results should be presented alongside the naive EFT results.

Three proposals for the treatment of EFT have been stated so far: (1) truncate using Q_{tr}, (2) truncate and iterate using Q_{tr}, and (3) truncate using E_{cm}. Another possibility is to present the raw EFT results, but qualify that they might not be valid. Finally, one can quantify the validity of the EFT result by presenting the sensitivity to R, the fraction of events that satisfy $\hat{s} > m^2_{\text{cut}}$, for example.

5.5 Recommendation for contact interaction theories with simplified models available

If a simplified model can be mapped to a given EFT, then the model's high-mediator-mass limit will converge to the EFT. This can be seen in Fig. 2.16, where the limits on the scale of the interaction of a Z'-like simplified model are presented in terms of the mediator mass. The limits at high mediator mass for this model are equivalent to those of the corresponding EFT benchmark. For this reason, experimental collaboration should deliver results for high-mass mediators instead of pure EFT results, and leave further reinterpretation to theorists.

We therefore recommend the addition of one point at very high mediator mass (5 TeV) to the scan, for each of the DM masses for the simplified models described in Section 2. The truncation procedure in Section 5.2 can be used to fine-tune the mediator mass to be simulated for this purpose. Studies are ongoing for $s-$channel vector mediators.

To do **The extrapolation to other couplings and mediator masses can be done using the Q_{tr} prescription for that model. (??)**

To do **Is this sufficient information for reinterpretation, or should we have instructions? (??)**

5.6 Recommendation for truncation of theories with no simplified models available

Whenever a UV completion is not available, EFT results can still be a source of useful information as described in Section 4.2.4. However, we can only naively control the validity of the EFT operator.

Despite the fact that a propagator was introduced to motivate the truncation procedure for $s-$ channel models, the prescription is only dependent upon the simplified model to derive the energy scaling. The simple fact remains that the effective coupling of the operator – g/Λ^n – should not allow momentum flow $Q > \Lambda$ or $g > 4\pi$. Given our ignorance of the actual kinematics, the truncation procedure suggested for this purpose is the one described in Section 5.2, as it is independent from any UV completion details.

Because there is no UV completion, the parameter m_{cut} can be treated more freely than an explicit function of g and Λ. It makes sense to choose m_{cut} such that we identify the transition region where the EFT stops being a good description of UV complete theories. This can be done using the ratio R, which is defined as the fraction of events for which $s_{hat} > m_{\text{cut}}^2$. For large values of m_{cut}, no events are thrown away in the truncation procedure, and R=1. As m_{cut} becomes smaller, eventually all events are thrown away in the truncation procedure, i.e. $R = 0$, and the EFT gives no exclusion limits for the chosen acceptance.

We propose a rough scan over m_{cut}, such that we find the values of m_{cut} for which R ranges from 0.1 to 1. The analysis can then perform a scan over several values of m_{cut} , and show the truncated limit for each one of them alongside the naive limit corresponding to $R = 1$.

To do **agree on how many? (??)**

6

Recommendations for evaluation of signal theoretical uncertainties

A prescription for determining the theoretical uncertainties (PDF and scale) from the POWHEGweights is being documented by the POWHEGauthors.

Here, we document some specific settings needed to run the POWHEGgeneration for the Dark Matter models:

A
Appendix: Implementation of Models

There are several matrix element implementations of the DM production through spin-0 and spin-1 mediators.

For a spin-1 mediator, the implementation in POWHEGgenerates DM pair production with 1 parton at next-to-leading order (NLO), whilst MadGraphand MCFMare at leading order (LO). As shown in POWHEGRef. [HKR13], including NLO corrections result in an enhancement in the cross section as compared to LO and though this is not significant, it does lead to a substantial reduction in the dependence on the choice of the renormalization and factorization scale and hence the theoretical uncertainty on the signal prediction. Since NLO calculations are available for the process in POWHEG, we recommend to proceed with POWHEGas the generator of choice.

For a spin-0 mediator, the top-quark loop is the most important consideration. The matrix element implementation of the $s-$ channel spin-0 mediated DM production is available in POWHEGwith the full top-loop calculation at LO [HR15]. The POWHEGimplementation includes the finite top quark mass dependence for DM pair production with 1 parton at LO. For consistency with the spin-1 generation, we recommend using POWHEGfor this case as well.

Here, we document some specific settings needed to run the POWHEGgeneration for the Dark Matter models. POWHEGcan handle the generation of events (be it at LO or NLO) in the 2 different modes explained in the following. The second one is the recommended one. The relevant keywords in the input card are `bornsuppfact`and `bornktmin`.

- POWHEGcan handle the generation of events (be it at LO or NLO) in the 2 different modes explained in the following. The second one is the recommended one. The relevant keywords in the input card are bornsuppfact and bornktmin.

- The POWHEGimplementation allows to generate a single sample that provides sufficient statistics in all signal regions. POWHEGgenerates weighted events and the `bornsuppfact`parameter is used to set the event suppression factor according to

$$F(k_{\mathrm{T}}) = \frac{k_{\mathrm{T}}^2}{k_{\mathrm{T}}^2 + \texttt{bornsuppfact}^2} \,. \tag{A.1}$$

In this way, the events at, for instance low $\not{E}_T$, are suppressed and receive higher event weights which ensures higher statistics at high $\not{E}_T$. We recommend to set `bornsuppfact`to 1000 (GeV).

- The `bornktmin`parameter allows to suppress the low $\not{E}_T$ region even further by starting the generation at a certain value of k_T. It is recommended to set this parameter to half the lower analysis $\not{E}_T$ cut, for the event selection used in the CMS/ATLAS monojet analyses for instance the proposed value for `bornktmin`is 150. However, this parameter should be set keeping in mind the event selection of all the analyses that will use these signal samples and hence a threshold lower than 150 may be required.
- Set `runningwidth`to 0.
- Set `mass_low`and `mass_high`to -1.
- The minimal values for `ncall1`, `itmx1`, `ncall2`, `itmx2`are 250000, 5, 1000000, 5 for the `DMV`model, respectively. In order to increase speed, set `foldsci`and `foldy`to 2 and keep `foldphi`at 1.
- The minimal values for `ncall1`, `itmx1`, `ncall2`, `itmx2`are 100000, 5, 100000, 5 for the `DMS_tloop`model, respectively.
- Allow negative weights for the `DMV`model by setting `withnegweights`to 1.
- Since the `DMS_tloop`model is a leading order process, set `LOeventsand` `bornonly`are set to 1 internally.
- Automatic calculation of systematic uncertainties associated with the choice of hard scale and PDFs.

[Comment on proper PDF sets to use, concerns about sea quark PDF in b-initiated diagrams (perhaps the latter belongs in the b-flavored DM section]

A.1 CKKW parton matching implementation

The parton matching techniques are implemented in the mono-jet like MC generation in order to avoid double counting the partons from matrix elements and parton showering. The CKKW matching is better developed and preferred [A$^+$14c] [A$^+$08]. As the illustration sample, the EFT D5 samples are generated with `MadGraph5_aMC@NLO`version 2.2.2. The technical implementations are shown as below.

On the generator side, i.e., `MadGraph5_aMC@NLO`:

- `ickkw = 0`
- `ktdurham =` matching scale
- `dparameter = 0.4`
- `dokt = T`

- `ptj=20`
- `drjj=0`
- `mmjj=0`
- `ptj1min=0`

On the parton showering side, i.e., PYTHIA 8:

- `Merging:ktType = 1`
- `Merging:TMS =` matching scale
- `1000022:all = chi chi  2 0 0 30.0 0.0 0.0 0.0 0.0`
- `1000022:isVisible = false`
- `Merging:doKTMerging = on`
- `Merging:Process = pp>chi,1000022chi ,-1000022`
- `Merging:nJetMax = 2`

The matching scales should be the same for the generation and parton showering. In MADGRAPH5aMCNLO, the particle data group ID `1000022` is used for weakly interacting dark matter candidates, which should be informed to PYTHIA 8.

In this test we are generating the process with up to two parton emissions, so the command `Merging:nJetMax = 2` is applied to PYTHIA 8. The different parton emission cases are generated separately:

- `p p > chi chi`
- `p p > chi chi  j`
- `p p > chi chi  j j`

Two matching scales are tested at 30 and 80 GeV. The differential jet rates are shown in Fig. A.1 for matching scale 30 GeV and Fig. A.2 for 80 GeV. The 80 GeV matching scale gives smoother distribution, which is desired to avoid artificial effect due to parton matching. There will be a small kink around the matching scale for both cases.

To compare the effect in a finer step, the matching scales at 30, 50, 70, 80 and 90 GeV are plotted in FigA.3. Globally good agreement is seen among different matching scales, with some difference observed around the matching scale. A closer look in this range shows that the 80 and 90 GeV matching scales produce very close distributions, so it is safe to use 80 GeV as the baseline matching scale.

The MC distributions for the missing transverse energy and transverse momenta for the leading and subleading jets are plotted in Fig.. For the mono-jet analysis, usually a missing transverse energy cut larger than 300 GeV is applied for offline selection, which makes the contribution of the 0-parton emission case negligible in the mono-jet analysis.

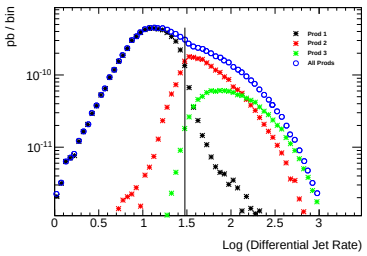

(a) $1 \to 2$ parton process

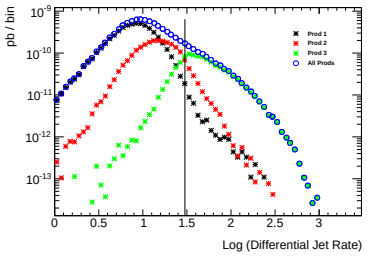

(b) $2 \to 3$ parton process

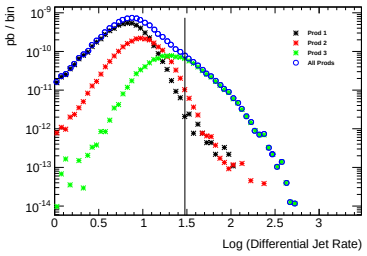

(c) $3 \to 4$ parton process

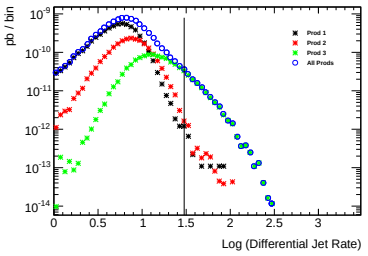

(d) $4 \to 5$ parton process

Figure A.1: Jet differential rates distributions for EFT D5 sample with CKKW matching scale at 30 GeV. 0-, 1- and 2-parton emission cases are generated separately. A vertical line is drawn at the matching scale.

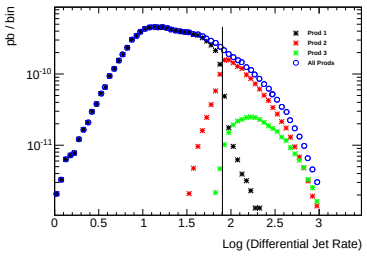

(a) $1 \to 2$ parton process

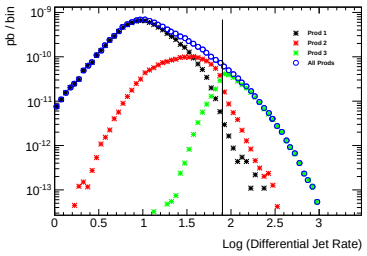

(b) $2 \to 3$ parton process

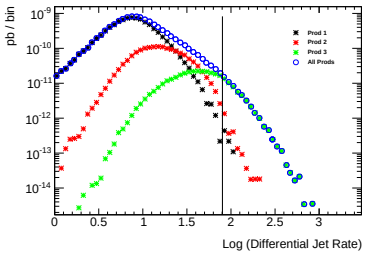

(c) $3 \to 4$ parton process

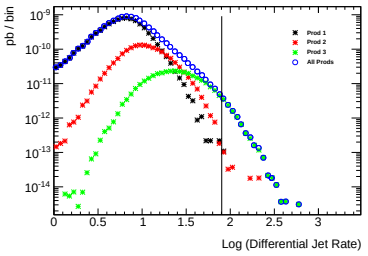

(d) $4 \to 5$ parton process

Figure A.2: Jet differential rates distributions for EFT D5 sample with CKKW matching scale at 80 GeV. 0-, 1- and 2-parton emission cases are generated separately. A vertical line is drawn at the matching scale.

A.2 *Parton emission generation*

In order to describe the signal kinematics correctly and save time in MC generation, the parton emissions will only be generated up to a certain numbers of parton and ignore the cases with more partons. The later ones usually have cross sections small enough and limited contribution in the interested kinematic regions.

It is found that the 3- or more-parton emission cases are negligible in our intersted regions, but the 2-parton emission case has significant contributions. The 0- and 1-parton emissions are out of discussion since they give the baseline signature in this analysis. The impacts of 2- and 3-parton emissions are quantified in this section.

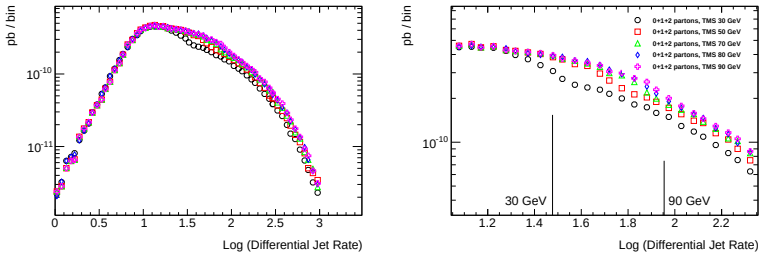

(a) $1 \to 2$ parton process

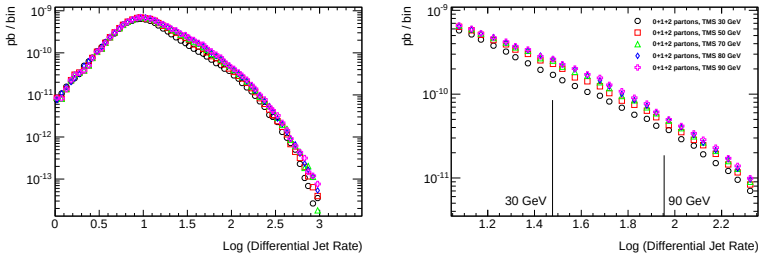

(b) $2 \to 3$ parton process

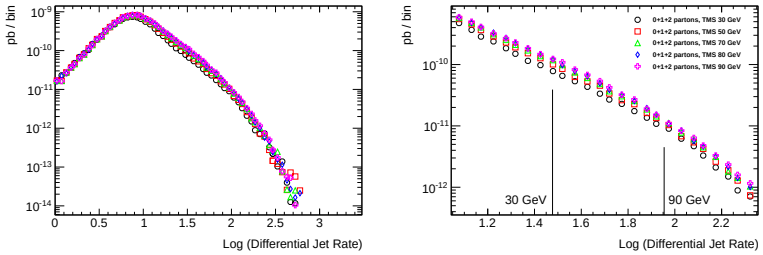

(c) $3 \to 4$ parton process

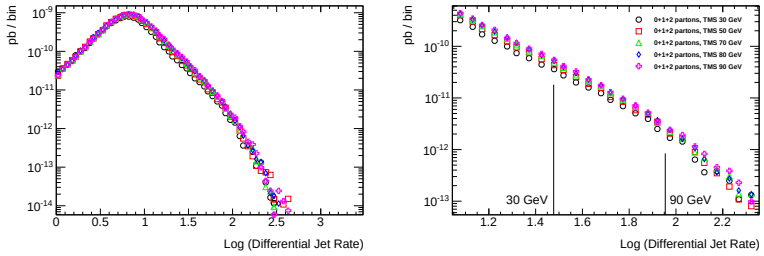

(d) $4 \to 5$ parton process

Figure A.3: Jet differential rates distributions for EFT D5 sample with CKKW matching scale at 30, 50, 70, 80 and 90 GeV. 0-, 1- and 2-parton emission cases are generated separately and the total merged contribution is shown. A closer look is shown around the matching scale.

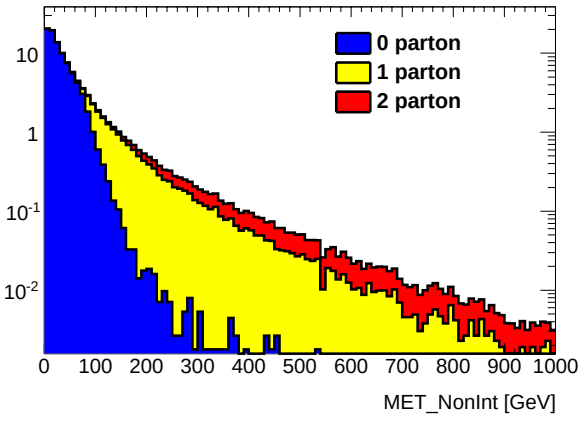

Figure A.4: Missing transverse momentum distributions for EFT D5 sample with CKKW matching scale at 80 GeV. 0-, 1- and 2-parton emission cases are generated separately and added together by cross sections. The 0-parton emission case has very limited contribution for missing transverse energy larger than 300 GeV region.

Here the 0-, 1-, 2- and 3-parton emissions are generated separately and requested in matching step with `Merging:nJetMax=3` and scale at 80 GeV in Pythia8for 0+1+2+3 parton emission case, while `Merging:nJetMax=2` requested for 0+1+2 case and `Merging:nJetMax=1` requested for 0+1 case. The MET distribution is plotted in Fig.A.5, while the jet multiplicity is shown in Fig.A.6.

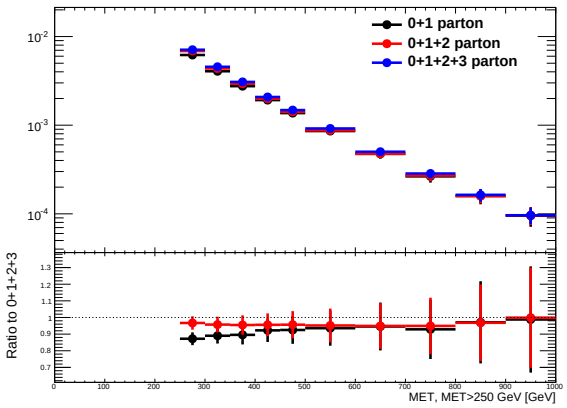

Figure A.5: Missing transverse momentum distributions for EFT D5 sample with CKKW matching scale at 80 GeV. 0-, 1-, 2- and 3-parton emission cases are generated separatedly and added together by cross sections.

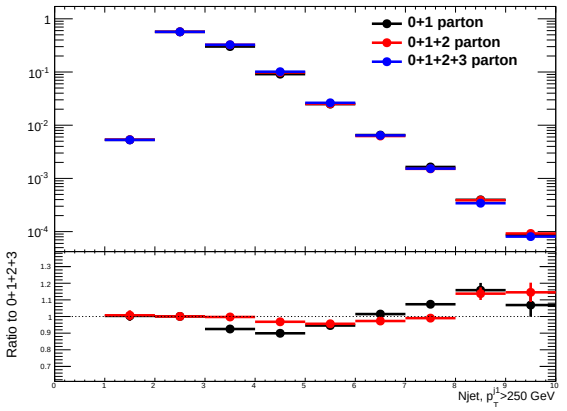

Figure A.6: Jet multiplicity distribution for EFT D5 sample with CKKW matching scale at 80 GeV. 0-, 1-, 2- and 3-parton emission cases are generated separatedly and added together by cross sections.

With the ATLAS run-I baseline cut (MET and leading jet p_T larger than 250 GeV, less than 4 jets), the 0+1 parton emission has 17.4% yield less compared to 0+1+2+3 parton emission, while the 0+1+2 has 2.2% less. With MET>400 GeV, 0+1 parton emission has 16.8% yield less and 0+1+2 parton emission has 2.4% less compared to 0+1+2+3 parton emission. With MET>600 GeV, 0+1 parton emission has 16.5% yield less and 0+1+2 parton emission has 2.9% less compared to 0+1+2+3 parton emission. The same numbers hold if a symmetric cut is added on leading jet transverse momentum.

A.3 Model implementation for mono-Higgs models

All three Higgs+MET models are generated at leading order with MadGraph 2.2.2, using Pythia8 for the parton shower. The MadGraph implementations of the scalar and vector models can be

found on the Forum SVN repository [For15f], while the 2HDM model can be found at this link [For15b].

In all cases, it is recommended not to handle the h decay through MadGraph as it does not include the proper h branching ratios, or, if using MadGraph, then the resulting cross section should be rescaled to match onto the correct branching ratio.

MADGRAPH DETAILS FOR SCALAR MEDIATOR HIGGS+MET MODEL

In this model, the contribution from the gghS box is included through an effective Lagrangian evaluated in the large m_t limit. This may overestimate the rates of the $h + \not{E}_T$ signal [HKU13], but a full evaluation is left to future studies.

MADGRAPH DETAILS FOR 2HDM HIGGS+MET MODEL

The two couplings that can be changed in the Madgraph model follow the nomenclature below:

- `Tb` - $\tan\beta$
- `gz` - g_z, gauge coupling of Z' to quarks

The other couplings are not changed, including `gx` (the $A\bar{\chi}\chi$ coupling) which has little impact on the signal. $\sin\alpha$ is fixed internally such that $\cos(\beta - \alpha) = 0$. The width of the Z' and A can be computed automatically within Madgraph. The couplings here don't affect the signal kinematics, so they can be fixed to default values and then the signal rates can be scaled appropriately.

The nomenclature for the masses in the Madgraph model is:

- `MZp` - PDG ID 32 - Z'
- `MA0` - PDG ID 28 - A
- `MX` - PDG ID 1000022 - dark matter particle

The other masses are unchanged and do not affect the result. Both $Z' \to hZ(\bar{\nu}\nu)$ and $Z' \to hA(\bar{\chi}\chi)$ contribute to the final state, scaling different with model parameters. We recommend to generate them separately, and then add the two signal processes together weighted by cross sections.

A.4 Heavy Flavor Models

In this particular model we recommend an additional care when choosing the flavor scheme generation. It is found that the best modeling of two b-quarks final states is achieved using a 4-flavor scheme and a massive treatment of the b-quarks . In addition, we recommend to calculate the cross sections of these models in the 5-flavor scheme, and as in the *tbart* case we provide values for the suggested coupling scan in the appendix. The PDF used to calculate these cross section is NNPDF3.0 (lhaid 263000).

.

To do **[TODO: Add reference] (??)**

To do **[TODO: The following figures are placeholders for now and will be added later] (??)**

Figure A.7: Comparison of the subleading jet p_T and b-jet multiplicity for bb+DM scalar model generated in the 4-flavor (left) and 5-flavor (right) schemes, respectively

A.5 Single Top Models

Card files for MadGraph are provided on the Forum SVN repository [For15d], corresponding to the Lagrangian from [AFM11]. Each coupling constant of this model can be set via the parameter card and the blocks which are relevant for the two models used for the experimental searches are described below. The relevant parameters in the MadGraph parameter cards, also expressed in the notation introduced in the previous Section, are as follows for the two models considered.

1. Resonant scalar model described by the Lagrangian (3.2)
   - `AQS` and `BQS`: 3×3 matrices (flavour space) fixing the coupling of the scalar ϕ (S stands for scalar) and *down*-type quarks (Q stands for quarks), previously called a^q/b^q_{SR}.
   - `A12S` and `B12S`: 3×1 matrices (flavor space) fixing the coupling of the new fermion χ (where 12 stands for spin-1/2 fermion) and up-type quarks, previously called $a^{1/2}_{VR}$.
2. Non-resonant vectorial model described by the Lagrangian (3.3)
   - `A1FC` and `B1FC`: 3×3 matrices (flavor space) fixing the coupling of the vector V (1 stands for vector) and up-type quarks, previously called a^1_{FC}.
   - particle name: the dark matter candidate χ is not implemented

The width of the scalar resonance and of the new vector are set to all allowed decays in the ATLAS implementation, while the only allowed decay in the CMS implementation to the new fermion and a top quark for the resonant model.

To do **Continue discussion between ATLAS and CMS to reach an agreement, or include instructions to compare results. (??)**

A.6 EFT Mono-Higgs implementation

These models are generated at leading order with MadGraph 2.2.2, using Pythia8 for the parton shower. No matching is performed. Parameter cards can be found on the Forum SVN repository: [For15f] for operators with Higgs+MET final states and [For15c] for $W/Z/\gamma$ final states.

A.7 Simplified Models of Mono-Higgs

These models are generated at leading order with MadGraph 2.2.2, using Pythia8 for the parton shower. No matching is performed. Parameter cards can be found on the Forum SVN repository [For15b, For15f].

B

Appendix: Detailed studies for EW models

B.1 Further W+MET models with possible cross-section enhancements

As pointed out in Ref. [BCD+15], the mono-W signature can probe the iso-spin violating interactions of dark matter with quarks. The relevant operators after the electroweak symmetry breaking is

$$\frac{1}{\Lambda^2}\overline{\chi}\gamma_\mu\chi\left(\overline{u}_L\gamma^\mu u_L + \xi\bar{d}_L\gamma^\mu d_L\right) . \tag{B.1}$$

Here, we only keep the left-handed quarks because the right-handed quarks do not radiate a W-gauge boson from the weak interaction. As the LHC constraints the cutoff to higher values, it is also important to know the corresponding operators before the electroweak symmetry. At the dimension-six level, the following operator

$$\frac{c_6}{\Lambda^2}\overline{\chi}\gamma_\mu\chi\,\overline{Q}_L\gamma^\mu Q_L \tag{B.2}$$

conserves iso-spin and provides us $\xi = 1$ [BCD+15]. At the dimension-eight level, new operators appear to induce iso-spin violation and can be

$$\frac{c_8^d}{\Lambda^4}\overline{\chi}\gamma_\mu\chi\,(H\overline{Q}_L)\gamma^\mu(Q_L H^\dagger) + \frac{c_8^u}{\Lambda^4}\overline{\chi}\gamma_\mu\chi\,(\tilde{H}\overline{Q}_L)\gamma^\mu(Q_L\tilde{H}^\dagger) . \tag{B.3}$$

After inputting the vacuum expectation value of the Higgs field, we have

$$\xi = \frac{c_6 + c_8^d\, v_{\rm EW}^2/2\Lambda^2}{c_6 + c_8^u\, v_{\rm EW}^2/2\Lambda^2} . \tag{B.4}$$

For a nonzero c_6 and $v_{\rm EW} \ll \Lambda$, the iso-spin violation effects are suppressed. On the other hand, the values of c_6, c_8^d and c_8^u depend on the UV-models.

There is one possible UV-model to obtain a zero value for c_6 and non-zero values for c_8^d and c_8^u. One can have the dark matter and the SM Higgs field charged under a new $U(1)'$. There is a small mass mixing between SM Z-boson and the new Z' with a mixing angle of $\mathcal{O}(v_{\rm EW}^2/M_{Z'}^2)$. After integrating out Z', one has different effective dark matter couplings to u_L and d_L fields, which are proportional to their couplings to the Z boson. For this model,

we have $c_6 = 0$ and

$$\xi = \frac{-\frac{1}{2} + \frac{1}{3}\sin^2\theta_W}{\frac{1}{2} - \frac{2}{3}\sin^2\theta_W} \approx -2.7 \tag{B.5}$$

and order of unity.

B.2 Simplified model corresponding to dimension-5 EFT operator

As an example of a simplified model corresponding to the dimension-5 EFT operator described in Section 4.2, we consider a Higgs portal with a scalar mediator. Models of this kind are among the most concise versions of simplified models that produce couplings of Dark Matter to pairs of gauge-bosons. Scalar fields may couple directly to pairs of electroweak gauge bosons, but must carry part of the electroweak vev. One may thus consider a simple model where Dark Matter couples to a a scalar singlet mediator, which mixes with the fields in the Higgs sector.

$$L \subset m_s S^2 + \lambda S^2 H^2 + \lambda^{'} S H^2 + y S \chi \overline{\chi} \tag{B.6}$$

Where H is a field in the Higgs sector that contains part of the electroweak vev, S is a heavy scalar singlet and χ is a Dark Matter field. There is then an S channel diagram where DM pairs couple to the singlet field S, which then mixes with a Higgs-sector field, and couples to W and Z bosons. This diagram contains 2 insertions of EW symmetry breaking fields, corresponding in form to the effective dimension-5 operator in the previous section.

B.3 Tabulated cross-sections

B.3.1 photon+MET signal, $s-$channel vector mediator model

B.3.2 Higgs+MET signal, vector mediator model

Figure B.1 shows the cross sections in this vector mediator model in the m_{med} vs m_{DM} plane. The tabulated values can be found in Table B.1

B.3.3 Higgs+MET signal, scalar mediator model

Figure B.2 shows the cross sections of the $pp \to H\chi\bar{\chi}$ process in this vector mediator model in the m_{med} vs m_{DM} plane. The tabulated values can be found in Table B.2

B.3.4 Higgs+MET signal from 2HDM model with a Z' and a new pseudoscalar

The leading order cross-sections from the Madgraph generator for the signal samples are listed in Tables B.3, B.4, B.5, for the various scan points recommended.

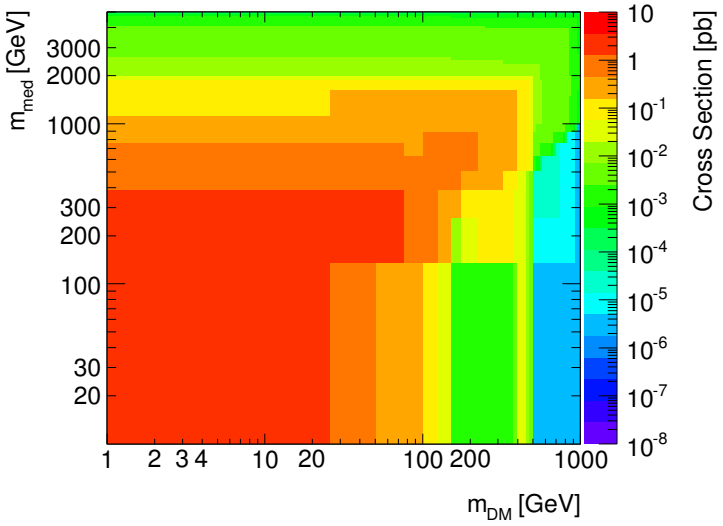

Figure B.1: Cross section of the $pp \to H\chi\bar{\chi}$ process in units of pico-barn for the vector mediator model.

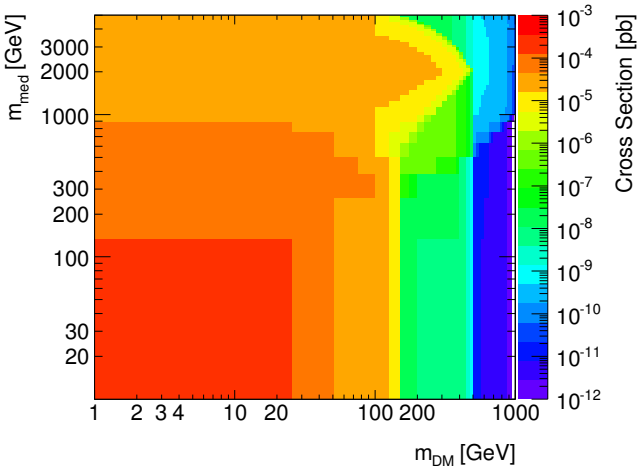

Figure B.2: Cross section of the $pp \to H\chi\bar{\chi}$ process in units of pico-barn for the scalar mediator model.

m_{DM} [GeV]	m_{med} [GeV]	$\sigma_{pp\to h\chi\bar{\chi}}$ [pb]
1	10	0.0003835
1	20	0.0003177
1	50	0.0001467
1	100	0.0001065
1	200	6.867e-05
1	300	7.388e-05
1	500	7.858e-05
1	1000	4.327e-05
1	2000	4.018e-05
1	5000	3.336e-05
10	10	3.603e-06
10	15	1.477e-05
10	50	0.0001547
10	100	0.0001104
10	5000	4.5e-05
50	10	1.401e-07
50	50	2.099e-07
50	95	2.813e-05
50	200	4.82e-05
50	300	7.485e-05
50	5000	3.384e-05
150	10	4.833e-09
150	295	3.65e-08
150	500	6.463e-07
150	5000	2.407e-08
500	10	8.672e-12
500	500	1.157e-11
500	995	5.254e-10
500	2000	7.138e-10
500	5000	5.87e-10
1000	10	5.946e-14
1000	1000	1.546e-13
1000	1995	8.316e-12
1000	5000	2.112e-11

Table B.1: Cross section of the $pp \to h\chi\bar{\chi}$ process in units of pico-barn for the vector mediator model.

m_{DM} [GeV]	m_{med} [GeV]	$\sigma_{pp\to h\chi\bar{\chi}}$ [pb]
1	10	2.389
1	20	2.483
1	50	2.98
1	100	2.881
1	200	2.344
1	300	2.041
1	500	0.9328
1	1000	0.1524
1	2000	0.008919
1	5000	1.39e-05
10	10	0.01895
10	15	0.7378
10	50	2.929
10	100	2.875
10	5000	1.387e-05
50	10	0.0003215
50	50	0.01127
50	95	0.2784
50	200	1.868
50	300	1.759
50	5000	1.391e-05
150	10	4.786e-06
150	200	0.004841
150	295	0.156
150	500	0.575
150	5000	1.391e-05
500	10	6.296e-09
500	500	2.855e-05
500	995	0.008244
500	2000	0.007899
500	5000	1.355e-05
1000	10	3.78e-11
1000	1000	7.372e-07
1000	1995	0.0004346
1000	5000	1.245e-05

Table B.2: Cross section of the $pp \to h\chi\bar{\chi}$ process in units of pico-barn for the scalar mediator.

$M_{Z'}$ (GeV)	$M_{A^0}(GeV)$	σ [pb]
600	300	1.55E-01
600	400	2.18E-02
800	300	8.30E-02
800	400	2.72E-02
800	500	1.09E-02
800	600	2.98E-03
1000	300	3.74E-02
1000	400	1.53E-02
1000	500	8.91E-03
1000	600	4.89E-03
1000	700	2.21E-03
1000	800	7.05E-04
1200	300	1.70E-02
1200	400	7.65E-03
1200	500	5.14E-03
1200	600	3.52E-03
1200	700	2.25E-03
1200	800	1.27E-03
1400	300	8.00E-03
1400	400	3.79E-03
1400	500	2.75E-03
1400	600	2.09E-03
1400	700	1.58E-03
1400	800	1.06E-03

Table B.3: LO cross-sections for $Z' \to A^0 h$ samples, varying $M_{Z'}$ and M_{A^0}, keeping the DM mass fixed to 100 GeV. The columns from left to right describe $M_{Z'}$, M_{A^0} and the sample cross section in pb.

$M_{Z'}$ (GeV)	$M_{A^0}(GeV)$	$M_{DM}(GeV)$	σ [pb]
1000	300	10	3.76E-02
1000	300	50	3.75E-02
1200	600	10	3.64E-03
1200	600	20	3.07E-03

Table B.4: LO cross-sections for $Z' \to A^0 h$ samples, when varying M_{DM}. The columns from left to right describe $M_{Z'}$, M_{A^0}, M_{DM}, and the sample cross section in pb.

$M_{Z'}$ (GeV)	σ [pb]
600	1.15E-01
800	3.21E-02
1000	1.13E-02
1200	4.54E-03
1400	2.00E-03

Table B.5: LO cross-sections for $Z' \to Zh$ exclusive samples, varying $M_{Z'}$. The columns from left to right describe $M_{Z'}$ and the sample cross section in pb.

C

Appendix: Table of cross sections for $t\bar{t}$+$\not{E}_T$ searches

C.1 Relic density constraints for b−flavored Dark Matter

For Dirac fermion DM the relic density is governed primarily by the s-wave annihilation cross section, which is given approximately given by:

$$\langle \sigma v \rangle = \frac{3g^4}{32\pi} \frac{m_\chi^2 \sqrt{1-(m_b/m_\chi)^2}}{\left(m_\Phi^2 + m_\chi^2 - m_b^2\right)} \approx \frac{3g^4 m_\chi^2}{32\pi(m_\Phi^2 + m_\chi^2)} \qquad \text{(C.1)}$$

We assume $\langle \sigma v \rangle = 1.5$ pb.

Figure C.1 shows the weights obtained for various dark matter and mediator massed required to obtain the correct relic density observed in the early universe.

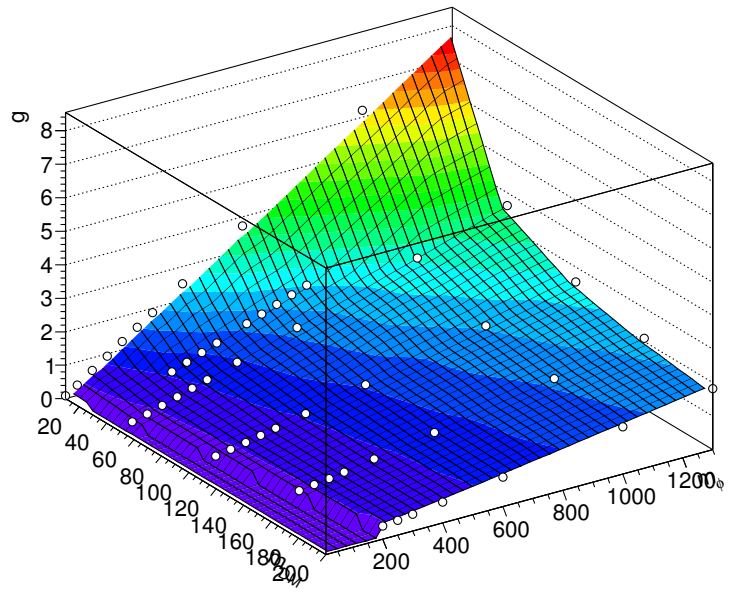

Figure C.1: Coupling constants required to obtain correct relic density in the early universe .

m_χ	m_Φ	σ [pb]	m_χ	m_Φ	σ [pb]
100	1000	5.48E-03	150	600	1.23E-01
100	100	1.91E-02	200	1000	4.94E-03
100	1300	8.90E-04	200	1300	7.82E-04
100	150	6.66E+00	200	200	2.66E-03
100	200	9.86E+00	200	250	6.48E-01
100	250	7.67E+00	200	300	1.69E+00
100	300	4.12E+00	200	400	9.41E-01
100	400	1.11E+00	200	600	1.16E-01
100	600	1.30E-01	35	250	9.75E+00
10	1000	5.80E-03	35	300	4.56E+00
10	100	7.84E+01	35	350	2.22E+00
10	10	4.09E-01	35	400	1.19E+00
10	1300	9.53E-04	35	500	3.76E-01
10	150	3.95E+01	35	550	2.24E-01
10	200	2.12E+01	35	600	1.37E-01
10	250	9.92E+00	35	650	8.62E-02
10	300	4.57E+00	35	700	5.54E-02
10	400	1.20E+00	50	1000	5.72E-03
10	50	1.59E+02	50	100	3.25E+01
10	600	1.38E-01	50	1300	9.34E-04
150	1000	5.22E-03	50	150	2.84E+01
150	1300	8.37E-04	50	200	1.84E+01
150	150	6.64E-03	50	250	9.52E+00
150	200	1.87E+00	50	300	4.49E+00
150	250	3.86E+00	50	400	1.17E+00
150	300	3.35E+00	50	50	7.06E-02
150	400	1.03E+00	50	600	1.36E-01

Table C.1: Dark matter masses m_χ and mediator masses m_Φ generated for $g = 1$ for 13 TeV. The resulting production cross sections are given in pb.

C.2 Cross sections for b−flavored Dark Matter

C.3 Cross sections for the $t\bar{t}$+DM scalar simplified model

Table C.5: Cross section calculation for each coupling choice and minimal width assumption for the $t\bar{t}$+DM scalar simplified model grid

Coupling (g)	m_{Phi} [GeV]	m_χ [GeV]	Γ_{min} [GeV]	σ [pb]
0.1	10	1	0.00374	0.1955 ± 0.00066
0.1	20	1	0.00785	0.1054 ± 0.00031
0.1	50	1	0.0199	0.03011 ± 9.1e-05
0.1	100	1	0.0398	0.006867 ± 2.5e-05
0.1	200	1	0.0797	0.0009397 ± 2.6e-06
0.1	300	1	0.120	0.0002942 ± 1e-06
0.1	500	1	0.311	5.289e-05 ± 1.9e-07
0.1	1000	1	0.881	3.717e-06 ± 1.5e-08

Continued on next page

Table C.5 – continued from previous page

Coupling (g)	m_{Phi} [GeV]	m_{χ} [GeV]	Γ_{min} [GeV]	σ [pb]
0.1	2000	1	1.91	7.81e-08 ± 3.2e-10
0.1	5000	1	4.89	1.111e-11 ± 5.5e-14
0.1	10	10	6.33	9.418e-06 ± 3.6e-08
0.1	50	10	0.0153	0.03016 ± 8.1e-05
0.1	100	10	0.0375	0.00686 ± 2.2e-05
0.1	5000	10	4.89	1.095e-11 ± 5.8e-14
0.1	15	10	3.84	1.2e-05 ± 4.8e-08
0.1	10	50	6.33	1.914e-07 ± 7.2e-10
0.1	50	50	2.34e-05	2.323e-07 ± 8.8e-10
0.1	200	50	0.0518	0.0009421 ± 2.8e-06
0.1	300	50	0.100	0.0002954 ± 9.8e-07
0.1	5000	50	4.88	1.059e-11 ± 5.3e-14
0.1	95	50	4.66e-05	6.548e-07 ± 2.3e-09
0.1	10	150	6.33	8.684e-09 ± 4.1e-11
0.1	200	150	0.000107	1.296e-08 ± 5.3e-11
0.1	500	150	0.214	3.92e-05 ± 1.6e-07
0.1	5000	150	4.87	9.079e-12 ± 5.9e-14
0.1	295	150	0.000185	3.969e-08 ± 2e-10
0.1	10	500	6.33	7.367e-11 ± 3.2e-13
0.1	500	500	0.112	9.86e-11 ± 3.9e-13
0.1	2000	500	1.63	5.953e-08 ± 2.3e-10
0.1	5000	500	4.77	5.768e-12 ± 2.6e-14
0.1	995	500	0.480	8.67e-10 ± 3.6e-12
0.1	10	1000	6.33	6.576e-13 ± 2.8e-15
0.1	1000	1000	0.483	9.426e-13 ± 4.2e-15
0.1	5000	1000	4.43	4.314e-12 ± 2e-14
0.1	1995	1000	1.11	1.589e-11 ± 9.2e-14
0.3	10	1	0.0337	1.766 ± 0.006
0.3	20	1	0.0706	0.9493 ± 0.0029
0.3	50	1	0.179	0.2695 ± 0.00082
0.3	100	1	0.358	0.06159 ± 0.00021
0.3	200	1	0.717	0.008466 ± 2.4e-05
0.3	300	1	1.08	0.002649 ± 8.5e-06
0.3	500	1	2.80	0.0004741 ± 1.6e-06
0.3	1000	1	7.93	3.349e-05 ± 1.3e-07
0.3	2000	1	17.2	7.227e-07 ± 3.2e-09
0.3	5000	1	44.0	5.42e-10 ± 3.5e-12
0.3	10	10	5.70	0.0007633 ± 2.5e-06
0.3	50	10	0.138	0.2706 ± 0.00082
0.3	100	10	0.337	0.06182 ± 0.00022
0.3	5000	10	44.0	5.386e-10 ± 2.7e-12
0.3	15	10	3.45e-05	0.0009761 ± 3.6e-06
0.3	10	50	5.70	1.561e-05 ± 6.1e-08
0.3	50	50	0.000210	1.892e-05 ± 7.3e-08
0.3	200	50	0.466	0.008444 ± 2.2e-05

Continued on next page

Table C.5 – continued from previous page

Coupling (g)	m_{Phi} [GeV]	m_{χ} [GeV]	Γ_{min} [GeV]	σ [pb]
0.3	300	50	0.902	0.002677 ± 7.7e-06
0.3	5000	50	44.0	5.012e-10 ± 3.1e-12
0.3	95	50	0.000420	5.306e-05 ± 2.3e-07
0.3	10	150	5.70	7.02e-07 ± 3.3e-09
0.3	200	150	0.000962	1.051e-06 ± 4.1e-09
0.3	500	150	1.92	0.000351 ± 1.3e-06
0.3	5000	150	43.9	3.805e-10 ± 2.4e-12
0.3	295	150	0.00166	3.211e-06 ± 1.5e-08
0.3	10	500	5.70	5.945e-09 ± 2.7e-11
0.3	500	500	1.01	7.991e-09 ± 4.9e-11
0.3	2000	500	14.7	5.347e-07 ± 2.3e-09
0.3	5000	500	42.9	1.264e-10 ± 6.9e-13
0.3	995	500	4.32	7.039e-08 ± 3e-10
0.3	10	1000	5.70	5.302e-11 ± 2.4e-13
0.3	1000	1000	4.35	7.606e-11 ± 3.4e-13
0.3	5000	1000	39.8	4.887e-11 ± 2.1e-13
0.3	1995	1000	10.0	1.279e-09 ± 6.4e-12
0.7	10	1	0.183	9.624 ± 0.034
0.7	20	1	0.384	5.129 ± 0.015
0.7	50	1	0.974	1.461 ± 0.0048
0.7	100	1	1.95	0.3324 ± 0.0014
0.7	200	1	3.90	0.04588 ± 0.00013
0.7	300	1	5.86	0.01442 ± 5e-05
0.7	500	1	15.2	0.002548 ± 9.6e-06
0.7	1000	1	43.2	0.0001813 ± 8.9e-07
0.7	2000	1	93.7	4.478e-06 ± 1.9e-08
0.7	5000	1	239	1.504e-08 ± 6.7e-11
0.7	10	10	3.10e-05	0.02264 ± 8.3e-05
0.7	50	10	0.752	1.462 ± 0.0041
0.7	100	10	1.84	0.3347 ± 0.0011
0.7	5000	10	239	1.494e-08 ± 6.7e-11
0.7	15	10	0.000188	0.02881 ± 0.00011
0.7	10	50	3.10e-05	0.0004597 ± 1.8e-06
0.7	50	50	0.00114	0.0005588 ± 2.3e-06
0.7	200	50	2.54	0.0458 ± 0.00013
0.7	300	50	4.91	0.01433 ± 4.9e-05
0.7	5000	50	239	1.363e-08 ± 6.9e-11
0.7	95	50	0.00228	0.00157 ± 7.3e-06
0.7	10	150	3.10e-05	2.097e-05 ± 8.5e-08
0.7	200	150	0.00524	3.123e-05 ± 1.6e-07
0.7	500	150	10.5	0.001889 ± 6.8e-06
0.7	5000	150	239	1.018e-08 ± 5.2e-11
0.7	295	150	0.00906	9.511e-05 ± 4e-07
0.7	10	500	3.10e-05	1.78e-07 ± 6.8e-10
0.7	500	500	5.48	2.373e-07 ± 9.8e-10

Continued on next page

Table C.5 – continued from previous page

Coupling (g)	m_{Phi} [GeV]	m_{χ} [GeV]	Γ_{min} [GeV]	σ [pb]
0.7	2000	500	80.0	2.877e-06 ± 1.2e-08
0.7	5000	500	234	2.682e-09 ± 1.7e-11
0.7	995	500	23.5	1.939e-06 ± 7.3e-09
0.7	10	1000	3.10e-05	1.584e-09 ± 7.6e-12
0.7	1000	1000	23.7	2.26e-09 ± 1.1e-11
0.7	5000	1000	217	5.244e-10 ± 2.4e-12
0.7	1995	1000	54.52	3.227e-08 ± 1.4e-10
1.	10	1	0.374	19.59 ± 0.062
1.	20	1	0.785	10.48 ± 0.03
1.	50	1	1.99	2.941 ± 0.0091
1.	100	1	3.98	0.6723 ± 0.0024
1.	200	1	7.97	0.09327 ± 0.00029
1.	300	1	12.0	0.0295 ± 0.00011
1.	500	1	31.1	0.00518 ± 2.2e-05
1.	1000	1	88.1	0.0003687 ± 1.7e-06
1.	2000	1	191	1.034e-05 ± 4.6e-08
1.	5000	1	489	6.17e-08 ± 2.4e-10
1.	10	10	6.33e-05	0.09487 ± 0.00036
1.	50	10	1.53	2.942 ± 0.0083
1.	100	10	3.75	0.6732 ± 0.0023
1.	5000	10	489	6.138e-08 ± 2.3e-10
1.	15	10	0.000384	0.1202 ± 0.0005
1.	10	50	6.33e-05	0.001906 ± 8.4e-06
1.	50	50	0.00234	0.002329 ± 1e-05
1.	200	50	5.18	0.09224 ± 0.00025
1.	300	50	10.0	0.02901 ± 0.0001
1.	5000	50	488	5.616e-08 ± 2.2e-10
1.	95	50	0.00466	0.006558 ± 2.7e-05
1.	10	150	6.33e-05	8.634e-05 ± 4e-07
1.	200	150	0.0107	0.00013 ± 5.7e-07
1.	500	150	21.4	0.003754 ± 1.9e-05
1.	5000	150	487	4.162e-08 ± 1.8e-10
1.	295	150	0.0185	0.000394 ± 1.6e-06
1.	10	500	6.33e-05	7.356e-07 ± 3.3e-09
1.	500	500	11.2	9.894e-07 ± 5e-09
1.	2000	500	163	5.808e-06 ± 2.4e-08
1.	5000	500	477	1.048e-08 ± 5.7e-11
1.	995	500	48.0	7.3e-06 ± 3.2e-08
1.	10	1000	6.33e-05	6.607e-09 ± 2.7e-11
1.	1000	1000	48.3	9.433e-09 ± 4e-11
1.	5000	1000	443	1.7e-09 ± 1e-11
1.	1995	1000	111	1.108e-07 ± 5.7e-10
1.5	10	1	0.842	44.1 ± 0.16
1.5	20	1	1.77	23.19 ± 0.078
1.5	50	1	4.47	6.471 ± 0.02

Continued on next page

Table C.5 – continued from previous page

Coupling (g)	m_{Phi} [GeV]	m_{χ} [GeV]	Γ_{min} [GeV]	σ [pb]
1.5	100	1	8.96	1.478 ± 0.0061
1.5	200	1	17.9	0.2074 ± 0.00068
1.5	300	1	26.9	0.0657 ± 0.00024
1.5	500	1	69.9	0.01123 ± 5.6e-05
1.5	1000	1	198	0.0008135 ± 3.5e-06
1.5	2000	1	430	2.873e-05 ± 1.2e-07
1.5	5000	1	1099	2.964e-07 ± 1.2e-09
1.5	10	10	0.000143	0.4772 ± 0.0019
1.5	50	10	3.45	6.499 ± 0.022
1.5	100	10	8.43	1.469 ± 0.0056
1.5	5000	10	1099	2.932e-07 ± 1.3e-09
1.5	15	10	0.000863	0.613 ± 0.0022
1.5	10	50	0.000143	0.009661 ± 3.4e-05
1.5	50	50	0.00526	0.0118 ± 4.2e-05
1.5	200	50	11.7	0.2032 ± 0.00064
1.5	300	50	22.6	0.06446 ± 0.00024
1.5	5000	50	1099	2.687e-07 ± 1.2e-09
1.5	95	50	0.0105	0.03298 ± 0.00013
1.5	10	150	0.000143	0.0004384 ± 1.8e-06
1.5	200	150	0.0241	0.0006557 ± 2.7e-06
1.5	500	150	48.1	0.008036 ± 3.9e-05
1.5	5000	150	1097	2.008e-07 ± 1.4e-09
1.5	295	150	0.0416	0.002022 ± 8.3e-06
1.5	10	500	0.000143	3.712e-06 ± 1.5e-08
1.5	500	500	25.2	5.001e-06 ± 1.9e-08
1.5	2000	500	367	1.223e-05 ± 6e-08
1.5	5000	500	1072	4.885e-08 ± 2.7e-10
1.5	995	500	108	2.975e-05 ± 1.5e-07
1.5	10	1000	0.000143	3.342e-08 ± 1.5e-10
1.5	1000	1000	109	4.786e-08 ± 2.1e-10
1.5	5000	1000	996	6.688e-09 ± 3.1e-11
1.5	1995	1000	250	3.982e-07 ± 2.2e-09
2.	10	1	1.50	78.28 ± 0.3
2.	20	1	3.14	40.52 ± 0.13
2.	50	1	7.95	11.12 ± 0.038
2.	100	1	15.9	2.531 ± 0.011
2.	200	1	31.9	0.3644 ± 0.0012
2.	300	1	47.8	0.1157 ± 0.00053
2.	500	1	124	0.01917 ± 9e-05
2.	1000	1	353	0.001382 ± 6.1e-06
2.	2000	1	765	5.899e-05 ± 2.7e-07
2.	5000	1	1954	8.392e-07 ± 3.4e-09
2.	10	10	0.0002532	1.509 ± 0.0052
2.	50	10	6.14	11.19 ± 0.037
2.	100	10	15.0	2.513 ± 0.0091

Continued on next page

Table C.5 – continued from previous page

Coupling (g)	m_{Phi} [GeV]	m_{χ} [GeV]	Γ_{min} [GeV]	σ [pb]
2.	5000	10	1954	8.317e-07 ± 3.6e-09
2.	15	10	0.00153	1.923 ± 0.0066
2.	10	50	0.000253	0.03065 ± 0.00011
2.	50	50	0.00934	0.03716 ± 0.00018
2.	200	50	20.7	0.3487 ± 0.0011
2.	300	50	40.1	0.1114 ± 0.00041
2.	5000	50	1953	7.612e-07 ± 4e-09
2.	95	50	0.0187	0.1045 ± 0.0005
2.	10	150	0.000253	0.001376 ± 6.3e-06
2.	200	150	0.0428	0.002081 ± 9.1e-06
2.	500	150	85.5	0.01343 ± 5.5e-05
2.	5000	150	1950	5.605e-07 ± 3e-09
2.	295	150	0.0740	0.006316 ± 2.8e-05
2.	10	500	0.000253	1.177e-05 ± 4.8e-08
2.	500	500	44.8	1.586e-05 ± 8.6e-08
2.	2000	500	653	1.953e-05 ± 9.5e-08
2.	5000	500	1907	1.333e-07 ± 6.5e-10
2.	995	500	192	7.427e-05 ± 3.9e-07
2.	10	1000	0.000253	1.056e-07 ± 5e-10
2.	1000	1000	193	1.507e-07 ± 6.7e-10
2.	5000	1000	1771	1.624e-08 ± 6.7e-11
2.	1995	1000	445	8.764e-07 ± 5.3e-09
2.5	10	1	2.34	122.2 ± 0.44
2.5	20	1	4.90	61.98 ± 0.21
2.5	50	1	12.4	16.62 ± 0.057
2.5	100	1	24.9	3.788 ± 0.016
2.5	200	1	49.8	0.551 ± 0.0021
2.5	300	1	74.7	0.1762 ± 0.00073
2.5	500	1	194	0.02816 ± 0.00014
2.5	1000	1	551	0.001971 ± 8.5e-06
2.5	2000	1	1195	9.628e-05 ± 4.1e-07
2.5	5000	1	3053	1.685e-06 ± 6.9e-09
2.5	10	10	0.000396	3.687 ± 0.016
2.5	50	10	9.59	16.9 ± 0.064
2.5	100	10	23.4	3.755 ± 0.014
2.5	5000	10	3053	1.68e-06 ± 6.7e-09
2.5	15	10	0.00240	4.719 ± 0.016
2.5	10	50	0.000396	0.07571 ± 0.00036
2.5	50	50	0.0146	0.09133 ± 0.00038
2.5	200	50	32.4	0.5224 ± 0.0016
2.5	300	50	62.6	0.1667 ± 0.00074
2.5	5000	50	3052	1.519e-06 ± 8e-09
2.5	95	50	0.0291	0.2547 ± 0.00089
2.5	10	150	0.000396	0.003396 ± 1.7e-05
2.5	200	150	0.0668	0.005081 ± 2.2e-05

Continued on next page

Table C.5 – continued from previous page

Coupling (g)	m_{Phi} [GeV]	m_{χ} [GeV]	Γ_{min} [GeV]	σ [pb]
2.5	500	150	133	0.01954 ± 8.7e-05
2.5	5000	150	3046	1.123e-06 ± 6.5e-09
2.5	295	150	0.116	0.01551 ± 6.8e-05
2.5	10	500	0.000396	2.874e-05 ± 1.2e-07
2.5	500	500	69.95	3.883e-05 ± 1.9e-07
2.5	2000	500	1020	2.555e-05 ± 1.2e-07
2.5	5000	500	2979	2.592e-07 ± 1.3e-09
2.5	995	500	300	0.0001417 ± 8e-07
2.5	10	1000	0.0003957	2.584e-07 ± 1.2e-09
2.5	1000	1000	302.2	3.668e-07 ± 1.5e-09
2.5	5000	1000	2767	2.841e-08 ± 1.3e-10
2.5	1995	1000	695.4	1.487e-06 ± 7.2e-09
3.	10	1	3.369	176.2 ± 0.67
3.	20	1	7.061	87.59 ± 0.35
3.	50	1	17.88	22.91 ± 0.078
3.	100	1	35.83	5.118 ± 0.024
3.	200	1	71.71	0.7647 ± 0.0027
3.	300	1	107.6	0.2474 ± 0.001
3.	500	1	279.8	0.0379 ± 0.00019
3.	1000	1	793.2	0.002521 ± 1.4e-05
3.	2000	1	1720	0.0001342 ± 4.9e-07
3.	5000	1	4396	2.668e-06 ± 1e-08
3.	10	10	0.0005698	7.631 ± 0.029
3.	50	10	13.81	23.27 ± 0.083
3.	100	10	33.73	5.138 ± 0.019
3.	5000	10	4396	2.62e-06 ± 1e-08
3.	15	10	0.003453	9.7 ± 0.044
3.	10	50	0.0005698	0.1553 ± 0.00062
3.	50	50	0.02102	0.1886 ± 0.0008
3.	200	50	46.61	0.7242 ± 0.0023
3.	300	50	90.2	0.2308 ± 0.0012
3.	5000	50	4395	2.394e-06 ± 1.4e-08
3.	95	50	0.04196	0.5301 ± 0.0019
3.	10	150	0.0005698	0.007036 ± 3.3e-05
3.	200	150	0.09621	0.01053 ± 4.4e-05
3.	500	150	192.4	0.02598 ± 0.00012
3.	5000	150	4387	1.767e-06 ± 1.2e-08
3.	295	150	0.1664	0.03185 ± 0.00013
3.	10	500	0.0005698	5.989e-05 ± 2.7e-07
3.	500	500	100.7	7.985e-05 ± 3.1e-07
3.	2000	500	1469	3.073e-05 ± 1.6e-07
3.	5000	500	4290	3.921e-07 ± 1.8e-09
3.	995	500	432.1	0.0002263 ± 9.7e-07
3.	10	1000	0.0005698	5.337e-07 ± 2.3e-09
3.	1000	1000	435.1	7.512e-07 ± 4.1e-09

Continued on next page

Table C.5 – continued from previous page

Coupling (g)	m_{Phi} [GeV]	m_{χ} [GeV]	Γ_{min} [GeV]	σ [pb]
3.	5000	1000	3984	4.011e-08 ± 1.7e-10
3.	1995	1000	1001	2.15e-06 ± 1e-08
3.5	10	1	4.585	242 ± 0.94
3.5	20	1	9.611	116.6 ± 0.36
3.5	50	1	24.34	29.39 ± 0.093
3.5	100	1	48.77	6.585 ± 0.027
3.5	200	1	97.6	0.993 ± 0.0042
3.5	300	1	146.4	0.3235 ± 0.0019
3.5	500	1	380.8	0.04713 ± 0.00021
3.5	1000	1	1080	0.00299 ± 1.5e-05
3.5	2000	1	2341	0.0001649 ± 6.2e-07
3.5	5000	1	5984	3.53e-06 ± 1.8e-08
3.5	10	10	0.0007756	14.23 ± 0.052
3.5	50	10	18.79	30.44 ± 0.11
3.5	100	10	45.91	6.51 ± 0.024
3.5	5000	10	5984	3.514e-06 ± 1.3e-08
3.5	15	10	0.004699	18.1 ± 0.067
3.5	10	50	0.0007756	0.2893 ± 0.0011
3.5	50	50	0.02861	0.3505 ± 0.0017
3.5	200	50	63.45	0.9325 ± 0.0035
3.5	300	50	122.8	0.2972 ± 0.0014
3.5	5000	50	5982	3.185e-06 ± 1.7e-08
3.5	95	50	0.05711	0.981 ± 0.0043
3.5	10	150	0.0007756	0.01295 ± 6.7e-05
3.5	200	150	0.131	0.01947 ± 8.7e-05
3.5	500	150	261.9	0.03264 ± 0.00016
3.5	5000	150	5971	2.316e-06 ± 1.3e-08
3.5	295	150	0.2265	0.05947 ± 0.00026
3.5	10	500	0.0007756	0.0001104 ± 4.8e-07
3.5	500	500	137.1	0.0001486 ± 7.1e-07
3.5	2000	500	2000	3.401e-05 ± 1.5e-07
3.5	5000	500	5839	5.061e-07 ± 2.6e-09
3.5	995	500	588.1	0.0003275 ± 1.4e-06
3.5	10	1000	0.0007756	9.835e-07 ± 4.7e-09
3.5	1000	1000	592.2	1.401e-06 ± 7.5e-09
3.5	5000	1000	5423	4.878e-08 ± 2.5e-10
3.5	1995	1000	1363	2.809e-06 ± 1.2e-08

Table C.6: Cross section calculation for each coupling choice and minimal width assumption for the $t\bar{t}$+DM pseudoscalar simplified model grid

Coupling (g)	m_{Phi} [GeV]	m_{χ} [GeV]	Γ_{min} [GeV]	σ [pb]
0.1	10	1	0.004	0.004237 ± 1.8e-05

Continued on next page

Table C.6 – continued from previous page

Coupling (g)	m_{Phi} [GeV]	m_{χ} [GeV]	Γ_{min} [GeV]	σ [pb]
0.1	20	1	0.008	0.003931 ± 1.5e-05
0.1	50	1	0.02	0.003005 ± 1.4e-05
0.1	100	1	0.04	0.001905 ± 8.1e-06
0.1	200	1	0.08	0.0008608 ± 3.3e-06
0.1	300	1	0.12	0.0004105 ± 1.6e-06
0.1	500	1	0.413	5.591e-05 ± 2.2e-07
0.1	1000	1	0.949	3.961e-06 ± 1.7e-08
0.1	2000	1	1.95	7.961e-08 ± 3.2e-10
0.1	5000	1	4.9	1.19e-11 ± 7.1e-14
0.1	10	10	2.0	1.489e-06 ± 9.6e-09
0.1	50	10	0.018	0.003 ± 1.5e-05
0.1	100	10	0.04	0.001926 ± 1e-05
0.1	5000	10	4.9	1.179e-11 ± 6.2e-14
0.1	15	10	5.9	1.798e-06 ± 1e-08
0.1	10	50	2.0	2.42e-07 ± 1.1e-09
0.1	50	50	2.5e-05	2.97e-07 ± 1.2e-09
0.1	200	50	0.069	0.0008585 ± 4.7e-06
0.1	300	50	0.11	0.0004108 ± 1.7e-06
0.1	5000	50	4.9	1.166e-11 ± 6.5e-14
0.1	95	50	5.4e-05	1.065e-06 ± 5.7e-09
0.1	10	150	2.0	2.359e-08 ± 1.2e-10
0.1	200	150	0.00019	4.119e-08 ± 2e-10
0.1	500	150	0.37	4.953e-05 ± 1.9e-07
0.1	5000	150	4.9	1.066e-11 ± 7.3e-14
0.1	295	150	0.00063	3.366e-07 ± 1.8e-09
0.1	10	500	2.0	2.276e-10 ± 9.7e-13
0.1	500	500	0.21	3.261e-10 ± 1.4e-12
0.1	2000	500	1.84	7.296e-08 ± 2.9e-10
0.1	5000	500	4.86	6.723e-12 ± 3.1e-14
0.1	995	500	0.55	1.418e-08 ± 9.2e-11
0.1	10	1000	2.0	2.593e-12 ± 1.2e-14
0.1	1000	1000	0.55	3.939e-12 ± 1.5e-14
0.1	5000	1000	4.74	4.964e-12 ± 2.1e-14
0.1	1995	1000	1.15	4.176e-10 ± 2.2e-12
0.3	10	1	0.035	0.03821 ± 0.0002
0.3	20	1	0.071	0.03519 ± 0.00017
0.3	50	1	0.179	0.02707 ± 0.00012
0.3	100	1	0.359	0.01728 ± 7e-05
0.3	200	1	0.718	0.007718 ± 3e-05
0.3	300	1	1.08	0.003678 ± 1.5e-05
0.3	500	1	3.72	0.0004992 ± 1.9e-06
0.3	1000	1	8.54	3.541e-05 ± 1.5e-07
0.3	2000	1	17.5	7.434e-07 ± 2.9e-09
0.3	5000	1	44.1	6.065e-10 ± 3.3e-12
0.3	10	10	1.8e-05	0.0001216 ± 7.6e-07

Continued on next page

Table C.6 – continued from previous page

Coupling (g)	m_{Phi} [GeV]	m_{χ} [GeV]	Γ_{min} [GeV]	σ [pb]
0.3	50	10	0.164	0.0273 ± 0.00013
0.3	100	10	0.351	0.01718 ± 6.8e-05
0.3	5000	10	44.1	6.164e-10 ± 4.3e-12
0.3	15	10	5.3e-05	0.0001503 ± 8.7e-07
0.3	10	50	1.8e-05	1.985e-05 ± 1e-07
0.3	50	50	0.000226	2.405e-05 ± 1.1e-07
0.3	200	50	0.622	0.007692 ± 2.8e-05
0.3	300	50	1.02	0.003682 ± 1.5e-05
0.3	5000	50	44.1	6.003e-10 ± 3.4e-12
0.3	95	50	0.00049	8.676e-05 ± 5.3e-07
0.3	10	150	1.8e-05	1.91e-06 ± 8.5e-09
0.3	200	150	0.00173	3.362e-06 ± 1.4e-08
0.3	500	150	3.36	0.0004437 ± 1.9e-06
0.3	5000	150	44.1	5.071e-10 ± 2.9e-12
0.3	295	150	0.00568	2.746e-05 ± 1.9e-07
0.3	10	500	1.8e-05	1.837e-08 ± 8.7e-11
0.3	500	500	1.93	2.647e-08 ± 1.1e-10
0.3	2000	500	16.6	6.605e-07 ± 2.6e-09
0.3	5000	500	43.8	1.956e-10 ± 1e-12
0.3	995	500	4.93	1.111e-06 ± 5.3e-09
0.3	10	1000	1.8e-05	2.107e-10 ± 8.3e-13
0.3	1000	1000	4.96	3.169e-10 ± 1.3e-12
0.3	5000	1000	42.6	6.77e-11 ± 3.4e-13
0.3	1995	1000	10.4	3.021e-08 ± 1.4e-10
0.7	10	1	0.191	0.213 ± 0.0011
0.7	20	1	0.389	0.1942 ± 0.00094
0.7	50	1	0.975	0.1483 ± 0.00074
0.7	100	1	1.95	0.09367 ± 0.00043
0.7	200	1	3.91	0.04172 ± 0.00017
0.7	300	1	5.89	0.01991 ± 7.9e-05
0.7	500	1	20.3	0.002681 ± 1.3e-05
0.7	1000	1	46.5	0.0001949 ± 8.2e-07
0.7	2000	1	95.5	4.648e-06 ± 2.2e-08
0.7	5000	1	240	1.714e-08 ± 7.6e-11
0.7	10	10	9.78e-05	0.00357 ± 1.7e-05
0.7	50	10	0.895	0.1482 ± 0.0007
0.7	100	10	1.91	0.09343 ± 0.00038
0.7	5000	10	240	1.71e-08 ± 8e-11
0.7	15	10	0.000289	0.004422 ± 2.6e-05
0.7	10	50	9.78e-05	0.0005819 ± 2.5e-06
0.7	50	50	0.00123	0.0007124 ± 3.3e-06
0.7	200	50	3.39	0.04143 ± 0.00018
0.7	300	50	5.55	0.01998 ± 9.3e-05
0.7	5000	50	240	1.661e-08 ± 1e-10
0.7	95	50	0.00266	0.002575 ± 1.7e-05

Continued on next page

Table C.6 – continued from previous page

Coupling (g)	m_{Phi} [GeV]	m_{χ} [GeV]	Γ_{min} [GeV]	σ [pb]
0.7	10	150	9.78e-05	5.65e-05 ± 2.9e-07
0.7	200	150	0.0094	9.979e-05 ± 4.8e-07
0.7	500	150	18.3	0.002329 ± 1.3e-05
0.7	5000	150	240	1.393e-08 ± 6.7e-11
0.7	295	150	0.0309	0.0008152 ± 4e-06
0.7	10	500	9.78e-05	5.458e-07 ± 2.2e-09
0.7	500	500	10.5	7.888e-07 ± 3.2e-09
0.7	2000	500	90.3	3.71e-06 ± 1.6e-08
0.7	5000	500	238	4.666e-09 ± 3e-11
0.7	995	500	26.9	2.182e-05 ± 9.7e-08
0.7	10	1000	9.78e-05	6.257e-09 ± 2.7e-11
0.7	1000	1000	27	9.46e-09 ± 3.7e-11
0.7	5000	1000	232	9.897e-10 ± 5.3e-12
0.7	1995	1000	56.4	4.386e-07 ± 2.2e-09
1.	10	1	0.39	0.4409 ± 0.0014
1.	20	1	0.793	0.3992 ± 0.0016
1.	50	1	1.99	0.3032 ± 0.0015
1.	100	1	3.98	0.1909 ± 0.001
1.	200	1	7.98	0.0836 ± 0.00035
1.	300	1	12	0.03999 ± 0.00016
1.	500	1	41.3	0.005408 ± 2.2e-05
1.	1000	1	94.9	0.0003973 ± 1.7e-06
1.	2000	1	195	1.087e-05 ± 5.2e-08
1.	5000	1	490	7.022e-08 ± 2.8e-10
1.	10	10	0.0002	0.01499 ± 8.4e-05
1.	50	10	1.83	0.3034 ± 0.0016
1.	100	10	3.9	0.1901 ± 0.00085
1.	5000	10	490	7.023e-08 ± 3e-10
1.	15	10	0.000589	0.01863 ± 9.3e-05
1.	10	50	0.0002	0.002444 ± 1.2e-05
1.	50	50	0.00251	0.002979 ± 1.5e-05
1.	200	50	6.91	0.08382 ± 0.00036
1.	300	50	11.3	0.03989 ± 0.00015
1.	5000	50	490	6.831e-08 ± 4.1e-10
1.	95	50	0.00544	0.01067 ± 5.7e-05
1.	10	150	0.0002	0.0002364 ± 1.1e-06
1.	200	150	0.0192	0.0004124 ± 1.8e-06
1.	500	150	37.4	0.004611 ± 1.9e-05
1.	5000	150	489	5.698e-08 ± 2.5e-10
1.	295	150	0.0631	0.003365 ± 1.7e-05
1.	10	500	0.0002	2.279e-06 ± 8.7e-09
1.	500	500	21.4	3.275e-06 ± 1.4e-08
1.	2000	500	184	7.611e-06 ± 3.7e-08
1.	5000	500	486	1.867e-08 ± 1.2e-10
1.	995	500	54.8	6.171e-05 ± 2.5e-07

Continued on next page

Table C.6 – continued from previous page

Coupling (g)	m_{Phi} [GeV]	m_{χ} [GeV]	Γ_{min} [GeV]	σ [pb]
1.	10	1000	0.0002	2.595e-08 ± 1e-10
1.	1000	1000	55.1	3.933e-08 ± 1.5e-10
1.	5000	1000	474	3.536e-09 ± 1.8e-11
1.	1995	1000	115	1.103e-06 ± 5e-09
1.5	10	1	0.878	1.041 ± 0.004
1.5	20	1	1.78	0.9304 ± 0.0037
1.5	50	1	4.48	0.6793 ± 0.003
1.5	100	1	8.96	0.4189 ± 0.002
1.5	200	1	17.9	0.1836 ± 0.00074
1.5	300	1	27	0.08863 ± 0.00038
1.5	500	1	93	0.01129 ± 5.5e-05
1.5	1000	1	214	0.000878 ± 4.1e-06
1.5	2000	1	439	3.1e-05 ± 1.2e-07
1.5	5000	1	1103	3.408e-07 ± 1.6e-09
1.5	10	10	0.000449	0.0747 ± 0.00036
1.5	50	10	4.11	0.6777 ± 0.0032
1.5	100	10	8.78	0.424 ± 0.002
1.5	5000	10	1103	3.418e-07 ± 1.3e-09
1.5	15	10	0.00133	0.09382 ± 0.00049
1.5	10	50	0.000449	0.01227 ± 6.9e-05
1.5	50	50	0.00566	0.01488 ± 7.4e-05
1.5	200	50	15.5	0.1861 ± 0.00087
1.5	300	50	25.5	0.08815 ± 0.00041
1.5	5000	50	1103	3.334e-07 ± 2e-09
1.5	95	50	0.0122	0.05397 ± 0.00029
1.5	10	150	0.000449	0.0012 ± 6.1e-06
1.5	200	150	0.0432	0.002092 ± 9.1e-06
1.5	500	150	84.1	0.009493 ± 4.2e-05
1.5	5000	150	1102	2.739e-07 ± 1.5e-09
1.5	295	150	0.142	0.01722 ± 0.00011
1.5	10	500	0.000449	1.147e-05 ± 4.7e-08
1.5	500	500	48.2	1.659e-05 ± 6.5e-08
1.5	2000	500	415	1.716e-05 ± 9e-08
1.5	5000	500	1094	8.722e-08 ± 3.9e-10
1.5	995	500	123	0.0001753 ± 6.8e-07
1.5	10	1000	0.000449	1.32e-07 ± 5.2e-10
1.5	1000	1000	124	1.975e-07 ± 7.7e-10
1.5	5000	1000	1065	1.508e-08 ± 6.2e-11
1.5	1995	1000	259	2.741e-06 ± 1.3e-08
2.	10	1	1.56	1.962 ± 0.0076
2.	20	1	3.17	1.718 ± 0.0064
2.	50	1	7.96	1.217 ± 0.0061
2.	100	1	15.9	0.7382 ± 0.0029
2.	200	1	31.9	0.3179 ± 0.0015
2.	300	1	48	0.1503 ± 0.00067

Continued on next page

Table C.6 – continued from previous page

Coupling (g)	m_{Phi} [GeV]	m_{χ} [GeV]	Γ_{min} [GeV]	σ [pb]
2.	500	1	165	0.01871 ± 0.0001
2.	1000	1	380	0.001487 ± 9.1e-06
2.	2000	1	780	6.481e-05 ± 3e-07
2.	5000	1	1961	9.619e-07 ± 3.9e-09
2.	10	10	0.000799	0.2395 ± 0.0012
2.	50	10	7.3	1.217 ± 0.0051
2.	100	10	15.6	0.7347 ± 0.003
2.	5000	10	1961	9.544e-07 ± 4.6e-09
2.	15	10	0.00236	0.2973 ± 0.0015
2.	10	50	0.000799	0.03855 ± 0.00018
2.	50	50	0.0101	0.04728 ± 0.00022
2.	200	50	27.6	0.3166 ± 0.0016
2.	300	50	45.3	0.149 ± 0.00061
2.	5000	50	1960	9.34e-07 ± 4.6e-09
2.	95	50	0.0217	0.1717 ± 0.00096
2.	10	150	0.000799	0.003778 ± 1.8e-05
2.	200	150	0.0768	0.006619 ± 2.7e-05
2.	500	150	149	0.01511 ± 8.1e-05
2.	5000	150	1959	7.835e-07 ± 3.9e-09
2.	295	150	0.253	0.05408 ± 0.00031
2.	10	500	0.000799	3.638e-05 ± 1.5e-07
2.	500	500	85.8	5.258e-05 ± 2.4e-07
2.	2000	500	736.9	2.857e-05 ± 1.7e-07
2.	5000	500	1945	2.44e-07 ± 1.1e-09
2.	995	500	219.2	0.0003371 ± 1.4e-06
2.	10	1000	0.0007987	4.139e-07 ± 1.7e-09
2.	1000	1000	220.5	6.26e-07 ± 2.8e-09
2.	5000	1000	1894	3.818e-08 ± 1.5e-10
2.	1995	1000	460.1	4.794e-06 ± 2.4e-08
2.5	10	1	2.44	3.313 ± 0.016
2.5	20	1	4.95	2.805 ± 0.013
2.5	50	1	12.4	1.92 ± 0.01
2.5	100	1	24.9	1.131 ± 0.0054
2.5	200	1	49.9	0.4734 ± 0.0021
2.5	300	1	75.0	0.2216 ± 0.0012
2.5	500	1	258	0.02611 ± 0.00012
2.5	1000	1	593	0.002111 ± 1e-05
2.5	2000	1	1218	0.0001072 ± 4.2e-07
2.5	5000	1	3064	1.927e-06 ± 9.9e-09
2.5	10	10	0.00125	0.5815 ± 0.0026
2.5	50	10	11.4	1.928 ± 0.011
2.5	100	10	24.4	1.131 ± 0.006
2.5	5000	10	3064	1.937e-06 ± 9.9e-09
2.5	15	10	0.00368	0.7216 ± 0.0041
2.5	10	50	0.00125	0.09521 ± 0.00048

Continued on next page

Table C.6 – continued from previous page

Coupling (g)	m_{Phi} [GeV]	m_{χ} [GeV]	Γ_{min} [GeV]	σ [pb]
2.5	50	50	0.0157	0.1158 ± 0.00055
2.5	200	50	43.2	0.475 ± 0.0018
2.5	300	50	70.8	0.2214 ± 0.0012
2.5	5000	50	3064	1.868e-06 ± 1e-08
2.5	95	50	0.034	0.421 ± 0.0022
2.5	10	150	0.00125	0.009221 ± 4.6e-05
2.5	200	150	0.12	0.01604 ± 6.7e-05
2.5	500	150	234	0.0206 ± 8.7e-05
2.5	5000	150	3062	1.55e-06 ± 7.6e-09
2.5	295	150	0.395	0.1314 ± 0.0007
2.5	10	500	0.00125	8.948e-05 ± 3.4e-07
2.5	500	500	134	0.0001273 ± 5e-07
2.5	2000	500	1151	3.922e-05 ± 1.8e-07
2.5	5000	500	3039	4.732e-07 ± 2e-09
2.5	995	500	343	0.0005315 ± 2.5e-06
2.5	10	1000	0.00125	1.014e-06 ± 4.2e-09
2.5	1000	1000	345	1.522e-06 ± 7e-09
2.5	5000	1000	2960	6.909e-08 ± 3.6e-10
2.5	1995	1000	719	6.791e-06 ± 3.3e-08
3.	10	1	3.51	5.17 ± 0.021
3.	20	1	7.13	4.262 ± 0.017
3.	50	1	17.9	2.814 ± 0.014
3.	100	1	35.9	1.595 ± 0.0073
3.	200	1	71.8	0.651 ± 0.0028
3.	300	1	108	0.3028 ± 0.0014
3.	500	1	372	0.03314 ± 0.00019
3.	1000	1	854	0.002641 ± 1.5e-05
3.	2000	1	1754	0.0001496 ± 5.3e-07
3.	5000	1	4412	3.035e-06 ± 1.4e-08
3.	10	10	0.0018	1.214 ± 0.0059
3.	50	10	16.4	2.849 ± 0.012
3.	100	10	35.1	1.611 ± 0.0071
3.	5000	10	4412	3.031e-06 ± 2.1e-08
3.	15	10	0.00530	1.509 ± 0.0076
3.	10	50	0.00178	0.1967 ± 0.00093
3.	50	50	0.0226	0.242 ± 0.0012
3.	200	50	62.2	0.6533 ± 0.0033
3.	300	50	102	0.3011 ± 0.0013
3.	5000	50	4412	2.974e-06 ± 1.6e-08
3.	95	50	0.0489	0.8669 ± 0.0046
3.	10	150	0.0018	0.01918 ± 8.3e-05
3.	200	150	0.173	0.03357 ± 0.00015
3.	500	150	336	0.02601 ± 0.00013
3.	5000	150	4409	2.417e-06 ± 1.1e-08
3.	295	150	0.568	0.2747 ± 0.0017

Continued on next page

Table C.6 – continued from previous page

Coupling (g)	m_{Phi} [GeV]	m_{χ} [GeV]	Γ_{min} [GeV]	σ [pb]
3.	10	500	0.0018	0.0001847 ± 7.2e-07
3.	500	500	193	0.0002634 ± 1.2e-06
3.	2000	500	1658	4.736e-05 ± 2.1e-07
3.	5000	500	4376	7.254e-07 ± 3.1e-09
3.	995	500	493	0.0007379 ± 3e-06
3.	10	1000	0.0018	2.087e-06 ± 9.5e-09
3.	1000	1000	496	3.142e-06 ± 1.3e-08
3.	5000	1000	4263	9.753e-08 ± 4e-10
3.	1995	1000	1035	8.775e-06 ± 3.8e-08
3.5	10	1	4.78	7.684 ± 0.025
3.5	20	1	9.71	6.209 ± 0.026
3.5	50	1	24.4	3.911 ± 0.024
3.5	100	1	48.8	2.138 ± 0.011
3.5	200	1	97.7	0.8426 ± 0.0034
3.5	300	1	147	0.3824 ± 0.0018
3.5	500	1	506	0.03921 ± 0.00026
3.5	1000	1	1163	0.003103 ± 1.6e-05
3.5	2000	1	2387	0.0001824 ± 8e-07
3.5	5000	1	6005	4.039e-06 ± 2.6e-08
3.5	10	10	0.00245	2.231 ± 0.011
3.5	50	10	22.4	3.911 ± 0.021
3.5	100	10	47.8	2.133 ± 0.0093
3.5	5000	10	6005	4.037e-06 ± 1.9e-08
3.5	15	10	0.00722	2.777 ± 0.013
3.5	10	50	0.00245	0.3644 ± 0.0016
3.5	50	50	0.0308	0.4471 ± 0.002
3.5	200	50	84.7	0.8484 ± 0.0041
3.5	300	50	139	0.3844 ± 0.002
3.5	5000	50	6005	3.938e-06 ± 2.2e-08
3.5	95	50	0.0666	1.603 ± 0.01
3.5	10	150	0.00245	0.03531 ± 0.00018
3.5	200	150	0.235	0.0618 ± 0.00027
3.5	500	150	458	0.03087 ± 0.00015
3.5	5000	150	6001	3.227e-06 ± 1.6e-08
3.5	295	150	0.773	0.5139 ± 0.0026
3.5	10	500	0.00245	0.0003434 ± 1.5e-06
3.5	500	500	263	0.0004874 ± 2e-06
3.5	2000	500	2257	5.311e-05 ± 2.5e-07
3.5	5000	500	5956	9.439e-07 ± 4.7e-09
3.5	995	500	672	0.0009553 ± 3.7e-06
3.5	10	1000	0.00245	3.857e-06 ± 1.9e-08
3.5	1000	1000	675	5.748e-06 ± 2.4e-08
3.5	5000	1000	5802	1.197e-07 ± 6.2e-10
3.5	1995	1000	1409	1.037e-05 ± 4.9e-08

m_χ	m_Φ	σ [pb]	m_χ	m_Φ	σ [pb]
100	1000	1.50E-02	150	600	1.22E-01
100	100	1.13E-04	200	1000	7.04E-03
100	1300	7.05E-03	200	1300	2.11E-03
100	150	6.12E+00	200	200	6.29E-05
100	200	9.60E+00	200	250	5.83E-01
100	250	7.57E+00	200	300	1.64E+00
100	300	4.01E+00	200	400	9.08E-01
100	400	1.06E+00	200	600	1.11E-01
100	600	1.45E-01	35	250	9.62E+00
10	1000	3.55E-01	35	300	4.56E+00
10	100	7.67E+01	35	350	2.35E+00
10	10	2.43E-05	35	400	1.33E+00
10	1300	2.35E-01	35	500	5.48E-01
10	150	3.92E+01	35	550	3.80E-01
10	200	2.13E+01	35	600	2.76E-01
10	250	1.05E+01	35	650	2.07E-01
10	300	5.57E+00	35	700	1.60E-01
10	400	2.35E+00	50	1000	3.69E-02
10	50	1.51E+02	50	100	3.07E+01
10	600	8.16E-01	50	1300	2.39E-02
150	1000	9.44E-03	50	150	2.76E+01
150	1300	3.44E-03	50	200	1.82E+01
150	150	8.84E-05	50	250	9.31E+00
150	200	1.69E+00	50	300	4.40E+00
150	250	3.76E+00	50	400	1.22E+00
150	300	3.29E+00	50	50	1.04E-04
150	400	9.83E-01	50	600	2.14E-01

Table C.2: Dark matter masses m_χ and mediator masses m_Φ generated such that relic density constraints are fullfilled for 13 TeV. The resulting production cross sections are given in pb.

C.4 Cross sections for the $b\bar{b}$+DM scalar simplified model

[TODO: add cross-sections, they will be available with plots]

m_χ	m_Φ	σ [pb]	m_χ	m_Φ	σ [pb]
100	1000	1.50E-02	150	600	1.22E-01
100	100	1.13E-04	200	1000	7.04E-03
100	1300	7.05E-03	200	1300	2.11E-03
100	150	6.12E+00	200	200	6.29E-05
100	200	9.60E+00	200	250	5.83E-01
100	250	7.57E+00	200	300	1.64E+00
100	300	4.01E+00	200	400	9.08E-01
100	400	1.06E+00	200	600	1.11E-01
100	600	1.45E-01	35	250	9.62E+00
10	1000	3.55E-01	35	300	4.56E+00
10	100	7.67E+01	35	350	2.35E+00
10	10	2.43E-05	35	400	1.33E+00
10	1300	2.35E-01	35	500	5.48E-01
10	150	3.92E+01	35	550	3.80E-01
10	200	2.13E+01	35	600	2.76E-01
10	250	1.05E+01	35	650	2.07E-01
10	300	5.57E+00	35	700	1.60E-01
10	400	2.35E+00	50	1000	3.69E-02
10	50	1.51E+02	50	100	3.07E+01
10	600	8.16E-01	50	1300	2.39E-02
150	1000	9.44E-03	50	150	2.76E+01
150	1300	3.44E-03	50	200	1.82E+01
150	150	8.84E-05	50	250	9.31E+00
150	200	1.69E+00	50	300	4.40E+00
150	250	3.76E+00	50	400	1.22E+00
150	300	3.29E+00	50	50	1.04E-04
150	400	9.83E-01	50	600	2.14E-01

Table C.3: Dark matter masses m_χ and mediator masses m_Φ generated such that relic density constraints are fullfilled for 13 TeV. The resulting production cross sections are given in pb.

m_χ	m_Φ	σ [pb]	m_χ	m_Φ	σ [pb]
100	1000	1.53E-03	150	600	1.61E-02
100	100	2.21E-05	200	1000	5.46E-04
100	1300	7.91E-04	200	1300	1.54E-04
100	150	1.58E+00	200	200	9.52E-06
100	200	2.48E+00	200	250	1.22E-01
100	250	1.82E+00	200	300	3.53E-01
100	300	8.77E-01	200	400	1.65E-01
100	400	1.94E-01	200	600	1.43E-02
100	600	2.00E-02	35	250	2.32E+00
10	1000	5.61E-02	35	300	1.00E+00
10	100	2.36E+01	35	350	4.73E-01
10	10	6.53E-06	35	400	2.51E-01
10	1300	3.62E-02	35	500	9.23E-02
10	150	1.12E+01	35	550	6.07E-02
10	200	5.61E+00	35	600	4.20E-02
10	250	2.50E+00	35	650	3.02E-02
10	300	1.21E+00	35	700	2.25E-02
10	400	4.53E-01	50	1000	4.70E-03
10	50	4.83E+01	50	100	8.88E+00
10	600	1.34E-01	50	1300	3.34E-03
150	1000	8.21E-04	50	150	7.83E+00
150	1300	3.07E-04	50	200	4.80E+00
150	150	1.52E-05	50	250	2.25E+00
150	200	3.93E-01	50	300	9.67E-01
150	250	8.86E-01	50	400	2.28E-01
150	300	7.19E-01	50	50	2.37E-05
150	400	1.79E-01	50	600	3.15E-02

Table C.4: Dark matter masses m_χ and mediator masses m_Φ generated for such that relic density constraints are fullfilled for 8 TeV. The resulting production cross sections are given in pb.

D
Appendix: Presentation of experimental results for reinterpretation

To do **Add a section on specific information that is necessary to have from experimentalists in DM searches (??)**

We suggest the following to collider searches, when presenting results from the recommended benchmarks:

- Provide limits in collider language, on fundamental parameters of interaction: couplings and masses of particles in simplified model.

- Translate limits to non-collider language, for a range of assumptions in order to convey a rough idea of the range of possibilities. The details of this point are left for work beyond the scope of this Forum.

- Provide all necessary material for theorists to reinterpret simplified model results as building blocks for more complete models (e.g. signal cutflows, acceptances, etc). This point is detailed further in this appendix.

Along with the design of new searches to hunt for new physics at the LHC, it is important to consider information needed in order to reinterpret the searches outside of the collaborations. The following is a non-exhaustive list of recommendations in order to make reinterpretation easier and faster. This appendix details considerations for reimplementation of the analysis as well as for using the simplified model results directly given by the collaborations.

One of the important developments in recent years is an active development of the analyses recasting codes [DFK+15, CDFW14, KSTR15]. The aim of these codes is to provide a public library of reimplemented and validated LHC analyses. Such libraries can then be used to analyze validity of a BSM scenario in a systematic and effective manner. The availability of public libraries further facilitates a unified framework and can lead to an organized and central structure to preserve LHC information in a long run.

In order to be able to develop such codes, it is important to get complete and systematic information from the collaborations.

- **Data digitization**: Availability of digitized data is one of the primary requirement. All information given by collaborations

in the form of plots should be made available in a digitized format. Platforms such as HepData can be used in oder to maintain a centralised manner. In case when HepData can not be used, digitised data can be provided via analyses twiki pages. This information primarily includes expected and observed exclusion lines along with their $\pm 1\sigma$ uncertainty, expected and observed upper limits in case of simplified models, efficiency maps and all kinematic distributions as reported in the analysis. Units should be clearly specified. If the digitised figures are made available as a C macro or a ROOT file, the names of the objects should be clearly identifiable e.g. expected upper limits of a particular topology/model given as a ROOT file can be labeled as `KEY: TH2D ExpectedUpperLimit;1`. Furthermore, these digitised files can potentially contain more information (larger axes ranges) than displayed on the plot. This will help facilitate understand what happens beyond the limits displayed in the plot, e.g. a distribution for number of jets can be artificially limited to a point in the plot (for the purpose of clarity of figure) , however, this artificial limit leads to a sharp cutoff in the plot. While validating the analysis it is often necessary to compare the distributions beyond such artificial limits, having this information digitised will be of a great help in such cases.

D.1 Reimplementing analyses

This section lists information necessary in order to reimplement an analysis. Analysis reimplementation usually consists of several stages. Usually, one starts with reading the analysis note carefully, following which the preselection and event selection cuts are identified. These are then mimicked using a code typically written in C++. The detector simulation is carried out by using public detector simulation softwares e.g. Delphes [dF+14]. The resulting ROOT file is then analysed using the C++ code written in the previous step.

- **Analysis documentation**: The collaborations should provide a cutflow table with every analysis, such a cutflow table will naturally define the order of cuts implemented in an analysis. There are several preselection criteria which can not be easily simulated in phenomenology, e.g. MET cleaning. Numbers should be provided after such cuts so that theorists can rescale their number of events in order to account for such cuts. Efficiencies of several reconstructed objects are given as an input to detector simulation softwares like Delphes. It is thus very useful to get parametrised efficiencies for reconstructed objects (as a function of the rapidity η and/or transverse momentum p_T), along with the working points at which they were evaluated (e.g. loose, tight selection). Object definitions should be clearly identifiable.

- **Validation**: Validation corresponds to re-deriving the results as given by collaborations in order to verify that the implementa-

tion of the analysis is correct. Usually most of the bug catching takes place in the phase of validation. The following items are necessary in order to recreate the results.

  - Monte Carlo generators: Monte Carlo generators along with the exact versions used to produce the event files should be listed.
  - Production cross sections: The order of production cross sections (e.g. LO,NLO,NLL) as well as the codes which were used to compute them should be provided. A table of reference cross sections for several values of particle masses such as ones provided by SUSY cross section working group will be highly appreciated.
  - Process Generation: Details of the generated process, detailing number of additional partons generated.
  - Availability of the LHE files: LHE files (detailing at least a few events if not the entire file) corresponding to the benchmarks listed in the analysis should be made available in order to cross check process generation. For models concerning SUSY, corresponding SLHA files of benchmark files should also be details. Special attention should be paid to list the parameters which change the production cross section or kinematics of the process e.g. mixing angles.
  - Process cards: Process cards includes PDF choices, details of matching algorithms and scales and details of process generation. If process cards are not available, above items should be clearly identified.
  - MadGraph model files: For models which are not already implemented in MadGraph, availability of the corresponding model files is highly desired. It details the exact notation used in the model and hence sets up a complete framework. In case MadGraph is not used, enough information should be provided in order to clearly identify the underlying model used for interpretations.

- **Limit setting**: Detailed description of the likelihood used in order to derive the limits should be given, this can contain statistical procedure within the analysis text itself, however direct availability of the limit setting code as a workspace in RooStats is highly desirable.

- **Binned backgrounds**: For analyses using techniques such as sliding windows or an unbinned technique, the Standard Model backgrounds should be given in the form of bins. These backgrounds can then be interpolated.

- **Recast code**: Finally, the collaborations can provide an analysis code directly implemented in one of the public recasting codes detailed above. Such codes can be published via INSPIRE in order to track the versioning and citations.

D.2 *Simplified model interpretations*

The analyses almost always provide at least one simplified model interpretation along with the search results. These interpretations are simple and can be used in order to take a quick survey of viability of parameter space. Codes such as [KKL$^+$14b, KKL$^+$14a, PSWZ14] can make use of the simplified model results given in the form of 95% Confidence Level (CLs) upper limit or efficiency maps in order to test Beyond the Standard Model parameter space. It will thus be extremely useful if the results are given in a form as easily usable by the theory community.

- **Direct usability of the results**: The results given should be as useful as possible. For example, for a simplified model containing dark matter mass m_{DM}, mediator mass M_{med} and couplings g_{DM}, g_{q} it will be extremely useful to have 95% CLs upper limits on the product of couplings $\sqrt{g_{\mathrm{DM}} g_{\mathrm{q}}}$ or cross section times branching ratio as a function of m_{DM}, M_{med}..

- **Smooth grids**: The usage of simplified model results relies on interpolating between upper limit values. In order to facilitate the interpolation, regions where large variation of upper limits is observed should contain denser grid, if a uniform grid over the entire plane is not possible. For simplified model involving more than three parameters (two masses and product of couplings), slices of upper limits in the additional dimensions will be very useful e.g. for a simplified model involving one step cascade decay, upper limits can be provided for several values of intermediate mass in the plane of mother - daughter masses. Results with only one slice often render invalid to be used in a general model testing.

- **Availability of efficiency maps**: Finally, efficiency maps for all the signal regions involved in the analysis should be made available. These results are not only useful for model testing using simplified models but also to validate implementation of the analysis. Information about the most sensitive signal region as a function of masses is also very useful in order to determine the validity of approximate limit setting procedures being used by theorists (in the absence of any other sophisticated limit setting technique).

Bibliography

[A+08] J. Alwall et al. Comparative study of various algorithms for the merging of parton showers and matrix elements in hadronic collisions. *Eur.Phys.J.*, C53(2):473–500, 2008.

[A+12] Daniele Alves et al. Simplified Models for LHC New Physics Searches. *J.Phys.*, G39:105005, 2012.

[A+14a] Georges Aad et al. Search for new particles in events with one lepton and missing transverse momentum in pp collisions at $\sqrt{s}$ = 8 TeV with the ATLAS detector. *JHEP*, 1409:037, 2014.

[A+14b] Jalal Abdallah et al. Simplified Models for Dark Matter and Missing Energy Searches at the LHC. *arXiv:1409.2893*, 2014.

[A+14c] J. Alwall et al. The automated computation of tree-level and next-to-leading order differential cross sections, and their matching to parton shower simulations. *JHEP*, 07(2):079, 2014.

[A+15a] G. Aad et al. Search for dark matter in events with heavy quarks and missing transverse momentum in pp collisions with the ATLAS detector. *Eur.Phys.J.*, C75(2):92, 2015.

[A+15b] Georges Aad et al. Search for new phenomena in final states with an energetic jet and large missing transverse momentum in pp collisions at $\sqrt{s} = 8$ TeV with the ATLAS detector. 2015.

[AAB+14] Jean-Laurent Agram, Jeremy Andrea, Michael Buttignol, Eric Conte, and Benjamin Fuks. Monotop phenomenology at the Large Hadron Collider. *Phys.Rev.*, D89(1):014028, 2014.

[Aad14a] Search for dark matter in events with a hadronically decaying W or Z boson and missing transverse momentum in pp collisions at $\sqrt{s} = 8$ TeV with the ATLAS detector. *Phys.Rev.Lett.*, 112(4):041802, 2014.

[Aad14b] Search for dark matter in events with a Z boson and missing transverse momentum in pp collisions at $\sqrt{s}$=8

TeV with the ATLAS detector. *Phys.Rev.*, D90(1):012004, 2014.

[Aad15] Search for new phenomena in events with a photon and missing transverse momentum in pp collisions at $\sqrt{s} = 8$ TeV with the ATLAS detector. *Phys.Rev.*, D91(1):012008, 2015.

[ABG14] Prateek Agrawal, Monika Blanke, and Katrin Gemmler. Flavored dark matter beyond Minimal Flavor Violation. *JHEP*, 1410:72, 2014.

[ABHL14] Prateek Agrawal, Brian Batell, Dan Hooper, and Tongyan Lin. Flavored Dark Matter and the Galactic Center Gamma-Ray Excess. *Phys.Rev.*, D90(6):063512, 2014.

[ADR+14] Mohammad Abdullah, Anthony DiFranzo, Arvind Rajaraman, Tim M.P. Tait, Philip Tanedo, et al. Hidden on-shell mediators for the Galactic Center γ-ray excess. *Phys.Rev.*, D90(3):035004, 2014.

[AFM11] J. Andrea, B. Fuks, and F. Maltoni. Monotops at the LHC. *Phys.Rev.*, D84:074025, 2011.

[AHW13] Haipeng An, Ran Huo, and Lian-Tao Wang. Searching for Low Mass Dark Portal at the LHC. *Phys.Dark Univ.*, 2:50–57, 2013.

[AJW12] Haipeng An, Xiangdong Ji, and Lian-Tao Wang. Light Dark Matter and Z' Dark Force at Colliders. *JHEP*, 1207:182, 2012.

[AOP+02] B.C. Allanach, K. Odagiri, M.J. Palmer, Michael Andrew Parker, A. Sabetfakhri, et al. Exploring small extra dimensions at the large hadron collider. *JHEP*, 0212:039, 2002.

[ATL14] Sensitivity to WIMP Dark Matter in the Final States Containing Jets and Missing Transverse Momentum with the ATLAS Detector at 14 TeV LHC. Technical Report ATL-PHYS-PUB-2014-007, CERN, Geneva, Jun 2014.

[AWZ14a] Haipeng An, Lian-Tao Wang, and Hao Zhang. Dark matter with t-channel mediator: a simple step beyond contact interaction. *Phys. Rev. D*, 89:115014, 2014.

[AWZ14b] Haipeng An, Lian-Tao Wang, and Hao Zhang. Dark matter with t-channel mediator: a simple step beyond contact interaction. *Phys.Rev.*, D89(11):115014, 2014.

[BB13a] Yang Bai and Joshua Berger. Fermion Portal Dark Matter. *JHEP*, 1311:171, 2013.

[BB13b] Yang Bai and Joshua Berger. Fermion Portal Dark Matter. *JHEP*, 11:171, 2013.

[BB14] Yang Bai and Joshua Berger. Lepton Portal Dark Matter. *JHEP*, 1408:153, 2014.

[BCD+15] Nicole F. Bell, Yi Cai, James B. Dent, Rebecca K. Leane, and Thomas J. Weiler. Dark matter at the LHC: EFTs and gauge invariance. 2015.

[BCDF15] Idir Boucheneb, Giacomo Cacciapaglia, Aldo Deandrea, and Benjamin Fuks. Revisiting monotop production at the LHC. *JHEP*, 1501:017, 2015.

[BDG+12] Nicole F. Bell, James B. Dent, Ahmad J. Galea, Thomas D. Jacques, Lawrence M. Krauss, et al. Searching for Dark Matter at the LHC with a Mono-Z. *Phys.Rev.*, D86:096011, 2012.

[BDM14] O. Buchmueller, Matthew J. Dolan, and Christopher McCabe. Beyond Effective Field Theory for Dark Matter Searches at the LHC. *JHEP*, 1401:025, 2014.

[BDSG+14] Giorgio Busoni, Andrea De Simone, Johanna Gramling, Enrico Morgante, and Antonio Riotto. On the Validity of the Effective Field Theory for Dark Matter Searches at the LHC, Part II: Complete Analysis for the *s*-channel. *JCAP*, 1406:060, 2014.

[BDSJ+14] Giorgio Busoni, Andrea De Simone, Thomas Jacques, Enrico Morgante, and Antonio Riotto. On the Validity of the Effective Field Theory for Dark Matter Searches at the LHC Part III: Analysis for the *t*-channel. *JCAP*, 1409:022, 2014.

[BDSMR14] Giorgio Busoni, Andrea De Simone, Enrico Morgante, and Antonio Riotto. On the Validity of the Effective Field Theory for Dark Matter Searches at the LHC. *Phys.Lett.*, B728:412–421, 2014.

[BFG15] Matthew R. Buckley, David Feld, and Dorival Goncalves. Scalar Simplified Models for Dark Matter. *Phys.Rev.*, D91(1):015017, 2015.

[BLW14] Asher Berlin, Tongyan Lin, and Lian-Tao Wang. Mono-Higgs Detection of Dark Matter at the LHC. *JHEP*, 1406:078, 2014.

[BT13] Yang Bai and Tim M.P. Tait. Searches with Mono-Leptons. *Phys.Lett.*, B723:384–387, 2013.

[CDFW14] Eric Conte, BÃl'ranger Dumont, Benjamin Fuks, and Chris Wymant. Designing and recasting LHC analyses with MadAnalysis 5. *Eur.Phys.J.*, C74(10):3103, 2014.

[CDM+14] Linda Carpenter, Anthony DiFranzo, Michael Mulhearn, Chase Shimmin, Sean Tulin, et al. Mono-Higgs-boson: A new collider probe of dark matter. *Phys.Rev.*, D89(7):075017, 2014.

[CEHL14] Spencer Chang, Ralph Edezhath, Jeffrey Hutchinson, and Markus Luty. Effective WIMPs. *Phys. Rev. D*, 89:015011, 2014.

[CGT13] Nathaniel Craig, Jamison Galloway, and Scott Thomas. Searching for Signs of the Second Higgs Doublet. 2013.

[CHH15] Andreas Crivellin, Ulrich Haisch, and Anthony Hibbs. LHC constraints on gauge boson couplings to dark matter. 2015.

[CHLR13] R.C. Cotta, J.L. Hewett, M.P. Le, and T.G. Rizzo. Bounds on Dark Matter Interactions with Electroweak Gauge Bosons. *Phys.Rev.*, D88:116009, 2013.

[CNS+13] Linda M. Carpenter, Andrew Nelson, Chase Shimmin, Tim M.P. Tait, and Daniel Whiteson. Collider searches for dark matter in events with a Z boson and missing energy. *Phys.Rev.*, D87(7):074005, 2013.

[CRTW14] Randel C. Cotta, Arvind Rajaraman, Tim M. P. Tait, and Alexander M. Wijangco. Particle Physics Implications and Constraints on Dark Matter Interpretations of the CDMS Signal. *Phys.Rev.*, D90(1):013020, 2014.

[dF+14] J. de Favereau et al. DELPHES 3, A modular framework for fast simulation of a generic collider experiment. *JHEP*, 1402:057, 2014.

[DFH+14] Tansu Daylan, Douglas P. Finkbeiner, Dan Hooper, Tim Linden, Stephen K. N. Portillo, et al. The Characterization of the Gamma-Ray Signal from the Central Milky Way: A Compelling Case for Annihilating Dark Matter. 2014.

[DFK+15] B. Dumont, B. Fuks, S. Kraml, S. Bein, G. Chalons, et al. Toward a public analysis database for LHC new physics searches using MADANALYSIS 5. *Eur.Phys.J.*, C75(2):56, 2015.

[DNRT13] Anthony DiFranzo, Keiko I. Nagao, Arvind Rajaraman, and Tim M. P. Tait. Simplified Models for Dark Matter Interacting With Quarks. *JHEP*, 1311, 2013.

[For15a] SVN repository for Madgraph input cards for model with s-channel exchange of vector mediator, for electroweak boson final states. `https://svnweb.cern.ch/cern/wsvn/LHCDMF/trunk/models/EW_DMV/`, 2015. [Online; accessed 15-May-2015].

[For15b] SVN repository for Madgraph inputs for 2HDM model leading to a mono-Higgs signature. https://svnweb.cern.ch/cern/wsvn/LHCDMF/trunk/models/EW_Higgs_2HDM/, 2015. [Online; accessed 12-May-2015].

[For15c] SVN repository for Madgraph inputs for dimension-7 EFT models with direct DM-EW boson couplings. https://svnweb.cern.ch/cern/wsvn/LHCDMF/trunk/models/EW_Fermion_D7/, 2015. [Online; accessed 24-April-2015].

[For15d] SVN repository for Madgraph inputs for mono-top models. https://svnweb.cern.ch/cern/wsvn/LHCDMF/trunk/models/HF_SingleTop/, 2015. [Online; accessed 27-April-2015].

[For15e] SVN repository for Madgraph inputs for simplified model with a colored scalar mediator coupling to DM and b-quarks. https://svnweb.cern.ch/cern/wsvn/LHCDMF/trunk/models/HF_S%2BPS/, 2015. [Online; accessed 24-April-2015].

[For15f] SVN repository for Madgraph inputs for vector and scalar mediator models leading to a mono-Higgs signature. https://svnweb.cern.ch/cern/wsvn/LHCDMF/trunk/models/EW_Higgs_all/, 2015. [Online; accessed 24-April-2015].

[For15g] SVN repository for Madgraph inputs with t-channel exchange of colored scalar mediator. https://svnweb.cern.ch/cern/wsvn/LHCDMF/trunk/models/Monojet_tChannel/, 2015. [Online; accessed 27-April-2015].

[GIR+10] Jessica Goodman, Masahiro Ibe, Arvind Rajaraman, William Shepherd, Tim M.P. Tait, et al. Constraints on Dark Matter from Colliders. *Phys.Rev.*, D82:116010, 2010.

[HKR13] Ulrich Haisch, Felix Kahlhoefer, and Emanuele Re. QCD effects in mono-jet searches for dark matter. *JHEP*, 1312:007, 2013.

[HKSW15] Philip Harris, Valentin V. Khoze, Michael Spannowsky, and Ciaran Williams. Constraining Dark Sectors at Colliders: Beyond the Effective Theory Approach. *Phys.Rev.*, D91(5):055009, 2015.

[HKU13] Ulrich Haisch, Felix Kahlhoefer, and James Unwin. The impact of heavy-quark loops on LHC dark matter searches. *JHEP*, 1307:125, 2013.

[HR15] Ulrich Haisch and Emanuele Re. Simplified dark matter top-quark interactions at the LHC. 2015.

[K+14] Vardan Khachatryan et al. Search for physics beyond the standard model in final states with a lepton and missing transverse energy in proton-proton collisions at $\sqrt{s}$ = 8 TeV. 2014.

[Kha14] Search for new phenomena in monophoton final states in proton-proton collisions at $\sqrt{s}$ = 8 TeV. 2014.

[KKL+14a] Sabine Kraml, Suchita Kulkarni, Ursula Laa, Andre Lessa, Veronika Magerl, et al. SModelS v1.0: a short user guide. 2014.

[KKL+14b] Sabine Kraml, Suchita Kulkarni, Ursula Laa, Andre Lessa, Wolfgang Magerl, Doris Proschofsky, and Wolfgang Waltenberger. SModelS: a tool for interpreting simplified-model results from the LHC and its application to supersymmetry. *Eur.Phys.J.*, C74:2868, 2014.

[KSTR15] Jong Soo Kim, Daniel Schmeier, Jamie Tattersall, and Krzysztof Rolbiecki. A framework to create customised LHC analyses within CheckMATE. 2015.

[LKW13] Tongyan Lin, Edward W. Kolb, and Lian-Tao Wang. Probing dark matter couplings to top and bottom quarks at the LHC. *Phys.Rev.*, D88(6):063510, 2013.

[LPS14] Hyun Min Lee, Myeonghun Park, and Veronica Sanz. Gravity-mediated (or Composite) Dark Matter. *Eur.Phys.J.*, C74:2715, 2014.

[LSWY13] Jia Liu, Brian Shuve, Neal Weiner, and Itay Yavin. Looking for new charged states at the LHC: Signatures of Magnetic and Rayleigh Dark Matter. *JHEP*, 1307:144, 2013.

[MMA+14] Sarah Malik, Christopher McCabe, Henrique Araujo, A. Belyaev, Celine Boehm, et al. Interplay and Characterization of Dark Matter Searches at Colliders and in Direct Detection Experiments. 2014.

[NCC+14] Andy Nelson, Linda M. Carpenter, Randel Cotta, Adam Johnstone, and Daniel Whiteson. Confronting the Fermi Line with LHC data: an Effective Theory of Dark Matter Interaction with Photons. *Phys.Rev.*, D89(5):056011, 2014.

[PS14] Alexey A. Petrov and William Shepherd. Searching for dark matter at LHC with Mono-Higgs production. *Phys.Lett.*, B730:178–183, 2014.

[PSWZ14] Michele Papucci, Kazuki Sakurai, Andreas Weiler, and Lisa Zeune. Fastlim: a fast LHC limit calculator. *Eur.Phys.J.*, C74(11):3163, 2014.

[PVZ14] Michele Papucci, Alessandro Vichi, and Kathryn M. Zurek. Monojet versus the rest of the world I: t-channel models. *JHEP*, 1411:024, 2014.

[RWZ15] Davide Racco, Andrea Wulzer, and Fabio Zwirner. Robust collider limits on heavy-mediator Dark Matter. 2015.

[WY12] Neal Weiner and Itay Yavin. How Dark Are Majorana WIMPs? Signals from MiDM and Rayleigh Dark Matter. *Phys.Rev.*, D86:075021, 2012.

[WY13] Neal Weiner and Itay Yavin. UV completions of magnetic inelastic and Rayleigh dark matter for the Fermi Line(s). *Phys.Rev.*, D87(2):023523, 2013.

[ZBW13] Ning Zhou, David Berge, and Daniel Whiteson. Mono-everything: combined limits on dark matter production at colliders from multiple final states. *Phys.Rev.*, D87(9):095013, 2013.